STUDIES OF DISORDER IN FASTIONICS AND OF A NUCLEAR QUADRUPOLE INTERACTION IN ORDERED MAGNETS

A.B. Walker

Department of Theoretical Physics,
University of Oxford

A Thesis submitted for the degree of

Doctor of Philosophy

at Oxford University

Wolfson College

Michaelmas Term 1980

RADCLIFFE SCIENCE LIBRARY OXFORD
DEPOSITED
THESIS
22.4.81

TO MY FAMILY

ACKNOWLEDGEMENTS

Warm thanks go to my supervisors, Gillian Gehring and Mike Gillan, who, besides suggesting the problems that form this thesis have constantly given advice and encouragement. I should also like to thank Maurice Dixon for his help and for reading part of the manuscript.

I should like to thank my colleagues in the Department of Theoretical Physics particularly John Chalker, Kimmo Kaski and Rafael Barno for some useful discussions, also the latter for dissecting some chapters of this thesis.

I am grateful to Lesley Taylor for her skillful typing.

The U.K.A.E.A. Harwell is thanked for financial support in my last two months in Oxford and for the use of computing facilities.

Finally, the St. Giles' fair deserves a mention for some opportune light relief.

ABSTRACT

This thesis consists of two completely separate parts. In Part I, we look at disorder in fastionic conductors, and in Part II we examine the pseudoquadrupole effect in ordered magnets.

Part I looks at two aspects of the disordered state in fastionics, where the disorder is due to ions moving off their regular sites to positions close to other regular sites, a feature especially characteristic of the fluorites.

The first aspect is how Coulomb interactions could be responsible for the co-operative behaviour of defects which causes the transition to fastionic behaviour. We look at this with a model of charged defects on a lattice, applying techniques involving classical diagrammatic perturbation theory to find the free energy of our model system. Using elementary thermodynamics, we show how this model can predict co-operative behaviour.

The second aspect is the nature of the disorder above the fastionic transition. We look at disorder in lead fluoride using a molecular dynamics simulation with an interionic potential that we obtained. We use the simulation to examine the distribution of anions in both real space and $\underline{k}$ space. Simulations have been made on the other fluorites CaF_2 and $SrCl_2$ and it is possible that the high dielectric constant of lead fluoride might lead to qualitatively different behaviour. Our results show that this is not the case and we find defect concentrations similar to those obtained

from CaF_2 and $SrCl_2$. Our $\underline{k}$ space analysis however gives defect concentrations an order of magnitude larger, in approximate agreement with experiment.

In Part II we set up a theory for the pseudoquadrupole effect in cubic ferromagnets and show that it is related to the difference in longitudinal and transverse magnetic susceptibilities. Model calculations are performed for a Heisenberg ferromagnet using molecular field theory near the critical temperature T_c, and spin wave theory at low temperatures; and the itinerant model at absolute zero and T_c.

We find that the pseudoquadrupole effect in iron and nickel and at impurities in these metals appears to be very much less than measured quadrupole effects. We also look at the effect in $GdAl_2$ and show that it can not explain a temperature dependent quadrupole interaction seen experimentally We therefore conclude that the observed quadrupole effects are due to real electric field gradients.

'You should understand, therefore, that there are two ways of fighting: by law or by force. The first way is natural to men and the second to beasts. But as the first way often proves inadequate one must needs have recourse to the second. So a prince must understand how to make a nice use of the beast and the man. The ancient writers taught princes about this by an allegory, when they described how Achilles and many other princes of the ancient world were sent to be brought up by Chiron, the centaur, so that he might train them his way. All the allegory means in making the teacher half beast and half man, is that a prince must know how to act according to the nature of both, and that he cannot survive otherwise.'

Nicolo Machiavelli 'The Prince'

(Transl. G. Bull)

TABLE OF CONTENTS

PART I: DISORDER IN FASTIONICS

		Page No.
1.	INTRODUCTION	2
2.	CLUSTER EXPANSION THEORY	10
	A) Preliminary: The Model	10
	B) Diagram Theory	13
	C) Debye-Hückel Theory	28
3.	THERMODYNAMICS OF MODEL	31
	A) Evaluation of Free Energy Series	31
	B) Padé Approximants	36
	C) Thermodynamics	41
4.	LEAD FLUORIDE SIMULATION	48
	A) The Molecular Dynamics Technique	48
	B) An Interionic Potential: Fitting of Parameters	51
	C) Tests of Stability	57
5.	MOLECULAR DYNAMICS RESULTS	69
	A) Real Space Analysis	69
	B) $\underline{k}$ Space Analysis	87
6.	CONCLUSIONS	100
	REFERENCES	107

PART II:

A NUCLEAR QUADRUPOLE INTERACTION IN ORDERED MAGNETS

		Page No.
1.	INTRODUCTION	111
2.	THE THEORY OF THE PSEUDOQUADRUPOLE EFFECT	115
	A) The Origin of the Effect	115
	B) Localised Magnets	119
	C) Itinerant Magnets	122
	D) Impurities	124
3.	THE MAGNITUDE OF THE PSEUDOQUADRUPOLE EFFECT	128
	A) The Localised Model	128
	B) Behaviour Near Criticality	136
	C) The Itinerant Model	140
4.	QUADRUPOLE EFFECTS IN $GdAl_2$	157
	A) Experimental Results	157
	B) The Pseudoquadrupole Effect	159
	C) Other Mechanisms Consistent with Experiment	162
5.	CONCLUSIONS	166
	REFERENCES	169

PART I

DISORDER IN FASTIONICS

CHAPTER 1

INTRODUCTION

Fastionic conductors are ionic solids which are known to show considerable disorder at high temperatures, the range of these temperatures varying considerably between fastionics. This disorder consists of ions moving off their regular sites and being distributed randomly on interstitial sites or close to regular sites. In part I of this thesis we study this disorder using techniques adapted from theories of liquids. We also look at the disorder in a specific case, lead fluoride, with a molecular dynamics simulation and make conclusions which are relevant to other fastionics particularly those of the fluorite structure.

The class of materials known variously as fastionic conductors, superionic conductors, or solid electrolytes has had so much interest focussed on it in the last few years that there is now a journal devoted entirely to the subject - 'Solid State Ionics' (published by North Holland Publishing Co.). These substances are characterised by the following properties: they are solid but have conductivities similar to those of electrolytes, the high conductivity is due to disorder in one or more component sublattices, and they are ionic thus little of the conductivity is due to electrons. Excellent reviews of the whole area of fastionics have appeared recently, these include Hayes (1978), Hooper (1978), Boyce and Huberman (1979) and Salamon (1979).

Research into fastionics started because of their technological interest for instance as potential materials for

solid state batteries - for a review see Holzapfel and Sickert (1975), there is also more recently an article by Steele (1978). However, it was quickly seen that they are of great scientific interest because of the way in which they combine ordered and disordered states.

Experimentally the disorder has been seen in a wide range of different types of measurement which are reviewed for fastionics by Hayes (1978). The measurements of particular interest to us are of dc conductivities, specific heats, X-ray diffraction and neutron diffraction.

The dc conductivity of a typical fastionic will show characteristic behaviour if $\log(\sigma)$ is plotted against $^{1000}/_{T}$. Figure 1 taken from Boyce and Huberman (1979) gives examples of this plot for different types of fastionic. This method of plotting, related to an Arrhenius plot gives a straight line from whose gradient the activation energy of the mobile species may be obtained. Fastionics show a noticeable change in slope over a narrow range of temperature (in some cases several changes of slope) indicating an apparent drop in the activation energy. It is over this range of temperature that the transition to fastionic behaviour appears to occur. Sometimes, as for silver iodide, the transition is sharp and is accompanied by a structural phase transition and in other cases, notably the fluorites, the transition is much more diffuse. Nevertheless all fastionics have associated with them a transition temperature T_s which indicates the onset of the high conductivity regime.

Fig. 1

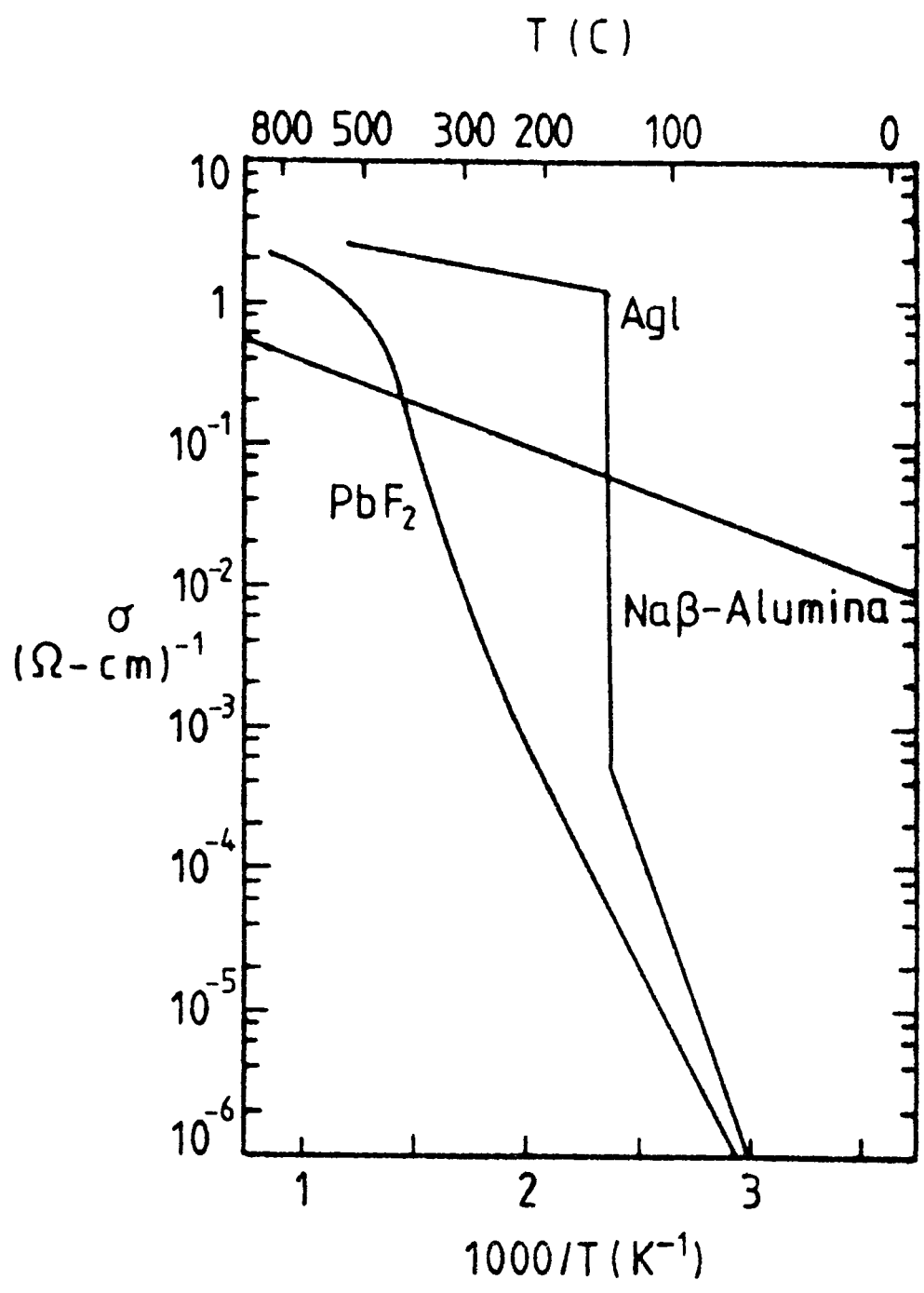

Conductivities of AgI, PbF_2 and $Na\beta Al_2O_3$ showing different types of behaviour on going from the low conductivity to the fastionic state.

The fact that there appears to be a transition to a new state is confirmed by specific heat anomalies at temperatures well below the melting temperature which correspond to the temperatures T_s in different fastionics. This phenomenon is generally assumed to be associated with the development of extensive disorder in a component sublattice, and the disorder is then associated with the high conductivity.

Such a specific heat anomaly is present in fluorite fastionics where the enthalpies were found to be 0.1 eV. Given the assumption that the defect energy does not fall below about 1 eV this indicates that for the fluorites there is an order-disorder transition, but in the disordered state there is only of the order of 10% of defects (Catlow et al 1978). It is known (Lidiard 1974) that for fluorites at low temperatures, defects are anion Frenkel pairs and it is assumed that the Frenkel pairs are also responsible for the fastionic disorder (this assumption is confirmed by molecular dynamics eg. Dixon and Gillan (1980)). The cation sublattice is not disordered (Dixon and Gillan 1980). Catlow et al (1978) conclude that the Coulomb interaction between the Frenkel defects plays a major role in the co-operative mechanism which gives rise to fastionic behaviour. Also the influence of Coulomb interactions on the fastionic transition in fluorites has been recently examined by March et al (1980) who demonstrate an empirical correlation between the transition temperature and the static lattice Frenkel energy and suggest that it could be explained by using Debye-Hückel theory following work by Kurosawa (1957).

In this thesis we look at the likelihood of Coulomb interactions being responsible for the fastionic behaviour by setting up a lattice gas model for Frenkel defects which we treat as charged mobile particles confined to a lattice. The particles in our model have only two interactions, an on site exclusion property and the Coulomb interaction. There are equal numbers of positively and negatively charged particles.

We look at the thermodynamics of this model to see whether it will predict a phase transition or diffuse transition and at what concentrations, and which temperatures. We do this by calculating the free energy of the particles in our model by applying methods more commonly used in theories of liquids. The approach is to start from the Debye-Hückel theory of electrolytes which was first applied to ionic conductors by Lidiard (1957). However as we will show, Debye-Hückel theory is not applicable to the defect concentrations found in the fluorites. We therefore use classical diagrammatic theory of the type first introduced by Mayer (1940) for imperfect gases and modified by Morita and Hiroike (1961), Stell (1964) and others to cope with the concentrations of particles found in liquids and with the long range Coulomb interaction. Application of this modified theory, known as cluster expansion theory to the case of our lattice gas model gives us an expansion for the free energy of our lattice gas due to the Coulomb interactions in increasing order of the electronic charge e. We then apply the theory of Padé approximants to obtain an expansion which is correct for both small and large concentrations and is thus an

interpolation between the two limits. The expression is then applied to establish the thermodynamics.(Alnatt and Cohen (1964) look at the free energy of charged defects on a lattice but do not apply Padé approximant theory nor are they interested in the same thermodynamics).

Neutron diffraction measurements (Dickens et al 1980) suggest that the defect concentration in lead fluoride is an order of magnitude larger than for other fluorites notably strontium chloride. As indicated the Coulomb interactions are considered to play an important role in fluorite fastionics. We tackle another aspect of this problem by looking at lead fluoride which has a very much larger static dielectric constant than the other fluorites to see whether it shows qualitatively different behaviour. Physically, this is because the interactions between defects will be affected by how much their charges are screened by the rest of the lattice and that is determined in a simple theory by the dielectric constant.

Thus a molecular dynamics simulation of this material might show up whether the disorder is of a different kind from that observed in CaF_2 (Dixon and Gillan 1978) and $SrCl_2$ (Gillan and Dixon (1980), (Dixon and Gillan 1980)). As the simulation programs already exist for the other fluorites and could be easily adapted to look at lead fluoride, it was quite feasible to look at this material in this way. This thesis describes how we found an interionic potential for lead fluoride to use in the simulation programs and discusses the results we obtained from the simulation. (The lead fluoride structure is shown in Figure 2. Anions occupy sites on a simple cubic lattice. Cation sites are at the centres of alternate cubes, the remaining cube centre sites are termed empty cube centre sites).

Fig. 2

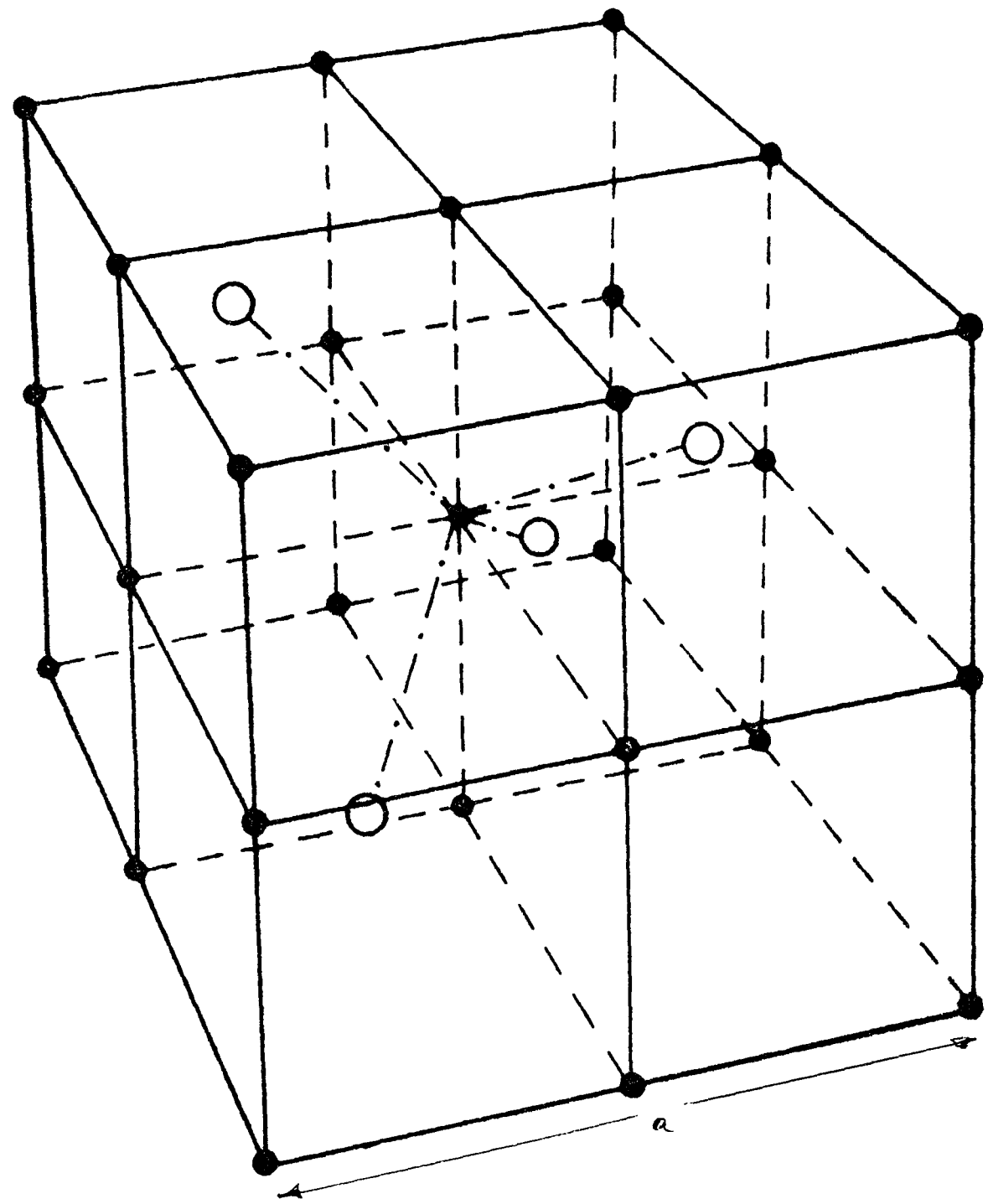

Lead fluoride structure

White circles represent cations (Pb^{2+})
Black circles represent anions (F^-).

In the simulation we tried a method of analysis that has not hitherto been used in a molecular dynamics simulation to our knowledge. The method looks at the simulation results in momentum space and shows how a distribution of defects may be obtained by fitting various models to the simulation results. We adopted this method as it is exactly how the defect concentrations from neturon scattering are obtained so it affords a comparison between simulation results and experiment that is much more direct than the comparisons used before.

Finally, the material is organised as follows: Chapters 2 and 3 describe the lattice gas model, the theory we used on it and the results we obtained. Chapters 4 and 5 contain a description of the molecular dynamics technique, the interionic potential that we found for lead fluoride and the results of the lead fluoride simulation. Chapter 6 contains our conclusions.

CHAPTER 2

CLUSTER EXPANSION THEORY

2A. Preliminary: The Model

Our model is intended to represent defects in a fluorite. As discussed in the introduction, one of the chief characteristics of fluorites is that the disorder is confined to a single sublattice, and it is intrinsic, involving mostly Frenkel defects. Thus we may consider half the defects as positively charged and half as negatively charged where the charges are equal in magnitude.

Furthermore, molecular dynamics simulations of $SrCl_2$ (Dixon and Gillan (1980)) have shown that here the motion of the defects is that of hopping rather than a liquid like diffusion. We model this behaviour by assuming that the defects are confined to sites on a simple cubic lattice, corresponding to the anion sublattice in the fluorites (since here it is the anions which disorder). We choose these sites because the molecular dynamics work on the fluorites has shown that the disorder can be represented by particles hopping between lattice sites and there is little evidence of stable interstitial sites. There is more discussion of this point in Chapter 5.

If we consider defects in a fastionic, it is clear that the probability of two defects of like charge being at the same lattice site is very low, from their strong repulsion and finite volumes. Furthermore, two defects of opposite charge represent a vacancy and an interstitial which would annihilate if they were at the same site. Thus effectively no config-

urations with two defects at the same site will be seen in a genuine fastionic. This can be modelled by giving the defects a 'hard core' by placing the condition in the model that no two defects are found at the same site.*

As we want to find the influence of Coulomb interactions on the order-disorder transition the only interaction in our model apart from the 'hard core' restriction will be the Coulomb potential

$$V(r) = \frac{Ze}{4\pi\epsilon_0\epsilon_r r} \qquad (2.1)$$

Here Z is the charge on the defect which we take as $\pm$ 1 (since fluorite anions are singly charged), e the electronic charge, ϵ_r the relative dielectric constant and r the distance between 2 defects. The effect of all the ions which are not defects, including cations, on the defect interactions is modelled by the dielectric constant. This we take as the macroscopic static dielectric constant.

To sum up, our model to represent the influence of Coulomb interactions on the order disorder transition in fluorite fastionics consists of: a lattice gas of defects of equal charges, half positive, half negative interacting with Coulomb forces only and with the restriction that no two defects can sit at the same site.

We wish to find out whether such a system would show a sharp change in the particle (ie. defect) concentration at some transition temperature T_s and at what concentration this transition would take place.

* We call this 'the excluded site property'

The number of each species of particles per site ν is governed by the chemical potential μ :

$$\mu = \frac{1}{N} \left. \frac{\partial F}{\partial \nu} \right|_{N,T} \qquad (2.2)$$

Here N is the number of lattice sites, F is the free energy. A system held at a fixed temperature and volume will minimise its free energy so that $\nu(T)$ is given by

$$\mu = 0 \qquad (2.3)$$

μ contains a constant term which is the Frenkel energy E_o. Thus lines for different E_o's on a plot of $\ln \nu$ against $^1/T$ will give the behaviour of the system for different Frenkel energies and if the sytem does show a phase transition, will indicate the critical values of T, ν and E_o. The Frenkel energy is treated by us as an experimental parameter which together with the dielectric constant ϵ_r and the lattice constant a will differentiate in its predictions between fluorites (and any other materials to which this model may apply).

Thus it is necessary to find an expression for the free energy in terms of the defect concentration. We may use diagrammatic perturbation theory to achieve this, following its application to liquids by Stell and others. This gives us an expansion for the free energy due to Coulomb interactions in increasing order of the electronic charge e. Our zeroth order term comes from Debye-Hückel theory which is only valid in the limit of very dilute defect concentrations, said to be those of charged ions in tap water. For fluorites we show in Chapter 3 section B that this limit does not apply.

However, we can use the Padé approximant technique successfully applied by Stell and Wu (1975) to a system of charged spheres. This technique is a method of interpolation between the low and high concentration limits so that our expression for the free energy should be valid even at the concentrations encountered in fastionics.

2B. Diagram Theory

As mentioned in the preliminary, we need to calculate the free energy of our system of charged mobile defects with the excluded site property. We split the free energy into two constituents, one, F_o being that of a lattice gas whose only interaction is that of site exclusion, the other, F_c, the contribution from Coulomb interactions. In this chapter we show how to find a diagrammatic series for F_c in increasing order of electronic charge to order e^6. Our zeroth order term is the free energy of charged particles in a continuum calculated using Debye-Hückel (D-H) theory. We describe how the discrete nature of our system can be taken into account through terms of increasing order in e and how charge fluctuations ignored by D-H theory can be included.

We commence by obtaining a diagrammatic series in continuum theory for the grand canonical partition function $\underline{\underline{\Xi}}$ from which the free energy series may be obtained. The free energy series is then modified to allow for the discrete nature of our lattice gas. We believe that the continuum theory we use should be valid for the discrete case but we present it as continuum theory since the methods are standard and have been described by Hansen and McDonald (1976).

Ξ may be written as follows:

$$\Xi = \sum_{N=0}^{\infty} \frac{(e^{\beta\mu})^N}{N!\, h^{3N}} \iint e^{-\beta H(\underline{r}_1 \cdots \underline{r}_N,\ \underline{p}_1 \cdots \underline{p}_N)} \, d\underline{r}_1 \cdots d\underline{r}_N \, d\underline{p}_1 \cdots d\underline{p}_N \tag{2.4}$$

$$= \sum_{N=0}^{\infty} \frac{1}{N!} \int \prod_{i=1}^{N} z^*(i) \prod_{i<j}^{N} e(ij)\, d\underline{r}_1 \cdots d\underline{r}_N \tag{2.4a}$$

where

$$H = \sum_{i=1}^{N} \frac{p_i^2}{2m} + \sum_{i=1}^{N} \phi(i) + \sum_{i<j}^{N} \sum v(ij) \tag{2.5}$$

$$e(ij) = \exp\left(-\beta v(|\underline{r}_i - \underline{r}_j|)\right) \tag{2.6}$$

$$z^*(i) = z \exp\left(-\beta \phi(\underline{r}_i)\right) \tag{2.7}$$

$$z = \frac{\exp(\beta\mu)}{(2m^*/h^2\beta)^{3/2}} \equiv \frac{\exp(\beta\mu)}{\lambda^3}, \quad \beta = \frac{1}{k_B T} \tag{2.8}$$

(k_B = Boltzmanns Constant, $\underline{r}_i$, $\underline{p}_i$ are position and momentum respectively of particle i)

We are assuming that the potential in our system is a central pair potential $v(|\underline{r}_i - \underline{r}_j|)$ and that there is an external field $\phi(\underline{r}_i)$ so that the technique of functional differentiation may be applied (later ϕ is set equal to zero). Following Mayer and Mayer (1940) we write

$$f(ij) = e(ij) - 1 \tag{2.9}$$

Since $f(i\ j) \to 0$ as $|\underline{r}_i - \underline{r}_j| \to \infty$ for all physically reasonable potentials, $f(i\ j)$ is small for most of the range of integration of $\underline{r}_i$ and $\underline{r}_j$. Thus Ξ becomes

$$\Xi = \sum_{N=0}^{\infty} \frac{1}{N!} \int \pi\, z^*(i) \sum \prod_{i<j} f(ij)\, d\underline{r}_1 \cdots d\underline{r}_N \tag{2.10}$$

where the unlabelled sum is taken over all terms resulting from the expansion of the product of $\prod_{i<j} (f(ij)+1)$. Ξ may be written in terms of diagrams:

$$\Xi = 1 + \left\{\text{the sum of all distinct diagrams consisting of one or more black circles and some or no f bonds}\right\} \tag{2.11}$$

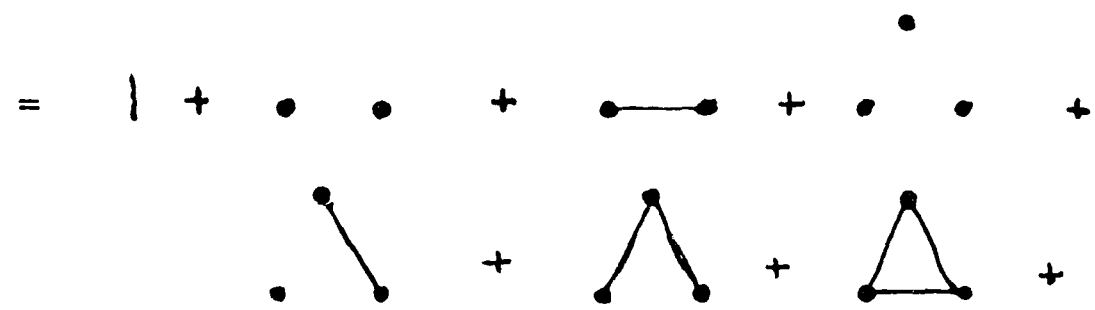

(2.11a)

(Hansen and McDonald 1976). Here 'distinct' implies 'topologically distinct'.

These diagrams represent integrals in our expansion; they contain in this theory the following elements:

(i) Root points represented by white circles which are associated with position variables that appear explicitly

(ii) Field points, represented by black circles, which are associated with functions of dummy variables over which integration has occurred

(iii) Bonds, represented by lines, associated with functions of two variables. We use straight, sawtoothed, dotted etc. lines to differentiate between the functional forms appearing.

The diagrams may be classified according to their topology into three classes

(a) Unlinked diagrams in which the diagram consists of two or more separate parts, the circles of the separate parts being unlinked by bonds - these are disconnected diagrams

eg 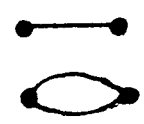

(b) Linked diagrams in which the diagram can be separated into two or more parts by cutting at one

or more circles; the points of separation are called 'articulation points' and the diagrams are termed 'reducible'

eg 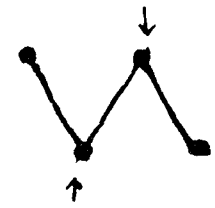

Here the articulation points are marked by arrows.

(c) Linked diagrams in which every circle is multiply connected. By definition the special case of the diagram of a single line between two circles is included in this category. There are no articulation points so that the diagrams are called 'irreducible'.

eg

The diagrams are a means of counting all the integrals in an expansion of a thermodynamic function. This technique allows for the fact that the value of an integral is independent of the way in which particle labels are attached to the dummy variables. We therefore represent the integral by a diagram with unlabelled field points. It is possible to show (see eg. Hansen and McDonald 1976) that the value of an unlabelled diagram is equivalent to the value of the equivalent diagram with arbitrary labels attached to the field points divided by the symmetry number S. S is the number of permutations of labels on a labelled diagram that leave the connectivity unchanged. The arbitrarily labelled diagram can then be written in terms of an integral with a given set of particle labels. In this way we can write down the integrals having allowed for the indistinguishability of the particles, eg. the set of terms in the expansion for the grand partition function $\underline{\underline{\Xi}}$ given by

$$\rho \frac{1}{4!} \int z_1^* z_2^* z_3^* z_4^* f(1,2) f(3,4) d\underline{r}_1 d\underline{r}_2 d\underline{r}_3 d\underline{r}_4$$

where P is the permutation operator acting on the dummy variables, may be represented by

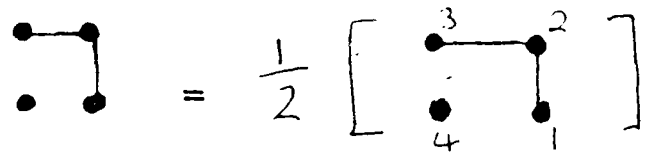

(2.12)

$$= \frac{1}{2} \int z_1^* z_2^* z_3^* z_4^* f(1,2) f(2,3) d\underline{r}_1 d\underline{r}_2 d\underline{r}_3 d\underline{r}_4 \qquad (2.12a)$$

By using the linked cluster theorum and functional differentiation of diagrams, Hansen and McDonald (1976) show that the following expansion may be derived from the expansion (2.11) for Ξ :

$\log(f_z) =$ {the sum of all distinct irreducible diagrams consisting of one white circle (associated with the function unity), and one or more black circles (associated with ρ) and f bonds}

(2.13)

Here ρ is the particle density and z the fugacity (defined in (2.8)):

$$\log z = \beta\mu + \log(\lambda^3) \qquad (2.14)$$

The chemical potential of a perfect gas (Hansen and McDonald 1976) is

$$\mu_{\rho_G} = (\log(\rho\lambda^3))/\beta \qquad (2.15)$$

Thus

$$\log(f_z) = \beta(\mu - \mu_{\rho_G}) \qquad (2.16)$$

Using the technique of functional differentiation,

$$\beta(\mu - \mu_{pg}) = \frac{\beta}{V}\frac{\partial}{\partial \rho}\left(F - F_{pg}\right)\Big|_{V,T} \tag{2.17}$$

$$= \beta \int dr \left[\frac{\delta}{\delta \rho(r)}\left(F - F_{pg}\right)\right]_{V,T}\Big|_{\rho = \text{const}} \tag{2.17a}$$

$$= \beta \frac{\delta}{\delta \rho}\left(F - F_{pg}\right)\Big|_{\rho = \text{const}} \tag{2.17b}$$

(where V is the volume of our system)

Here F is the total free energy of our system, F_{pg} the free energy of a perfect gas. The condition ρ = constant applies to our model since we are only interested in a homogeneous system. It is possible to apply the technique of functional differentiation to a series of diagrams (Hansen and McDonald 1976). It is also possible to show that there is only one series whose functional derivative is the series on the right of equation (2.13) and that hence

$$A \equiv -\frac{\beta(F - F_{pg})}{V} \tag{2.18}$$

$$= \frac{1}{V}\{\text{sum of all simple irreducible diagrams with two or more field points (ρ points) and no more than a single bond connecting any pair of field points}\} \tag{2.18a}$$

$$= \quad f \quad + \quad \triangle \quad + \cdots \qquad \rho \quad \rho \tag{2.18b}$$

We now modify the theory to cope with the discrete nature of our lattice gas. Our method is to introduce a new type of field point, represented in diagrams by the symbol ■ and

defined as multiplication by ρ_α, the density of particles of species α and summation over all lattice sites $\underline{R}_i$ multiplied also by a dimensional factor of the volume per lattice site (= $1/a^3$ for a simple cubic lattice where a is the lattice constant). This is analogous to the field points (•) used above which represent dummy variables that are integrated over all space. We also introduce a new root point, whose symbol is □ and is defined as being associated with a lattice site $\underline{R}_i$.

Then our expression for A (2.18b) is modified to

A = 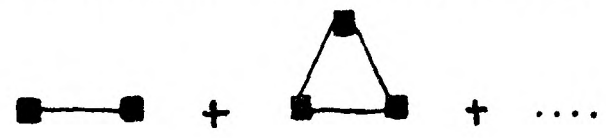 (2.19)

but the statement of the expansion, (2.18a) still holds.

Our next step is to separate out the influence of the Conlomb interactions by the standard technique of decomposing the f bonds into f° bonds and γ bonds (defined below) as the γ bonds are very much easier to treat when evaluating the diagrams:

$$f_{\alpha\beta} = f^\circ_{\alpha\beta} + (1+f^\circ_{\alpha\beta}) \sum_{n=1}^{\infty} \frac{1}{n!} (\gamma_{\alpha\beta})^n \qquad (2.20)$$

$$f^\circ_{\alpha\beta} = e^{-\beta u^\circ_{\alpha\beta}} - 1 \qquad (2.21)$$

$$\gamma_{\alpha\beta} = -\beta u^c_{\alpha\beta} \qquad (2.22)$$

$$= \frac{z_\alpha z_\beta e^2}{4\pi \epsilon_0 \epsilon_r k_B T} \left\{ \frac{1}{|\underline{R}|} \left[1 - \delta_{\underline{R},0} \right] + c\,\delta_{R,0} \right\} \qquad (2.23)$$

($v_{\alpha\beta}(|\underline{r}_i - \underline{r}_j|) = u^\circ_{\alpha\beta} + u^c_{\alpha\beta}$ where $u^c_{\alpha\beta}$ = potential for particles with excluded site property only)

The subscripts α, β refer to the species of the particles and $\underline{R}$ is a lattice vector. The other variables in (2.23) are defined after (2.1). Because of the excluded site property our final result should be independent of c and we shall show in section A of Chapter 3 that this is the case, at least to the order we take our expansion.

The result of our decomposition is:

$$A = \frac{1}{V} \times \left\{ \begin{array}{l} \text{sum of all irreducible diagrams containing} \\ \text{two or more field points, at most one } f^{o} \\ \text{bond and any number of } \gamma \text{ bonds connecting} \\ \text{any pair of field points} \end{array} \right\} \tag{2.24}$$

We can considerably reduce the number of diagrams in the expansion (2.24) by taking advantage of the technique of topological reduction which is explained by Andersen (1977). The basic idea is as follows: In certain cases it is possible to resum a series of diagrams $\mathcal{S}$ in such a way that a new bond may be introduced. This new bond can itself be represented by a series of diagrams, each of which has two root points and bonds of the type appearing in the series $\mathcal{S}$. By summing certain series of diagrams in $\mathcal{S}$ we are able to replace each series by a single diagram containing the new bond (in addition to other bonds). Thus we achieve the reduction in diagrams mentioned above.

In this case we resum the series for A, equation (2.24) such that we replace series of diagrams containing f^{o} bonds (and γ bonds) by diagrams containing h^{o} bonds (and γ bonds). h^{o} is by definition the total correlation function for our lattice gas if Coulomb interactions are excluded; thus it is the correlation function of a lattice gas with the site exclusion property as the only interaction. The total correlation function for a discrete system is given by

$$h^{o}_{\alpha\beta}(\underline{R}_1, \underline{R}_2) = g^{o}_{\alpha\beta}(\underline{R}_1, \underline{R}_2) - 1 \tag{2.25}$$

Here $\nu_\alpha \nu_\beta \, g^c_{\alpha\beta}(\underline{R}_1, \underline{R}_2)$ is the probability that site $\underline{R}_1$ is occupied by a particle of species α and site $\underline{R}_2$ is occupied by a particle of species β. It is easy to show that

$$h^o(\underline{R}_1, \underline{R}_2) = -\delta(\underline{R}_1, \underline{R}_2) \qquad (2.25a)$$

($\delta(\underline{R}_1, \underline{R}_2)$ is the Kronecker delta function)

Assuming as before that the basic results of diagram theory are as valid for the discrete case as for the continuum case, we modify an expansion by Hansen and McDonald (1976) for the total correlation function of particles with hard core repulsion and no other interaction (the continuum equivalent of h^o) to give

$h^o_{\alpha\beta}$ = {sum of all irreducible diagrams containing two root points, any number of field (ρ) points and at most one f^o bond, but no φ bonds, between any pair of points} (2.26)

= 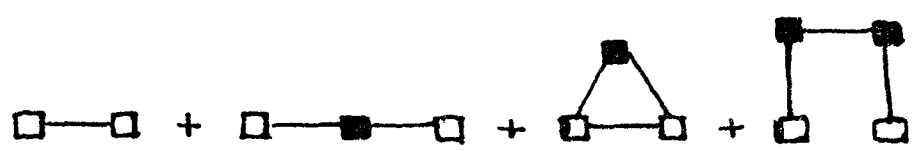 (2.26a)

We then express the diagrammatic series for A, (2.23), in terms of $h^o_{\alpha\beta}$ to give

$$A = A^o + \frac{1}{V} \times \{\text{sum of all irreducible diagrams containing two or more field points at most one } h^o \text{ bond and any number of } \varphi \text{ bonds connecting any pair of points. In addition the diagram contains at least one } \varphi \text{ bond and is free of 'articulation pairs'}\} \qquad (2.27)$$

(Hansen and McDonald 1976). Here an 'articulation pair' has the meaning of: a pair of field points whose removal causes the diagram to become disconnected and one of the disconnected points contains at least one field point and no φ bonds. (The term is somewhat more specialised in its definition than 'articulation point' which we have already defined). $\checkmark A^{o}_{/\beta}$ is the free energy of the lattice gas without Conlomb interactions (but with the excluded site property). We could write down a diagrammatic series for A^{o} but it is much easier to evaluate without the use of diagrams as we will show in Chapter 3, section C. Thus we are interested simply in A^{c}, related to the free energy from the Coulomb interactions in the lattice gas F_c by

$$A^{c} = A - A^{o} \qquad (2.28)$$

$$= \beta F_c / V \qquad (2.28a)$$

A^{c} (given by (2.27) and (2.28)) contains diagrams which diverge. This is because the Coulomb potential $\varphi(\underline{R})$ is summed over all lattice sites at each field point. We can however remove these divergencies with the aid of topological reduction. The method is to renormalise the $\varphi(\underline{R})$ bonds by summing the series of chain bonds:

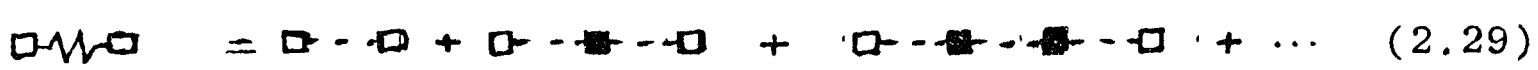

$$= \hat{\varphi}_D(\underline{R} - \underline{R}') \qquad (2.29a)$$

where □-□ = $\varphi_{\alpha\Delta}(\underline{r}-\underline{r}')$

In a continuum context, this method was first used by Mayer (1950) for ionic solutions. Here the analogous bond

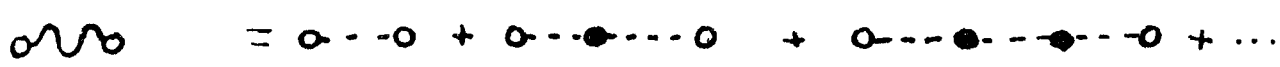

where ○-○ = $\varphi^{c}(\underline{r}-\underline{r}')$ defined in (2.34) below

is summed to give the following:

$$\varphi_{\alpha\beta}(\underline{r}-\underline{r}') + \sum_{\gamma} \int d\underline{r}_1 \, \varphi_{\alpha\gamma}(\underline{r}-\underline{r}_1)\,\varphi_{\gamma\beta}(\underline{r}_1-\underline{r}')\,\rho_\gamma + \sum_{\gamma,\delta} \int d\underline{r}_1\, d\underline{r}_2 \, \varphi_{\alpha\gamma}(\underline{r}-\underline{r}_1)\,\varphi_{\gamma\delta}(\underline{r}_1-\underline{r}_2)\,\varphi_{\delta\beta}(\underline{r}_2-\underline{r}')\,\rho_\gamma\rho_\delta$$

$$+ \text{etc.} \tag{2.31}$$

$$= \frac{z_\alpha z_\beta e^2}{4\pi\epsilon_0\epsilon k_B T} \frac{e^{-k|\underline{r}-\underline{r}'|}}{|\underline{r}-\underline{r}'|} \tag{2.32}$$

$$\equiv \hat{\varphi}_c(\underline{r}-\underline{r}') \tag{2.32a}$$

where $k^2 = \sum_\alpha \frac{\rho_\alpha z_\alpha^2 e^2}{k_B T \epsilon_0 \epsilon}$ (2.33)

and $\varphi^c(\underline{r}-\underline{r}') = \frac{-z_\alpha z_\beta}{4\pi\epsilon_0\epsilon k_B T} \times \frac{1}{|\underline{r}-\underline{r}'|}$ (2.34)

(Andersen 1977). k^{-1} is the Debye-Hückel screening length.

Unfortunately it is not possible to obtain a closed form for $\hat{\varphi}_D(\underline{r}-\underline{r}')$ (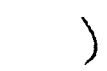) as we have done for $\hat{\varphi}_c(\underline{r}-\underline{r}')$ ( ). We can however write it as an expansion about the limit where the lattice spacing goes to zero and the lattice becomes a continuum. We do this by introducing the field point ▲ where

(2.35)

Thus

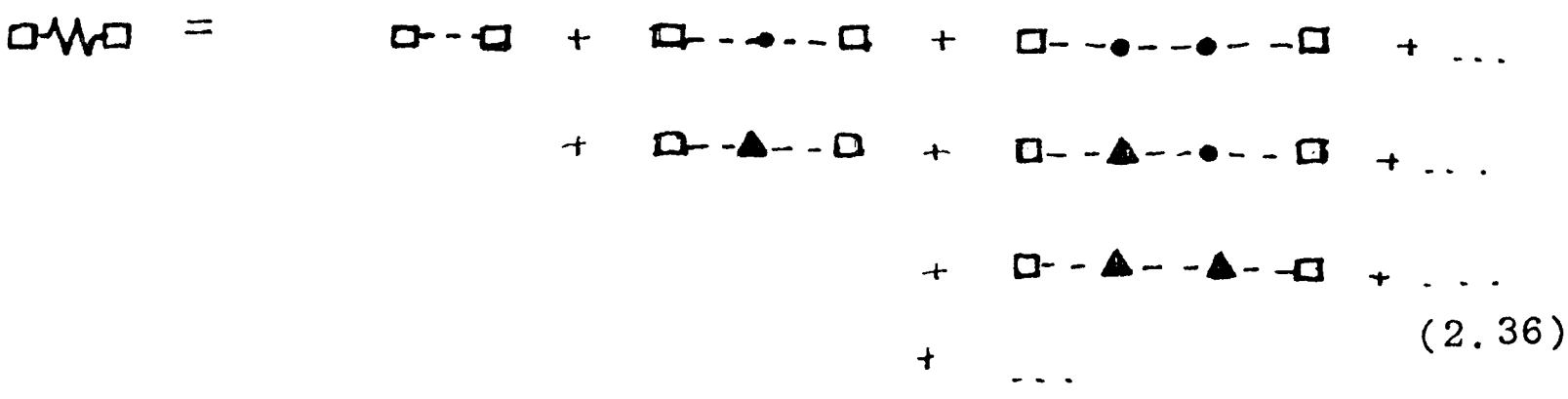

(2.36)

By resumming the diagrams in (2.36) in terms of the continuous renormalised Conlomb bond $\hat{\varphi}(\underline{r}-\underline{r}')$( )we find that

(2.37)

Here $\hat{\varphi}_c(\underline{R}-\underline{R}') \equiv$ 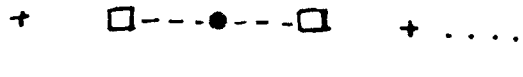 (2.38)

We can sum all the terms in (2.38) barring because for these terms, all the φ's are functions of continuous variables and are therefore given by (2.34). Thus, from (2.32a),

$$= \frac{-Z_\alpha Z_\beta}{4\pi\epsilon_0\epsilon K_B T}\left[\frac{e^{-K|\underline{R}-\underline{R}'|}-1}{|\underline{R}-\underline{R}'|}\right] \tag{2.39}$$

Then from equation (2.23)

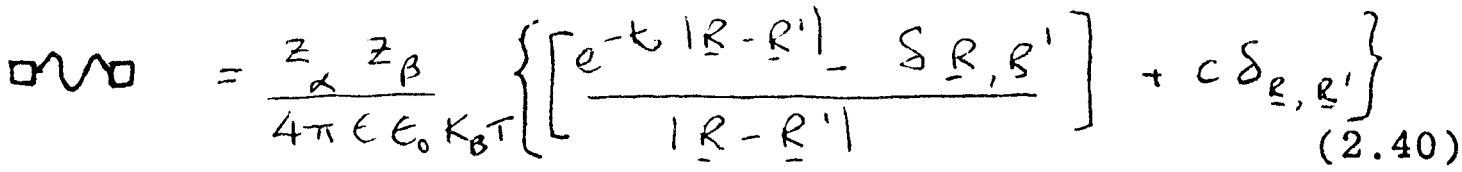

$$= \frac{Z_\alpha Z_\beta}{4\pi\epsilon\epsilon_0 K_B T}\left\{\left[\frac{e^{-K|\underline{R}-\underline{R}'|}-\delta_{\underline{R},\underline{R}'}}{|\underline{R}-\underline{R}'|}\right] + C\delta_{\underline{R},\underline{R}'}\right\} \tag{2.40}$$

$\hat{\varphi}_c(\underline{r}-\underline{R}')$ is given by

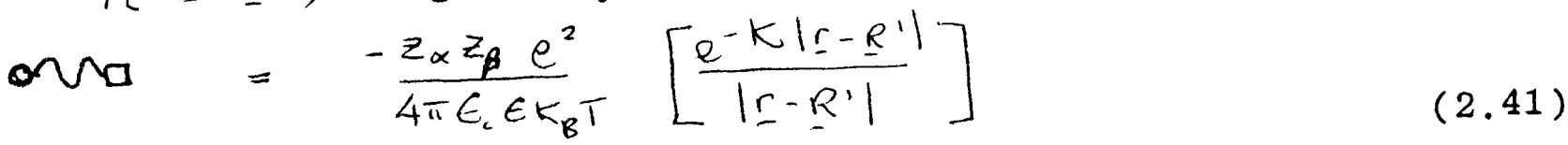

$$= \frac{-Z_\alpha Z_\beta e^2}{4\pi\epsilon_0\epsilon K_B T}\left[\frac{e^{-K|\underline{r}-\underline{R}'|}}{|\underline{r}-\underline{R}'|}\right] \tag{2.41}$$

since here all the φ's in the constituent chain diagrams are functions of continuous variables. Thus

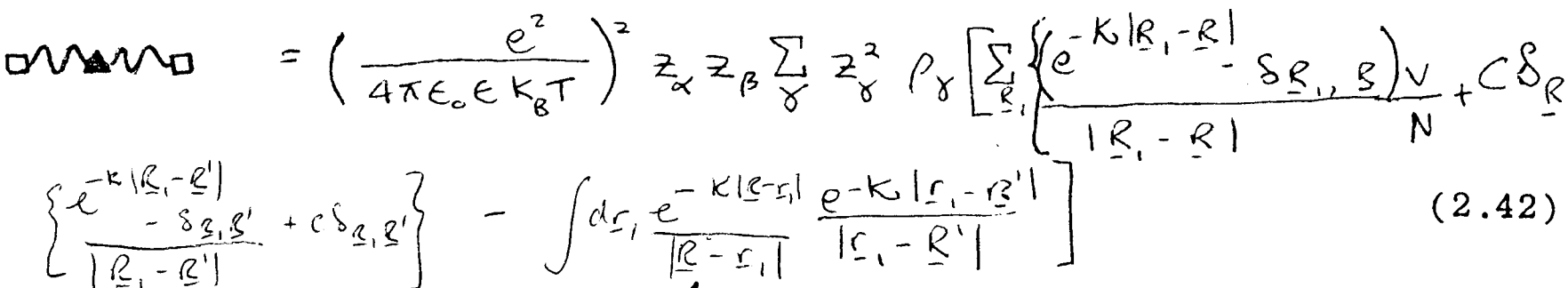

$$= \left(\frac{e^2}{4\pi\epsilon_0\epsilon K_B T}\right)^2 Z_\alpha Z_\beta \sum_\gamma Z_\gamma^2 \rho_\gamma \left[\sum_{\underline{R}_1}\left\{\frac{\left(e^{-K|\underline{R}_1-\underline{R}|}-\delta_{\underline{R}_1,\underline{R}}\right)\frac{V}{N}}{|\underline{R}_1-\underline{R}|} + C\delta_{\underline{R}_1,\underline{R}}\frac{V}{N}\right\}\times\right.$$

$$\left.\left\{\frac{e^{-K|\underline{R}_1-\underline{R}'|}-\delta_{\underline{R}_1,\underline{R}'}}{|\underline{R}_1-\underline{R}'|} + C\delta_{\underline{R}_1,\underline{R}'}\right\} - \int d\underline{r}_1 \frac{e^{-K|\underline{R}-\underline{r}_1|}}{|\underline{R}-\underline{r}_1|}\frac{e^{-K|\underline{r}_1-\underline{R}'|}}{|\underline{r}_1-\underline{R}'|}\right] \tag{2.42}$$

This term is of order e^4 from the following heuristic argument. The two bonds contribute a factor e^2 each from their definition (2.32a). The field point ▲ does not reduce the

order of the diagram because it gives the difference between the sum over all $\underline{R}_i$ of $e^{-\kappa|\underline{R}_i|}/|\underline{R}_i|$ (excluding the origin) and the integral over all $\underline{r}$ of $e^{-\kappa|\underline{r}|}/|\underline{r}|$. The integral and the sum will separately contribute a factor $1/\kappa \sim 1/e$ (from (2.33)) to the order of the diagram. We know that these factors must cancel when one takes the difference between the integral and the sum. This is because in the limit as $\kappa \to 0$ both $\lim_{\kappa \to 0} \int e^{-\kappa r}/r \, d\underline{r} = \int 1/r \, d\underline{r}$ and $\lim_{\kappa \to 0} \sum_{\underline{R}_i} \frac{e^{-\kappa R_i}}{R_i} = \sum_{\underline{R}_i} \frac{1}{R_i}$ diverge. However the difference $\sum 1/R - \int dr/r$ does not diverge as we shall argue in section C. Therefore in the limit as $\kappa \to 0$, the difference between the integral over $e^{-\kappa r}/r$ and the sum over $e^{-\kappa R_i}/R_i$ does not diverge and thus ▲ can not contribute any terms varying inversely with κ and hence inversely with e.

It follows that (2.37) is an expansion in increasing order of e about the bond $\hat{\varphi}_c(\underline{R}-\underline{R}')$ which from its definition (2.38) is of order e^2. Each term in (2.37) is at least of order e^2 greater than the preceeding term.

We now return to the expansion of A_c, equation (2.27) Because of the fact that the unrenormalised bonds φ (- - -) create divergences, we have to renormalise them to $\hat{\varphi}(\underline{R})$ The latter is written as an expansion in terms of $\hat{\varphi}_c$ and the field points (▲). There is an important exception to this, diagrams which consist entirely of rings of φ bonds

ie 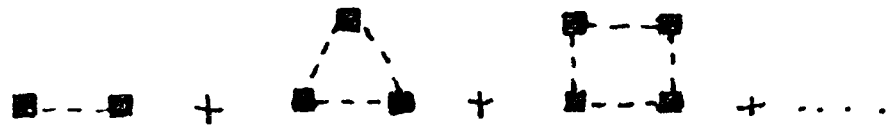

It can be shown (see Andersen 1977) that it is not possible to renormalise the φ bonds in this series which is in fact

the D-H series. The series is further discussed in section B. We therefore consider these diagrams separately from the rest of the diagrams in (2.27). The contents of this paragraph can be turned into a rule for evaluating the diagrams in A_c:

Rule 1 All the coulomb bonds φ in the series for A_c are to be renormalised to become $\hat{\varphi}_D$ bonds which may then be expanded in terms of $\hat{\varphi}_c$ bonds and ▲ field points. D-H diagrams, the ring diagrams, are excepted from this rule. (D-H = Debye Hückel)

Another rule is obtained from the charge symmetry of the system namely the fact that

$$\sum_{\alpha} z_{\alpha} \rho_{\alpha} = 0 \qquad (2.43)$$

The result of (2.43) is

Rule 2 If there is an odd number of φ bonds incident on a field point, the value of the diagram is zero.

As a result of Rule 1, a typical diagram consists entirely of m x h_o bonds (——), n x $\hat{\varphi}_c$ bonds (∿), p x discrete field points (■) and q x 'difference' field points (▲). From our earlier discussion, the order of the diagram will be at least (e^{2n}) . Thus

Rule 3 The order of a diagram with n $\hat{\varphi}_c$ bonds is at least e^{2n}

Finally we show how to sum all the diagrams with up to three $\hat{\varphi}$ bonds and any number of h^o bonds by taking advantage

of the simple definition of h_o ($= -\delta(\underline{r}_1, \underline{r}_2)$), equation (2.25a). Diagrams with only one $\hat{\varphi}_c$ bond have zero value (Rule 2). The only allowed diagram with two $\hat{\varphi}_c$ bonds and any number of h^o bonds is as all the rest contain articulation pairs.

Diagrams with three $\hat{\varphi}_c$ bonds can be represented as:

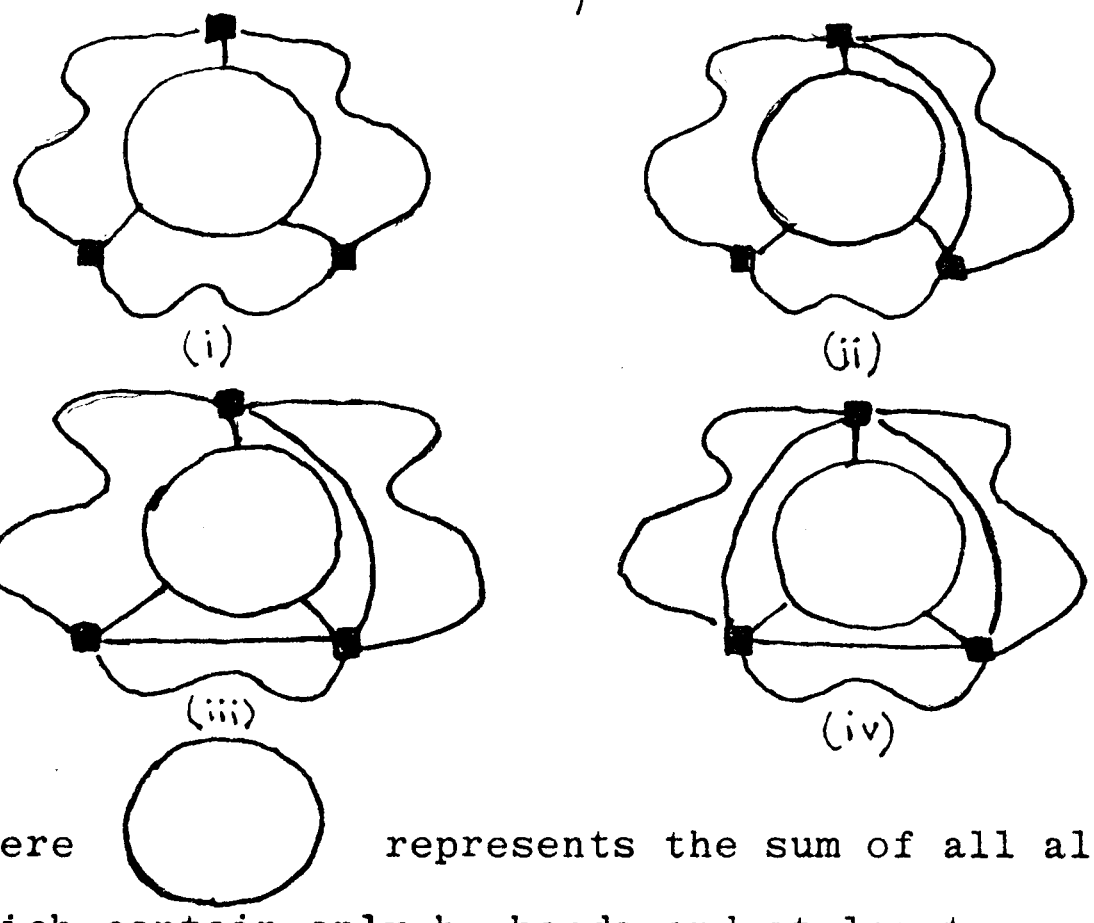

where represents the sum of all allowed diagrams which contain only h_o bonds and at least one field point ■ . Diagrams (i) and (iv) above have the same symmetry number and it is easy to show from (2.25a) that they have the same value but are of opposite sign. Therefore they cancel as do (ii) and (iii) by the same argument. Therefore the only diagrams with three renormalised Coulomb bonds and any number of h^o bonds that give a net contribution to our series are

$D_1 =$ 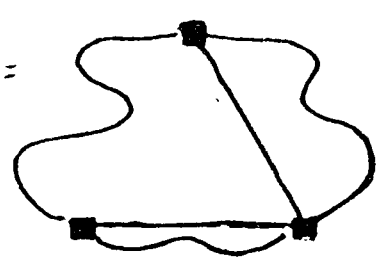 and $D_2 =$ 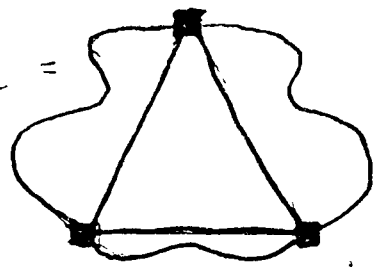 (2.43a)

These diagrams give only terms at $\underline{R} = \underline{R}' = 0$ and these cancel with all terms at $\underline{R} = \underline{R}' = 0$ in the D-H diagram (3.15), or give terms of higher order than κ^6.

We can also show that all diagrams in our series with ▲ points and those with more than three φ_c bonds are of higher order than e^6. Then we are left with the following diagrams in our expansion:

(a) The D-H series diagrams evaluated to order e^6. We show how to deal with these diagrams in section C.

(b) The diagram 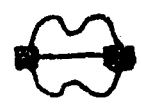 . This will be evaluated along with the renormalised D-H diagrams in Section A of Chapter 3.

2C. Debye-Hückel Theory

We have indicated in section B that the D-H diagrams

$A^{Discr}_{(D-H)} =$ 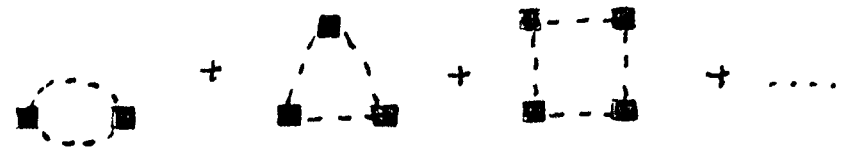 (2.44)

have to be considered separately because of their special structure. This series of ring diagrams has a physical significance in that they correspond to a mean field theory for finding the free energy due to Coulomb interactions.

It is readily shown that the series

$A^{Cont}_{(D-H)} =$ 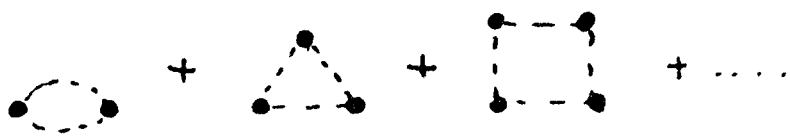 (2.45)

ie. the D-H series in the continuum limit can be summed to give

$$A^{cont}_{(D-H)} = \frac{+k^3}{12\pi} \qquad (2.46)$$

(Résibois 1968). The same result may be obtained without the aid of diagrams Résibois (1968) from the assumption that the

distribution of mobile charges seen by one ion is the same for all ions - here in the mean field assumption. Thus our theory essentially corresponds to expanding the free energy from the Coulomb interactions about the mean field limit.

We have shown in section B that the fluctuations about the mean field, namely all terms in our series for A_c (2.27) that do not come from D-H theory, are (to order e^6) given by the diagram 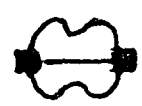 . We now look at the D-H terms and show how to obtain the D-H contribution for a discrete lattice, $A^{Discr}(D\text{-}H)$ The problem we have to solve here is how to find an expression for $A^{Discr}(D\text{-}H)$ given that the contributions from individual diagrams in it diverge because the Coulomb interaction is summed out to infinity at each field point. There is no closed form expression for the series unlike the continuum case so that we have to expand about the continuum limit. We do this in exactly the same way as we did when finding an expansion for the discrete renormalised Coulomb bond ($\hat{\varphi}_D(k)$ = 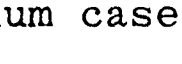)

Thus we introduce the field point ▲ (= ■ - •) and write

$A^{Discr}(D\text{-}H)$ = 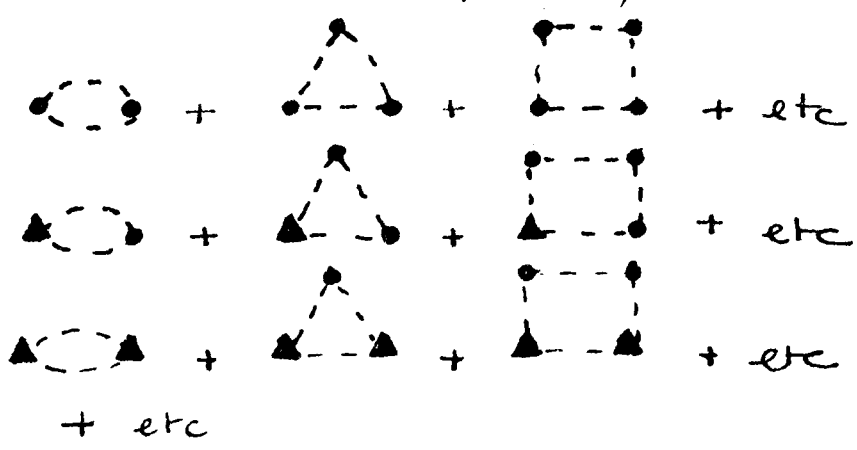

(i)

(ii)

(2.47)

series (i) in (2.47) is simply $A^{cont}(D\text{-}H)$, series (ii) is zero. We can see this by looking at the first term

$$= \sum_{\alpha,\beta} \frac{1}{V} \frac{V}{N} \frac{1}{2} \int \sum_{\underline{k}_0} \frac{1}{|\underline{R}_0 - \underline{r}|^2} d\underline{r} \; \frac{z_\alpha z_\beta}{4\pi\epsilon_0 \epsilon k_B T} \rho_\alpha \rho_\beta$$

$$- \sum_{\alpha,\beta} \frac{1}{V} \frac{V}{N} \frac{1}{2} \int \frac{d\underline{r}\, d\underline{r}'}{|\underline{r} - \underline{r}'|^2} \; \frac{z_\alpha z_\beta}{4\pi\epsilon_0 \epsilon k_B T} \rho_\alpha \rho_\beta \qquad (2.48)$$

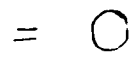

(2.48a)

The factor of ½ comes from $^{1}/_{S}$, $^{V}/_{N}$ from our definition of and the other factors from the definition of $\varphi_{\alpha\beta}(R)$. Similarly all the other terms in (ii) in (2.47) are zero. Diagrams on the righthand side of (2.47) above which contain two or more▲points may be summed to give:

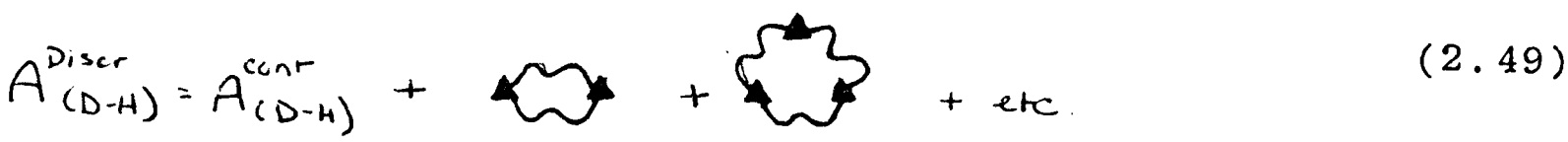

(2.49)

Here ∿∿ is the renormalised continuous Coulomb bond $\hat{\varphi}_c(r)$ defined in equations (2.38), (2.40) and (2.41).

In section A we showed how to evaluate the order of a diagram containing ∿∿ bonds and ▲ points and argued that the ▲ points do not reduce the order of the diagram but each ∿∿ bond contributed a factor e^2 to the value of the diagram. Then a ring diagram with n ▲ points and n ∿∿ bonds will be at least of order $(e^2)^n$. Thus (2.49) is an expansion of increasing order in e. To order (e^6), then

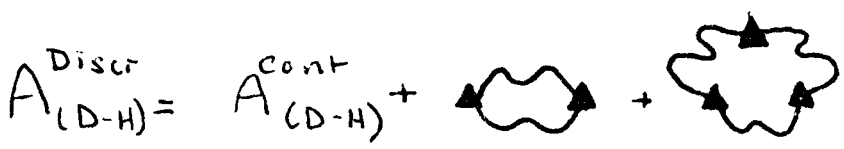

(2.50)

Thus our series A_c for the free energy consists of the following terms

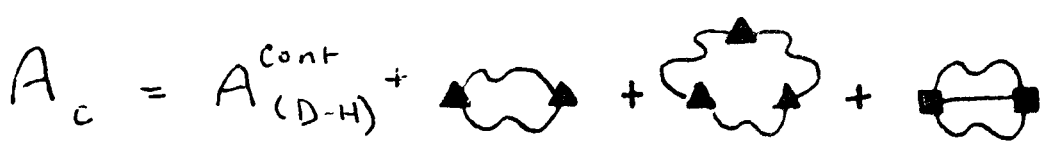

(2.51)

In section A of Chapter 3 we show how to find the values of these diagrams.

CHAPTER 3

THERMODYNAMICS OF MODEL

3A. Evaluation of Free Energy Series

We have shown in Chapter 2 that in order to find the free energy A_c as an expansion in e to order e^6, we need to evaluate the three diagrams

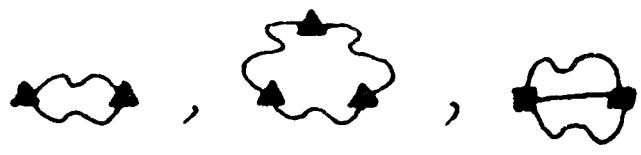

First we look at the diagram

Using the definition of the discrete field point, (after equation (2.18)), the renormalised Coulomb bond $\hat{\varphi}_c(\underline{r})$, equation (2.32) and the total correlation function h_o, equation (2.25a), we can write down the value of this diagram as

$$= -\frac{1}{V}\frac{1}{4}\sum_{\alpha,\beta}(-1)^2\frac{z_\alpha^2 z_\beta^2 \rho_\alpha \rho_\beta}{(4\pi\epsilon\epsilon_0)^2(k_B T)^2} \times \tag{3.1}$$

$$\times \frac{V^2}{N^2}\sum_{\underline{R}^1\underline{R}^2}\left[\frac{e^{-\kappa|\underline{R}_1-\underline{R}_2|}}{|\underline{R}_1-\underline{R}_2|}-\delta_{\underline{R}_1\underline{R}_2}+c\,\delta_{\underline{R}_1\underline{R}_2}\right]^2\delta_{\underline{R}_1\underline{R}_2}$$

$$= -\frac{\kappa^4 a^3}{64\pi^2}\left[\frac{e^{-\kappa R_{-1}}}{R}+c\right]^2\Bigg|_{R=0} \tag{3.1a}$$

given that V/N for a simple cubic lattice is simply the lattice spacing a^3, and given equation (2.33) for κ

Next we look at

$$= \frac{1}{V}\frac{1}{4}\sum_{\alpha,\beta}\frac{(-1)^2 z_\alpha^2 z_\beta^2 \rho_\alpha \rho_\beta}{(4\pi\epsilon\epsilon_c)^2(k_B T)^2}$$

$$\times\left[\frac{V^2}{N^2}\sum_{\substack{\underline{R}_1\underline{R}_2\\ \underline{R}_1+\underline{R}_2}}\left[\frac{e^{-2\kappa|\underline{R}_1-\underline{R}_2|}}{|\underline{R}_1-\underline{R}_2|^2} - 2\int d\underline{r}_1\sum_{\underline{R}_2}\frac{e^{-2\kappa|\underline{R}_2-\underline{r}_1|}}{|\underline{R}_2-\underline{r}_1|^2}\right.\right.$$

$$\left.\left.+\int d\underline{r}_1\, d\underline{r}_2\,\frac{e^{-2\kappa|\underline{r}_1-\underline{r}_2|}}{|\underline{r}_1-\underline{r}_2|^2}+\left[\frac{e^{-\kappa R_{-1}}}{R}+c\right]^2\Bigg|_{R=0}\right] \tag{3.2}$$

$$= \frac{K^4}{16\pi^2} \times \frac{1}{4}\left[a^3 \sum_{\underline{R}\neq 0} \frac{e^{-2KR}}{R^2} + \left[\frac{e^{-KR}-1}{R} + C\right]_{R=0}^{2} - \int d\underline{r}\, \frac{e^{-2Kr}}{r^2}\right] \qquad (3.2a)$$

We then need to find the expansion in powers of K of

$$D = \left[a^2 \sum_{\underline{R}} \frac{e^{-2KR}}{R^2} - \int d\underline{r}\, \frac{e^{-2Kr}}{r^2}\right]$$

$$= \left[a^3 \sum_{\underline{R}} \frac{1}{R^2} - \int \frac{d\underline{r}}{r^2}\right.$$

$$+ \frac{(-2K)}{}\left(a^3 \sum_{\underline{R}} \frac{1}{R} - \int \frac{d\underline{r}}{r}\right)$$

$$\left. + \frac{(-2K)^2}{2!}\left(a^3 \sum_{\underline{R}} 1 - \int d\underline{r}\right)\right] \qquad (3.3)$$

giving us terms up to K^6 (and hence e^6). Let us define

$$D_1 \equiv a^3 \sum_{\underline{R}} \frac{1}{R^2} - \int \frac{d\underline{r}}{r^2} \qquad (3.4)$$

This represents the difference between the function $f(R) = {}^1/R^2$ evaluated at the centre of a unit cell and summed over m^1 unit cells and the function integrated over the volume taken up by the m^1 unit cells, in the limit as m^1 goes to ∞ . Consider the value of D_1 for finite m^1 .for cells on or near the surface of the volume covered by the m^1 unit cells, the difference between the integral and the sum is small and tends to zero as the distance from the centre of the unit cell to the origin of R tends to infinity. Thus, the value of D in the limit that m^1 (and hence the volume integrated or summed over) tends to infinity converges to a finite value. We calculated D_1 in two ways: firstly by approximating the volume integrated or summed over by a sphere and finding the limit for D_1 as the volume increases in size. Secondly we took the volume as

a cube and used the same procedure. In both cases we found that

$$D_1 = 8.91\, a \tag{3.5}$$

Now consider

$$D_2 = a^3 \sum_{R} \frac{1}{R} - \int \frac{dr}{r} \tag{3.6}$$

There are problems here because if the same method is used as for D_1, we find that we obtain different results for taking the volume as a sphere and as a cube. This is because there are points on the surface of the (smooth) sphere which contribute to D_2 which consist of parts of unit cells. However if we choose a cubic as our volume, only complete unit cells are integrated over. Unfortunately $1/r$ does not decrease sufficiently fast as $\underline{r}$ decreases so that the extra terms in the integration over the sphere do count.

However this problem is resolved when it is seen that D is given by the Taylor series

$$D \simeq \lim_{K\to 0} G(K) + K \lim_{K\to 0} \frac{\partial G}{\partial K} + \frac{K^2}{2} \lim_{K\to 0} \frac{\partial^2 G}{\partial K^2} \tag{3.7}$$

(to order K^2)

where $$G(K) = a^3 \sum_{R\neq 0} \frac{e^{-2KR}}{R^2} - \int d\underline{r}\, \frac{e^{-2Kr}}{r^2} \tag{3.8}$$

Then $$D_1 = \lim_{K\to 0} G(K) \tag{3.9}$$

$$D_2 = \lim_{K\to 0} \frac{\partial G}{\partial K} \tag{3.10}$$

$$D_3 = \lim_{K\to 0} \frac{\partial^2 G}{\partial K^2} \tag{3.11}$$

We have shown that D_1 is uniquely defined if the limit $K \to 0$ is taken and then the difference between the sum (over $1/R^2$) and the integral (over $1/r^2$) is found. However we will only find a unique value for D_2 if the limit $K \to 0$ is taken <u>after</u> the difference of the sum (over e^{-2KR}/R) and the integral (over e^{-2Kr}/r) is found. Thus the e^{-2Kr} (or e^{-2KR}) acts as a convergance factor. It is possible to find the difference numerically between $\sum_R e^{-2KR}/R$ and $\int d\underline{r}\, e^{-2Kr}/r$ for various values of K and find D_2 by extrapolating to $K = 0$. In this way we obtained

$$D_2 = 2.84\, a^2 \tag{3.12}$$

D_3 can be evaluated after the limit $K \to 0$ is taken since it is then simply

$$D_3 = a^3 \sum_{R \neq 0} 1 - \int d\underline{r} \tag{3.13}$$

$$= a^3 \tag{3.13a}$$

We can then substitute the values D_1, D_2 and D_3 into (3.3), the value of D into (3.2a) and we then obtain

$$= \frac{K^4}{64\pi^2}\left[8.91 + 2.84\,K_a + K^2a^2 + \left[\frac{e^{-KR}-1}{R} + C\right]^2\Big|_{R=0}\right] \tag{3.14}$$

Finally we need to evaluate the diagram

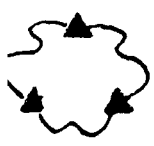

$$= \sum_{\alpha,\beta,\gamma} \frac{(-1)^3 Z_\alpha^2 Z_\beta^2 Z_\gamma^2 \rho_\alpha \rho_\beta \rho_\gamma}{(4\pi\epsilon\epsilon_0)^3 (K_B T)^3}$$

$$\times \frac{V^3}{N^3} \sum_{\substack{\underline{R}_1 \underline{R}_2 \underline{R}_3 \\ \underline{R}_1 \neq \underline{R}_2 \neq \underline{R}_3}} \frac{e^{-K|\underline{R}_1 - \underline{R}_2|}}{|\underline{R}_1 - \underline{R}_2|} \frac{e^{-K|\underline{R}_2 - \underline{R}_3|}}{|\underline{R}_2 - \underline{R}_3|} \frac{e^{-K|\underline{R}_3 - \underline{R}_1|}}{|\underline{R}_3 - \underline{R}_1|}$$

$$- 3\frac{V^2}{N^2} \int d\underline{r}_1 \sum_{\underline{R}_1 \neq \underline{R}_3} \frac{e^{-K|\underline{r}_1 - \underline{R}_2|}}{|\underline{r}_1 - \underline{R}_2|} \frac{e^{-K|\underline{r}_1 - \underline{R}_3|}}{|\underline{r}_1 - \underline{R}_3|} \frac{e^{-K|\underline{R}_2 - \underline{R}_3|}}{|\underline{R}_2 - \underline{R}_3|}$$

$$+ 3\frac{V}{N}\int d\underline{r}_1 d\underline{r}_2 d\underline{r}_3 \; \frac{e^{-K|\underline{r}_1-\underline{r}_2|}}{|\underline{r}_1-\underline{r}_2|}\,\frac{e^{-K|\underline{r}_2-\underline{r}_3|}}{|\underline{r}_2-\underline{r}_3|}\,\frac{e^{-K|\underline{R}_3-\underline{r}_1|}}{|\underline{r}_3-\underline{r}_1|}$$

$$+ \int d\underline{r}_1 d\underline{r}_2 d\underline{r}_3 \; \frac{e^{-K|\underline{r}_1-\underline{r}_2|}}{|\underline{r}_1-\underline{r}_2|}\,\frac{e^{-K|\underline{r}_2-\underline{r}_3|}}{|\underline{r}_2-\underline{r}_3|}\,\frac{e^{-K|\underline{r}_3-\underline{r}_1|}}{|\underline{r}_3-\underline{r}_1|} \qquad (3.15)$$

$$= -\frac{K^6 a^3}{64\pi^3} \times \frac{1}{6} \times D' \qquad (3.15a)$$

Terms at $\underline{R}_1 = \underline{R}_2$, $\underline{R}_1 = \underline{R}_3$, $\underline{R}_2 = \underline{R}_3$ are ignored - see comments after (2.43a)

where

$$D' = \underset{K\to 0}{Lt}\left[\left(\frac{V}{N}\right)^2 \sum_{\substack{R R' \\ R+R'}} \frac{e^{-KR}}{R}\,\frac{e^{-KR'}}{R'}\,\frac{e^{-K|\underline{R}+\underline{R}'|}}{|\underline{R}+\underline{R}'|}\right.$$

$$- 3\left(\frac{V}{N}\right)\sum_{\substack{R \\ R\neq 0}} \int d\underline{r}\; \frac{e^{-Kr}}{r}\,\frac{e^{-K|\underline{r}+\underline{R}|}}{|\underline{r}+\underline{R}|}\,\frac{e^{-KR}}{R}$$

$$\left. + 2\int d\underline{r}\, d\underline{r}'\; \frac{e^{-Kr}}{r}\,\frac{e^{-Kr'}}{r'}\,\frac{e^{-K|\underline{r}+\underline{r}'|}}{|\underline{r}+\underline{r}'|}\right] \qquad (3.16)$$

$$= 38.32 \qquad (3.16a)$$

As when evaluating the diagram with two ▲ points, we have to be careful to take the limit $K \to 0$ after the expression inside the square brackets, $D(K)$ has been evaluated. In this case we run into a difficulty with convergance. The problem is, that for each value of K it is necessary to evaluate D^1 over an increasing volume until convergance to a well defined figure is obtained. As K becomes smaller, the maximum volume that is taken becomes prohibitively large numerically. We were therefore forced to replace all terms $e^{-K\mathcal{R}}$ where $\mathcal{R}$ is a discrete or a continuous variable by the function

$$f(\mathcal{R}) = 2\mathcal{R}^3/R_0^3 - 3\mathcal{R}^2/R_0^2 + 1 \quad \mathcal{R} \le R_0 \qquad (3.17)$$
$$= 0 \quad \mathcal{R} > R_0$$

This function has the desirable properties that it is flat close to $\mathcal{R} = 0$, that it tails off rapidly close to $\mathcal{R} = R_0$ and that it is unity at $\mathcal{R} = 0$. The limit $K \to 0$ corresponds to taking $R_0 \to \infty$

We believe, though we have no proof, that the result we have obtained (equation 3.16a) from this method would be the same as the result had we had sufficient computer time to evaluate the limit using the exponential functions. Substituting equation (3.16a) into (3.15a) we find

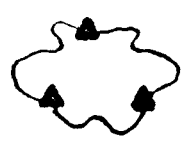

$$= \frac{-K^6}{64\pi^3} \times \frac{38 \cdot 32}{6} \qquad (3.18)$$

Summing all the diagrams, equations (3.1a), (3.14) and (3.18) we finally obtain using equations (2.46), (2.51)

$A_c =$ $+ A^{cont}_{(D-H)}$ (3.19)

$$= \frac{K^3}{12\pi}\left[1 - 0.532(Ka) + 0.3386(Ka)^2 - 0.2467(Ka)^3\right] \qquad (3.19a)$$

(3.19b)

$= -\beta F_c / V$

We note that all terms containing the parameter c cancel, thus avoiding divergencies in the final result. It also proves that to order e^6, the value of the potential at the origin does not affect the final result as we indicated in section B. Finally we note that the dependence on e comes in only through the D-H inverse screening length K, again to order e^6. This point arises because of the properties of the diagrams that contribute to the expansion to e^6.

3B. Padé Approximants

We have found an expansion for the free energy, F_c, equations (3.19) that goes to order e^6 and we have written it in terms of powers of (Ka) where K is the inverse D-H screening length. As we have said in section A, this expansion cannot

be applied directly to fastionics where, as we show at the end of this section, κa is of the order of unity. We now treat κa as our expansion parameter since we have shown that, to order e^6, all the charge, temperature and concentration dependence of the interaction can be written in terms of this one parameter.

To find a theory that would be more appropriate for systems where κa is of the order of unity, we turn to Padé approximants. The general idea of this approach is that it creates a means of interpolating between low and high κ limits, as follows. If the function we are looking at is given for low κ as a series to order κ^m and further arguments can be used to show that in the high κ limit, the function goes as $\kappa^{m'}$ an interpolation formula for the function is

$$f(\kappa a) = \frac{a_1 + b_1(\kappa a) + c_1(\kappa a)^2 + \ldots . d_1(\kappa a)^{m''}}{a_2 + b_2(\kappa a) + \ldots \ldots d_2(\kappa a)^{m''-m'}} \qquad (3.20)$$

Here a, b, ... and a_2, b_2 .... are found such that on expanding $f(\kappa a)$ up to $(\kappa a)^m$, the low κ series is recovered. Clearly for large κ , $f(\kappa a)$ will vary in the correct manner. $f(\kappa a)$ is known as a Padé approximant.

We adapt an argument due to Onsager (1939) to find the behaviour of the free energy as a function of κ for large κ . Onsager (1939) looked at a charged hard sphere system and showed that there is a lower bound to the internal energy per particle of the system E_u this being

$$E_u = \frac{-Z_p^2 e^2}{\sigma} \qquad (3.21)$$

where Z_p is the charge on each sphere and σ its diameter.

Fig. 3a

Padé approximants for lattice gas model

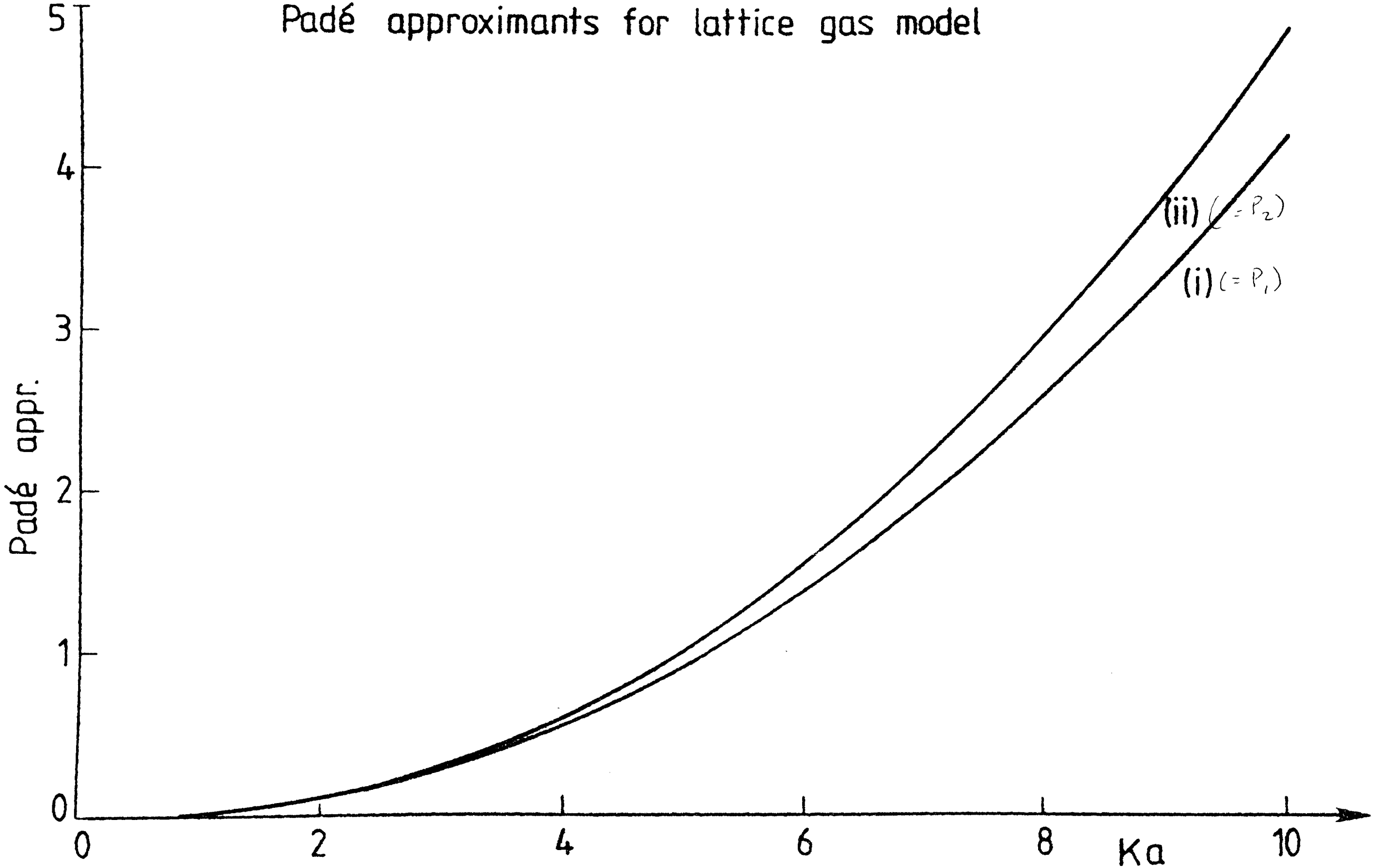

Assuming that Onsager's theory will be valid for our lattice gas, we may assume that in the limit of the charge on the particles becoming large, the internal energy will vary as the square of the total charge. In this limit, the internal energy will dominate over the entropy terms in the free energy and so the free energy will also vary as the square of the total charge. Since $K \sim Z$ (equation (2.33)), this implies that the free energy varies as K^2 in the limit of large K .

Clearly by taking the low K expansion to arbitrary order in K one may generate several Padé approximants. These should all converge for small K and be sufficiently close at the magnitude of Ka for which the theory is of interest. By finding terms up to e^6 we could only obtain two approximants viz:

$$P_1 = (Ka)^3 \frac{N k_B T}{12\pi} \frac{p'}{1 + r'(Ka)} \qquad (3.22)$$

and

$$P_2 = (Ka)^3 \frac{N k_B T}{12\pi} \frac{p + q(Ka)}{1 + r(Ka) + s(Ka)^2} \qquad (3.23)$$

This is because when we obtained the approximants and plotted them (figure 3a) they were both nearly equal for $(Ka) \lesssim 6$ up to where we would expect to apply our theory. Figure 3a provides a useful indication that even the two lowest order approximants are converging sufficiently that we may consider P_2 as a valid approximant for the free energy.

Given that our low K series for the free energy is from equations (2.28) and (3.19)

$$F_c = \frac{-\beta A_c}{V} \tag{3.24}$$

$$= -\frac{(\kappa a)^3}{12\pi}\left[1 + B(\kappa a) + C(\kappa a)^2 + D(\kappa a)^3\right] \tag{3.24a}$$

where

$$B = -0.532 \tag{3.25}$$

$$C = 0.3386 \tag{3.26}$$

$$D = -0.2407 \tag{3.27}$$

then from simple algebra

$$p^1 = 1 \tag{3.28}$$

$$r^1 = -B = 0.532 \tag{3.29}$$

and

$$p = 1 \tag{3.30}$$

$$q = \frac{D - 2BC + C^3}{B^2 - C} = 0.558 \tag{3.31}$$

$$r = \frac{D - BC}{B^2 - C} = 1.089 \tag{3.32}$$

$$s = \frac{BD - C^2}{C - B^2} = 0.243 \tag{3.33}$$

It is interesting to note that r^1 is close to 0.5. This approximant is therefore very similar (and is identical in form) to the modified D-H theory (Lidiard 1957) in which account is taken of site exclusion.

We may thus take

$$F_c = P_2 \tag{3.34}$$

as our expansion for the free energy due to the Coulomb interactions in our lattice gas. (P_2 is given by (3.23)).

Finally we evaluate what (κa) would be for lead fluoride to indicate what size (κa) would be if we wished to apply our

theory to the fluorites. Given the definition of κ (equation (2.33)) and assuming the following parameters: $a^3 \times \rho_\pm \sim 2\%$, $\epsilon_r = 31.7$, a = 3 Å, T ~ 800K and Z = 1, we find that

$$\kappa a \simeq 1 \tag{3.35}$$

The value of $\rho_\pm$ was obtained from the results of the molecular dynamics simulations described in Chapter 5, ϵ_r is from Samara (1976). a is the distance between nearest neighbour anions - a value of 3Å from the measurements quoted in Hayes (1974). The fastionic transition temperature is 705 K (Derrington et al 1976) and in the fluorites the anions are singly charged.

3C. Thermodynamics

We have shown how to find the free energy F_c due to Coulomb interactions in our lattice gas, this being given by equation (3.34). There are other contributions to the free energy of our system namely the energy required to create the defects, the Frenkel energy per defect E_o and the entropy of the defects. Part of this entropy is implicitly included in F_c as here we have calculated the free energy and not the internal energy due to the interactions. The remainder comes from the entropy S_o when the Coulomb interactions are switched off. S_o is the entropy of non interacting particles on a lattice where no two particles are allowed on the same site and it is given by

$$\frac{S_o}{k_B} = \ln \frac{N!}{[(N\nu)!]^2 (N - 2N\nu)!} \tag{3.36}$$

$$= N \ln N - 2N\nu \ln N\nu - (N - 2N\nu) \ln (N - 2N\nu) \tag{3.36a}$$

using Stirling's theorem. Here ν is the number of defects per lattice site, N is the number of lattice sites and k_B is Boltzmann's constant.

Thus the total free energy of our system,

$$F = N\nu E_c - TS_c + F_c \tag{3.37}$$

where E_o is assumed independent of temperature.
As described in section A of Chapter 2 we can immediately calculate the chemical potential μ of our system.

$$\mu = \frac{1}{N} \left.\frac{\partial F}{\partial \nu}\right|_{N,T} \tag{3.38}$$

F_c is a function of (κa) which we write in terms of ν using equation (2.33) as follows

$$\kappa a = a \sqrt{\sum_\alpha \frac{Z_\alpha^2 \rho_\alpha e^2}{k_B T \epsilon \epsilon_o}} \tag{3.39}$$

$$= \sqrt{\frac{2\nu e^2}{k_B T \epsilon \epsilon_o a}} \tag{3.39a}$$

since $\rho_\alpha = \nu_\alpha / a^3 \qquad Z_\pm = \pm 1$ (3.40)

Since in our model we have equal numbers of positively and negatively charged defects, $\rho = \rho_+ = \rho_-$. If we define a reduced temperature

$$t = T/T_o \tag{3.41}$$

where

$$T_o = \frac{e^2}{k_B \epsilon \epsilon_o a} \tag{3.42}$$

then from (3.39),

$$\kappa a = \sqrt{\frac{2\nu}{t}} \tag{3.43}$$

Equations (3.37) and (3.38) then give

$$\mu_r = \mu_o + \mu_c \tag{3.44}$$

where

$$\mu_r \equiv \mu / k_B T_o \tag{3.45}$$

and is the reduced chemical potential,

$$\mu_0 = \frac{E_0}{k_B T_c} + 2t \ln \frac{\nu}{1-2\nu} \tag{3.46}$$

$$\mu_c = \frac{1}{12\pi}\sqrt{\frac{t}{2\nu}}\left[\frac{\{3p(2\nu/t)+4q(2\nu/t)^{3/2}\}\{1+r(2\nu/t)^{1/2}+s\left(\frac{2\nu}{t}\right)\} - \{r+2s(2\nu/t)^{1/2}\}\{p(2\nu/t)^{3/2}+q(2\nu/t)^2\}}{[1+r(2\nu/t)^{1/2}+s(2\nu/t)]^2}\right] \tag{3.47}$$

and we define

$$\mu' \equiv \mu_r - E_0 / k_B T_0 \tag{3.48}$$

We found (3.47) from the equations (3.34), (3.37) and (3.38)

We use equation (3.48) to plot lines of constant μ' on a graph of $^1/t$ against $\log\nu$. The plot is shown in figure.3b. It shows clearly that our system does have first order, second order and diffuse transitions depending on the value of the reduced Frenkel energy ($E_o/k_B\ T_o$).

This graph resembled the plot for a van der Waal's gas in which $\log \rho$ is plotted against the reciprocal of the temperature (ρ is the density of the gas). for lines of constant chemical potential. By this analogy its significance may readily be understood. It is possible to obtain t_c, ν_c and μ_c', the critical reduced temperature, critical defect concentration, and the critical chemical potential less the reduced Frenkel energy, as follows:

first we calculated the pressure p from

$$p = -\frac{\partial F}{\partial N}\Big)_{n,T} \tag{3.49}$$

g. 3b

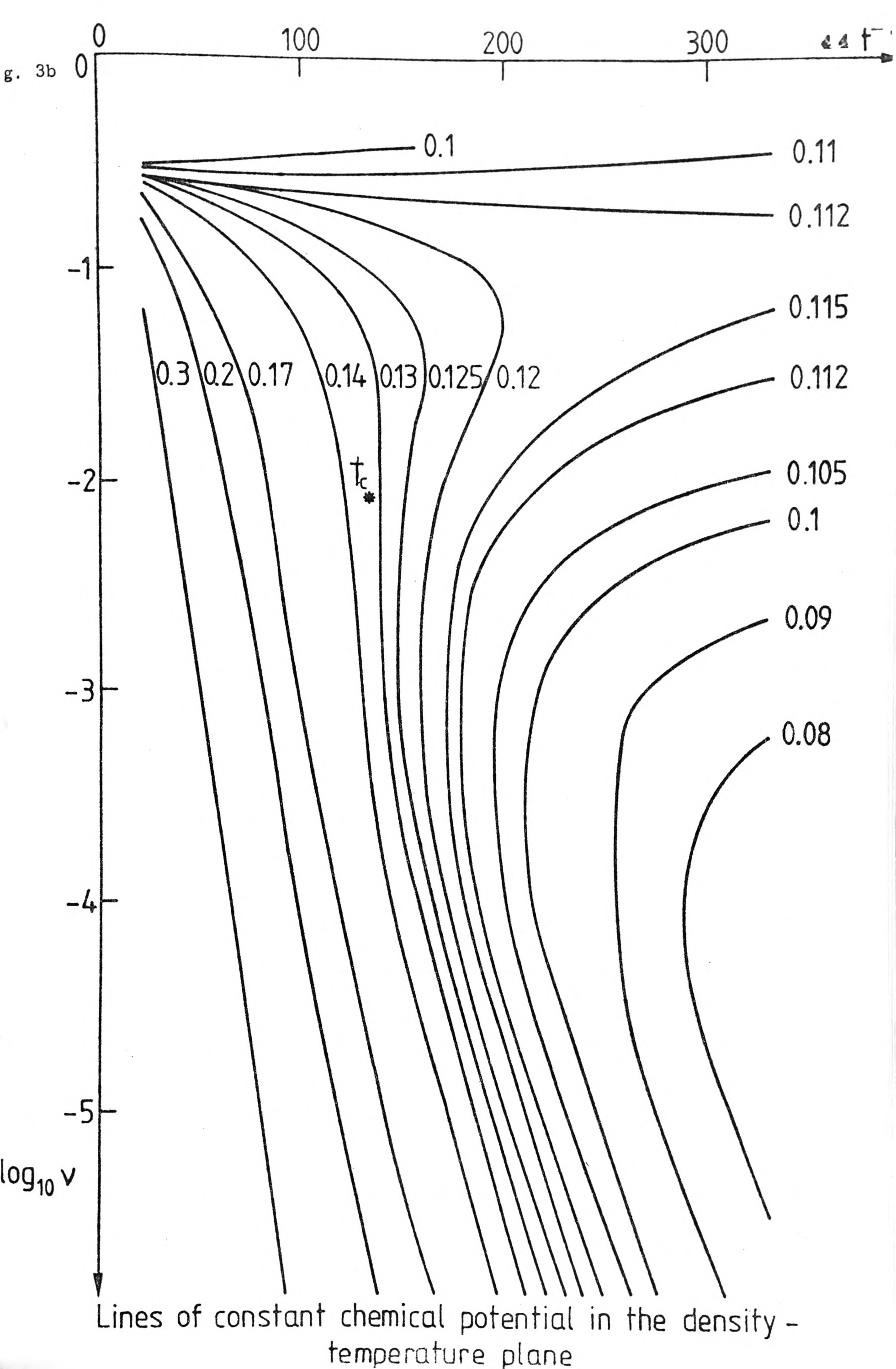

Lines of constant chemical potential in the density - temperature plane

where n is the number of particles. The critical pressure is by definition the pressure at which

$$\left.\frac{\partial P}{\partial N}\right)_{n_c, T_c} = \left.\frac{\partial^2 P}{\partial N^2}\right)_{n_c, T_c} = 0 \qquad (3.50)$$

Using equations (3.34), (3.37), (3.50)

we can show that

$$(Ka)_c = \sqrt{\frac{2\nu_c}{t_c}} = 1.538 \qquad (3.51)$$

$$\mu'_c = -0.13 \qquad (3.52)$$

and that

$$\nu_c = 8.92 \cdot 10^{-3} \qquad (3.53)$$

$$t_c = 7.54 \cdot 10^{-3}$$

Hence (3.53a)

t_c is marked in figure 3b

We can see immediately that the critical defect concentration is very low (equation (3.53)). Furthermore figure 3b indicates that a diffuse transition will also occur at low concentrations in agreement with the behaviour noted for the fluorites where the disorder appears to come from defect concentrations of 10% or less (see the introduction). Figure 3b which for given chemical potential is an Arrhenius plot also shows that the change in the logarithm of the defect concentration with the reciprocal of the reduced temperature is very much slower above the transition temperature if there is a diffuse transition. However this does not indicate a genuine saturation of defect concentration which was suggested by Catlow et al (1978) as being due to

defect repulsions. Therefore in this respect the model does not appear entirely satisfactory.

Another way of testing the model is to look at the ratio

$$\zeta_c = \frac{|\mu'_c|}{E_c} = 17.24 \qquad (3.54)$$

This is because

$$\mu' = \frac{-E_c}{K_B T_0} \qquad (3.55)$$

where E_c is the Frenkel energy for a static lattice of a system which shows critical behaviour. Assuming that μ'_c is close to the value of μ' for a system with a diffuse transition, we can assume that ζ_c gives the correlation between the static lattice Frenkel energy and the transition temperature of a system which shows a diffuse transition. Since the reduced temperature cancels in equation (3.54), ζ_c is universal in the sense that it is the same figure for all systems to which our model may apply. The point is that ζ_c has been examined for the fluorites by March et al (1980) where they find that it is approximately 20. This compares favourably with the value of 17.4 that we find (equation (3.54)).

Finally we calculate the values of the critical temperatures and E_c's for CaF_2 and PbF_2. For CaF_2 we use $\epsilon_r = 6.47$ Catlow and Norgett (1973) $a = 2.72$ Å Hayes (1974) to obtain

$$T_0 = 9650\,K \qquad (3.56)$$

Then $T_c = \epsilon_c T_0 = 728\,K$, cf $T_s = 1423\,K$ (3.57)

Dworkin and Bredig (1968)

and $E_c = 1.09\,eV$ cf $E_o = 2.71\,eV$ March et al (1980) (3.58)

for PbF_2 we use ϵ_r and a quoted when finding (k_a) to give

$$T_o = 22080\,K \tag{3.59}$$

and $$T_c = 166\,K, \text{ cf } T_s = 705\,K^{*} \tag{3.60}$$

$$E_c = 0.25\,eV \text{ cf } E_o = 1.0\,eV^{\dagger} \tag{3.61}$$

We see that whilst we obtain a rough agreement with experimental values of T_s, the fastionic transition temperature and E_o for CaF_2, the agreement is poor for PbF_2. The reason for the poor agreement in the latter case may be that the static dielectric constant is not the correct parameter to use when writing down the Coulomb interaction between particles in our lattice gas. This is because the dielectric constant may be affected by local electric fields but it is difficult to see how to improve this without considerably complicating the theory by introducing a position dependent dielectric constant.

Despite a major defect of the theory, namely the neglect of the temperature dependence of E_o (this could easily be modified), the agreement we have with data on the fluorites strongly suggestes that the Coulomb interactions do play a major role in the transition to fastionic behaviour.

* Derrington et al (1976)

† March et al (1980)

CHAPTER 4

LEAD FLUORIDE SIMULATION

4A. The Molecular Dynamics Technique

As we said in the introduction, we have simulated lead fluoride using molecular dynamics programmes that already exist and that needed no adapting for this work. Therefore this technique will not be described in great detail here since it has been reviewed by Sangster and Dixon (1976) for alkali halides and discussed by Gillan and Dixon (1980) for the fluorite $SrCl_2$.

The purpose of molecular dynamics is to numerically simulate the time evolution of a material by calculating the trajectories of a large number N (of the order of a hundred) of particles from Newtonian equations of motion. The N simulated particles are enclosed in a cube (in our case) of volume V containing an integral number N_u of unit cells. Periodic boundary conditions can then be imposed (they are described in Hansen and McDonald 1976) such that the cube may be regarded as N_u unit cells in an infinite crystal. The use of the periodic boundary conditions avoids surface effects which would clearly be important in only a hundred or so particles and enables calculation of the long range Coulomb forces as we describe below.

The input for a molecular dynamics programme is the interionic potential which is assumed to be pairwise additive and central. Thus if Φ is the total potential energy of the system it is assumed that

$$\Phi = \frac{1}{2} \sum_{\alpha,\beta} \sum_{i=1}^{N_\alpha} {\sum_{j=1}^{N_\beta}}' \phi_{\alpha\beta}(r_{ij}) \qquad (4.1)$$

where α, β are the species of the ions (anions or cations) and $\phi_{\alpha\beta}(r_{ij})$ is the potential between ions i and j which are separated by $r_{ij} = |\underline{r}_i - \underline{r}_j|$. The prime excludes self interactions. The force on the ith ion is then given classically by

$$\underline{F}_i = -\sum_{j \neq i}^{N_\beta} \nabla \phi_{\alpha\beta}(r_{ij}) \qquad (4.2)$$

When calculating the forces from equation (4.2) the short range forces are truncated on a sphere of diameter equal to the box length. The Coulomb forces however have to be dealt with using special techniques described by Sangster and Dixon (1976). For the lead fluoride simulation, Ewald summation was used which we describe in section C of this chapter. The Coulomb forces are calculated between a given particle and other particles in the box, also their images and the particles' own images in the repeated boxes.

Once the forces have been calculated, the particle positions $\underline{r}_i$ and their velocities $\underline{v}_i$ are obtained by numerical integration of the equations of motion. At this point approximations are introduced since we have to replace the continuous equations of motion by difference equations involving the time step used in numerical integration, Δt . Sangster and Dixon (1976) discuss various ways of obtaining the difference equations. We use Beeman's algorithm (Beeman 1976) since it has been found that it achieves very good energy conservation. This algorithm approximates $\underline{r}_i$ and

$\underline{r}_i$ as follows:

$$\underline{r}_i(t+\Delta t) \simeq \underline{r}_i(t) + \underline{v}_i(t)\,\Delta t + \tfrac{1}{6}\left[4\underline{a}_i(t) - \underline{a}_i(t-\Delta t)\right](\Delta t)^2 \tag{4.3}$$

and

$$\underline{v}_i(t+\Delta t) \simeq \underline{v}_i(t) + \tfrac{1}{6}\left[2\underline{a}_i(t+\Delta t) + 5\underline{a}_i(t) - \underline{a}_i(t-\Delta t)\right]\Delta t \tag{4.4}$$

where $\underline{a}_i$ is the acceleration. Δt was taken to be $\sim 10^{-14}$ sec, ca 1/20 of the minimum vibration period. It cannot be too small or the computer time required for the simulations would be excessive. Equally, it cannot be too large as we need to avoid unacceptably big fluctuations in the internal energy of the system. The Δt that was chosen gave fluctuations that were only 10^{-4} of the total internal energy.

During the simulation, the volume, number density, momentum and total energy are conserved variables. At the start of the first run, the ions were set on the regular fluorite positions with the lattice parameter chosen to give the required density. The initial velocities were taken from a gaussian random distribution with the constraints

$$\sum_{i,\alpha} m_{i\alpha}\,\underline{v}_{i\alpha} = 0 \tag{4.5}$$

and

$$T = \frac{1}{3NK_B}\sum_{i,\alpha} m\,\underline{v}^2_{i,\alpha} \tag{4.6}$$

Here T was set to a value considerably lower than that required in any of the runs and the system is 'heated' to the first temperature desired in steps of $\sim$ 150K by scaling the

velocities. The initial conditions for subsequent runs at different densities and temperatures are constructed by scaling the positions and velocities obtained at the end of a previous run. With this kind of initialisation, the fastion behaviour we will describe in Chapter 5 is in no way built into the system.

Before taking the results for a given run, the system is allowed to come into equilibrium, thus the first few hundred steps are ignored. Subsequent steps were used in two ways: for static properties the system at each step was taken as a member of an ensemble and a thermal average would simply be the average over all the time steps. For dynamic properties, in this work only the hopping analysis, we are able directly to look at microscopic events as a function of time with a resolution of $\Delta t = 10^{-14}$ sec.

In the next chapter we indicate how physical properties which indicate the disorder present are evaluated from the simulation and discuss our results.

4B. An Interionic Potential: Fitting of Parameters

It is clear that to simulate a given material one needs to produce an interionic potential that will not throw up instabilities in the simulation. In this section we show how we found an interionic potential for lead fluoride and in the following section how we tested the potential using a static lattice to check for basic instabilities, and how we revised the potential accordingly.

The type of interionic potential that we used is of the

Born-Mayer-Huggins form

$$\varphi_{\alpha\beta}(r) = \underset{(i)}{\frac{Z_\alpha Z_\beta e^2}{4\pi\epsilon_0 r}} + \underset{(ii)}{A_{\alpha\beta} e^{-r/\rho_{\alpha\beta}}} - \underset{(iii)}{\frac{C_{\alpha\beta}}{r^6}} \qquad (4.7)$$

Where α, β denote the ionic species, e is the electronic charge, ϵ_0 the permitivity of the vacuum and Z_α is the charge on ions of species α in units of $|e|$. We chose such a potential as we want to compare the results for our lead fluoride simulation directly with those from simulations of CaF_2 and $SrCl_2$ (Dixon and Gillan (1978), Dixon and Gillan (1980) respectively) which use precisely this form for the interionic potential.

The first term (i) in (4.7) is clearly the Coulomb potential where the ions are represented by unpolarisable point charges. This is clearly inaccurate, especially for lead fluoride for which the high frequency dielectric constant is 2.99 (Jones 1955). This may be compared with the value of unity that is predicted by the rigid ion model. We would redeem this failing by using shell model potentials (for a review see Cochran 1971) where the outer electrons are represented by a rigid shell coupled through a harmonic spring to a charged core which has the mass of the ion. However Dixon and Gillan (1980a) found that for CaF_2 the introduction of polarisability through this approach does not qualitatively alter the characteristics of the system. We do not therefore attempt to obtain a shell model potential for lead fluoride in this study as we found a rigid ion potential that appears to represent lead fluoride satisfactorily on simulation (see Chapter 5), and shell model simulations require considerably more computer time than could

be justified for a first look at lead fluoride.

Term (ii) in (4.7) is a short range repulsive potential whose origin lies in the opposition to overlap of closed electronic shells when the ions approach each other at distances close to the sum of the radii of the outermost closed shell. The form assumed for this term, known as the Born-Mayer potential, has been found to represent well this type of interaction from quantum mechanical calculations. (Sangster and Dixon 1976).

The final term, (iii) in (4.7) is aimed at representing the Van der Waals attraction. The dependence on r^{-6} is argued on the basis that the physical origin of this attractive form is fluctuating dipole interactions (see eg. Kittel 1971). However it is very difficult to make first principles calculations of this form and it is the area most subject to arbitrary assumptions (Sangster and Dixon 1976).

We should also say that lead fluoride is assumed to be fully ionic and that no attempt has been made to fit non integral charges in the Coulomb term in our work. This may be justified by the agreement we obtain with experiment when we calculate the cohesive energy (for a static solid), for the potential we adopt in our simulation.

Now we show how we found values of the nine parameters in the short range interaction viz. A_{++}, C_{++}, ρ_{++}, A_{+-}, C_{+-}, ρ_{+-}, A_{--}, C_{--} and ρ_{--}. It must be emphasised that the procedure we use is somewhat ad hoc. This is because it is difficult to find a unique reliable method for fitting an

interionic potential based on first principles reasoning because of the sheer complexity of the system that one is attempting to represent with very few parameters.

Whilst all nine parameters could be fitted by experimental results, this would not necessarily produce a good potential from the combination of many different experimental measurements in one potential. We therefore made certain assumptions to find our initial potential which fixed six of the parameters (some of these subsequently had to be modified as described in section C). These assumptions were used in the work of Catlow and Norgett (1973) in their defect studies on CaF_2, SrF_2 and BaF_2 and are as follows: the cation-cation short range interactions are set equal to zero. The justification here is that the cations in the fluorite lattice are some distance apart ($^1/\sqrt{2}$ x the lattice constant) especially by comparison with the anions. The cations do not approach each other either as defects (since the cation sublattice does not disorder, see the introduction) or under the influence of an external electric field being all of like charge. Another assumption is that C_{+-} may be set equal to zero on the basis of 'quenching' (see Diller (1975) for a description of this phenomenon and how it may be used to justify our assumption). Finally, the short range anion-anion interaction parameters A_{--}, ρ_{--} and C_{--} are assumed to be equal to values for fluorine ions in other fluorites. This is an assumption which was made by Catlow and Norgett (1973) and found to work well for CaF_2, SrF_2 and BaF_2. We used initially the values for A_{--}, ρ_{--} and C_{--} quoted in Catlow and Norgett (1973) although we were later forced to alter them, vide discussion in section C.

This leaves two parameters, A_{+-} and C_{+-} to be fitted to experimental quantities. The low temperature lattice constant is one of those chosen, as a potential which did not get this right is unlikely to be considered realistic. In practice what is done is to calculate the parameters such that for an assumed value of the lattice constant, the pressure is zero. The pressure is calculated from

$$P = -\frac{dU}{dV} \tag{4.8}$$

where V is the volume of the system and U its internal energy. It is easily shown then that

$$P = \frac{-4}{3a^3}\left[\frac{1}{2}\sum_{lkk'} \left.\frac{\partial \varphi_{kk'}}{\partial r}\right|_{r_{lkk'}} r_{lkk'} - \frac{e^2 \alpha_m}{8\pi\epsilon_o a}\right] \tag{4.9}$$

where α_M is the Madelung constant, a is the lattice constant, $(a+T=0)$, ϵ_o is the permittivity of the vacuum. a = 6·0 A (Hayes 1974)

The other parameter chosen is the static dielectric constant ϵ_r. This is because, as we discuss in the introduction, lead fluoride is differentiated from the other fluorites by an exceptionally large value of ϵ_r which might give rise to qualitatively different behaviour. Thus it is essential to have a potential which simulates the correct value of ϵ_r. Furthermore Hardy and Flocken (1970) and Faux and Lidiard (1971) have shown that the Frenkel energy in the static lattice E_o is not generally well represented unless ϵ_r is correct. As we argue in the introduction, it is necessary to have a reasonable value of E_o to obtain fastionic behaviour in the correct range of temperatures.

We evaluate ϵ_r using the parameters of the interionic potential which is being fitted from

$$\epsilon_r = 1 - \frac{3}{1 + 3M\epsilon_0 a^3/8e^2} \tag{4.10}$$

where

$$M = -\frac{1}{6}\sum_{\underline{r}_a}\left[\left.\frac{\partial^2 \varphi^{SR}_{+-}}{\partial r^2}\right|_{\underline{r}_a} + \frac{2}{r}\left.\frac{\partial \varphi^{SR}_{+-}}{\partial r}\right|_{\underline{r}_a}\right] \tag{4.11}$$

Here $\underline{r}_a$ are the anion positions on the regular lattice.*

Other parameters which have been measured experimentally can be calculated for our system with the parameters that have been fitted to ϵ_r and a. Following Catlow and Norgett (1973) we use the elastic constants C_{11}, C_{12} and C_{14}, together with the cohesive energy to test our potential. The elastic constants are obtained for nearest neighbour positions in the fluorite lattice from

$$C_{11} = \frac{2}{a}\left(\frac{1}{3}A_1 + A_2 + \frac{2}{3}B_1\right) \tag{4.12}$$

$$C_{12} = \left(A_1 - B_1\right)\frac{2}{3a} \tag{4.13}$$

$$C_{14} = \left[\left(\frac{1}{3}A_1 + \frac{1}{6}B_1 + \frac{1}{2}B_2\right) - \frac{1}{3}\frac{(A_1 - B_1)^2}{A_1 + 2B_1 + 3A_2 + 6B_2}\right]\frac{2}{3a} \tag{4.14}$$

Here $$A_1 = \left.\frac{\partial^2 \varphi^{SR}_{+-}}{\partial r^2}\right|_{r = \sqrt{3}a/4} \tag{4.15}$$

$$A_2 = 2/a \left.\frac{\partial^2 \varphi^{SR}_{+-}}{\partial r^2}\right|_{r} \tag{4.16}$$

$$B_1 = \frac{4}{\sqrt{3}a}\left.\frac{\partial \varphi^{SR}_{+-}}{\partial r}\right|_{r = \sqrt{3}a/4} \tag{4.17}$$

$$B_2 = \frac{2}{a}\left.\frac{\partial \varphi^{SR}_{--}}{\partial r}\right|_{r = a/2} \tag{4.18}$$

These expressions were obtained from Axe (1965).

*We fit ϵ_r to the value of 31.7 (Samara 1976) and φ^{SR} is the short range part of φ (terms (ii) and (iii) in (4.7)).

We have also calculated the cohesive energy directly from the potential. It is the total internal energy consisting of the Coulomb energy (found from the Madelung sum) and the short range contribution found from summing the interaction energy out to nearest neighbours.

This is a very useful test particularly of the ionicity of the solid.

4C. Tests of Stability

In this section we describe how, having obtained a potential by fitting to the lattice and static dielectric constants, we apply various tests to the potential. We show how in this study the potential had to be modified to avoid an instability which resulted in the longitudinal Raman mode at the Brillouin zone boundary (hereafter simply called the boundary Raman mode) having a negative squared eigen-frequency.

As we commented in section B, it is essential to obtain approximately the right value for the Frenkel energy for a static lattice E_o. Thus the first test we applied was to use the HADES (Harwell Automatic Defect Evaluation System) program to calculate E_o . This is a program designed to evaluate defect energies in a static lattice. HADES divides the simulated material into two regions; an inner region (region I) containing Ca 100 ions where the ions are represented explicitly on a lattice using the interionic potential under test and an outer region (region II) which is treated as a matched dielectric continuum. The defect energies required are calculated by allowing the ions in region I to

relax to equilibrium and taking account of displacements in region II obtained using macroscopic polarisation and elastic fields. The programme has been described in detail by Lidiard and Norgett (1972) and Norgett (1974). We used HADES to find the energy required to take an anion off the regular site and put it on the empty cube centre site, to check that the intestitial is stable at the cube centre site. This can be done by using the HADES program to calculate the energies (relative to the energy of the perfect lattice) of interstitials which are slightly displaced from the cube centre. Another check is that the interstitial is stable against interstitialcy motion in which a lattice ion is displaced into an adjacent interstitial site (Catlow and Norgett 1973). We also look at vacancy migration energies, the energy barrier against movement of a vacancy at one lattice site to a nearest neighbour lattice site. Clearly a potential with large energy barriers against interstialcy motion and vacancy migration in the static lattice is less likely to create problems in the molecular dynamics simulation at finite temperatures.

The final test we consider necessary is that the potential should show up no instabilities when evaluating the phonon spectrum for the regular lattice.

Having detailed the tests that we consider necessary to obtain an acceptable potential we now describe how a potential we obtained using the approach described in section B failed the final test, that of giving stable phonon modes, and how we modified it accordingly.

We found that by making all the assumptions described in section B concerning the parameters, A_{++}, C_{++}, ρ_{++}, A_{--}, C_{--}, ρ_{--} and C_{+-} and fitting A_{+-} and ρ_{+-} to a and ϵ_r that we had a potential which gave good values for the elastic constants, cohesive energy and Frenkel energy. It also showed none of the instabilities tested for with the HADES program. However when we evaluated its phonon spectrum using a standard programme we found that the boundary Raman mode in the $(1\ 0\ 0)$ direction (or $(0\ 1\ 0)$ or $(0\ 0\ 1)$ directions by symmetry) had a negative eigenvalue (square of the eigen-frequency) whose magnitude was approximately that of the square of the experimental frequency (Dickens and Hutchings 1978). Thus not only was an instability present, but it was also severely unstable. It is worth noting that this soft mode is an indication of the weakness of the fluorite structure in these directions and the same mode has been observed to show a tendency to soften in $SrCl_2$ (Dixon 1980, private communication). Its eigen-vectors show that the anions are displaced along adjacent parallel lines in the fluorite structure and that the cations are not displaced at all.

The way we chose to cure the instability was to fit another of the nine parameters in the potential so that in addition to the correct ϵ_r and a we would have a positive eigenvalue W_R^2 for the boundary Raman mode.

We were able to do this by choosing the parameter C_{--} to be the extra parameter fitted to experiment. The reason for this was that equation (4.10) shows that only the cation-

anion short range interaction contributes to the expression for ϵ_r and it comes in the combination $\left({}^{2}/_{r} \frac{\partial \varphi_{+-}^{SR}}{\partial r} + \frac{\partial^2 \varphi_{+-}^{SR}}{\partial r^2} \right)$ From (4.26) below we see that if nearest neighbour interactions only are considered for the short range potential, the cation-anion short range interaction contributes to W^2_R in exactly the same combination. Therefore it is pointless to alter W^2_R by fitting the cation-anion parameter C_{+-} in addition to A_{+-} and ρ_{+-} as we have to obtain the correct dielectric constant which fixes the combination $\left({}^{2}/_{r} \frac{\partial \varphi_{+-}^{SR}}{\partial r} + \frac{\partial^2 \varphi_{+-}^{SR}}{\partial r^2} \right)$. As the cations are not displaced in this mode, there is no point either in altering the cation-cation interaction. We are therefore left with the short range anion-anion interaction. We chose C_{--} rather than A_{--} and ρ_{--} because it is not well understood so that the value obtained by Catlow and Norgett (1973) for fluorine ions in fluorites is not as reliable as their values for A_{--} and ρ_{--}.

We calculated W^2_R as follows. The phonon modes for a perfect lattice are found from the equation of motion in the harmonic approximation

$$\omega^2 \underline{\underline{m}}\, \underline{U}_q = \underline{\underline{M}}(q)\, \underline{U}_q \qquad (4.19)$$

Here $\underline{U}$ is a column matrix whose elements are the displacements of ions on each sublattice, $\underline{\underline{m}}$ is a diagonal matrix with the mass of the ions on each sublattice and $\underline{\underline{M}}$ is the force constant matrix (Cochran 1966). The Raman mode that we want is longitudinal and we take it as being parallel to the x direction (1 0 0) although y or z could equally well be chosen by symmetry. Thus it is only necessary to diagonalise

$$\underline{\underline{M}}^{xx}(q) = \begin{pmatrix} M_{11}^{xx}(q) & M_{12}^{xx}(q) & M_{13}^{xx}(q) \\ M_{21}^{xx}(q) & M_{22}^{xx}(q) & M_{23}^{xx}(q) \\ M_{31}^{xx}(q) & M_{32}^{xx}(q) & M_{33}^{xx}(q) \end{pmatrix} \qquad (4.20)$$

Here 1, 2, 3 respectively refer to the cation in each unit cell, an anion within the unit cell (displaced by a ($\frac{1}{4}$ $\frac{1}{4}$ $\frac{1}{4}$) from the cation) and the other anion in the unit cell (displaced by a ($-\frac{1}{4}$ $\frac{1}{4}$ $\frac{1}{4}$) from the cation). $\underline{q}$ is the wave vector of the mode. We ascertained from this matrix that the eigenvector of the mode that was going soft was

$$\frac{1}{\sqrt{2}} \begin{pmatrix} 0 \\ 1 \\ -1 \end{pmatrix}$$

and its eigenvalue, $W_R^2 = M_{22}^{xx}(q) - M_{23}^{xx}(q)\Big|_{q = q_{BZ}}$ (4.20a)

where q_{BZ} is the zone boundary wave vector

Cochran (1966) shows that

$$M_{kk'}^{xx}(q) = N^{xx}(kk', q) \qquad k \neq k' \qquad (4.21)$$

$$= N^{xx}(kkq) - \sum_{k'} N^{xx}(kk', 0) \quad k = k' \qquad (4.21a)$$

Here k specifies the ion within the unit cell

$$N^{xx}(kk', q) = -\sum_{l'} \frac{\partial^2 \varphi_{kk'}}{\partial x^2} e^{i q \cdot r}\Big|_{\underline{r} = \underline{r}_{l'k'} - \underline{r}_{lk}} \qquad (4.22)$$

where l specifies the unit cell of one ion k and l' goes over all the unit cells in the lattice.

We split the potential into the short range component φ_{sR} and the Coulomb potential φ_c.

We define R^{xx}, C^{xx} :

$$M^{xx}_{KK'}(q) = R^{xx}(KK'q) + C^{++}(KK'q) \qquad K \neq K$$
$$= R^{xx}(KK'q) - \sum_{K'} R^{xx}(KK'0) \tag{4.23}$$
$$+ C^{xx}(KK'q) - \sum_{K'} C^{xx}(KK'0) \qquad K = K' \tag{4.23a}$$

where

$$R^{xx}(KK'q) = -\sum_{l'} \frac{\partial \varphi_{SR}^{KK'}}{\partial x^2} e^{iq\cdot r}\Big|_{r = r_{l'K'} - r_{lK}} \tag{4.24}$$

where $\varphi_{SR}^{KK'}$ is the short range potennial

and

$$C^{xx}(KK'q) = -\sum_{l'} \frac{\partial^2 \varphi_c}{\partial x^2} e^{iq\cdot r}\Big|_{r = r_{l'K'} - r_{lK}} \tag{4.25}$$

where $\varphi_c^{KK'}$ is the Coulomb potennial

Then truncating φ_{SR} at nearest neighbours,

$$R^{xx}(22q) = \left(-6\varphi_{SR}^{--}\right)''\Big|_{r = a/2}$$
$$-\frac{4}{3}\left[\frac{2}{r}\left(\varphi_{SR}^{+-}\right)' + \left(\varphi_{SR}^{+-}\right)''\right]_{r = \frac{\sqrt{3}a}{4}} \tag{4.26}$$

where $\varphi' = \partial\varphi/\partial r$, $\varphi'' = \partial^2\varphi/\partial r^2$

$$R^{xx}(23q) = \left(\varphi_{SR}^{--}\right)''\Big|_{r = a/2}\left(\cos\left(\frac{q_x a}{2}\right) + \cos\left(\frac{q_y a}{2}\right)\right.$$
$$\left. + \cos\left(q_z \tfrac{a}{2}\right)\right) \tag{4.27}$$

Now we look at the Coulomb potential φ_c. Because of its long range, the lattice sums do not converge if attempted directly so we use the Ewald transformation and write the Coulomb potential as a sum of two series, one in real space, one in reciprocal space as follows:

$$\varphi_c^{KK'}(r) = \frac{1}{r} \times \frac{Z_K\, Z_{K'}\, e^2}{4\pi\epsilon_0} \tag{4.28}$$

$$= \left[\psi(r) + \left(\frac{1}{r} - \psi(r)\right)\right] \frac{Z_K\, Z_{K'}\, e^2}{4\pi\epsilon_0} \tag{4.28a}$$

where

$\psi(r)$ = potential due to the gaussian charge

$$\rho(r) = \left(\frac{p}{\pi}\right)^{3/2} e^{-pr^2} \tag{4.29}$$

$$= \frac{1}{r}\, erf(\sqrt{p}\, r) \tag{4.29a}$$

and Z_k is the charge of the ion k in the unit cell in units of the electronic charge $|e|$. Then

$$\varphi^{kk'}(r) = \left[\frac{4\pi}{\Omega}\sum_{g}\frac{e^{-g^2/4p}}{g^2}\, e^{ig\cdot r} + \frac{1}{r}\, erfc(\sqrt{p}\, r)\right]\frac{Z_k Z_{k'} e^2}{4\pi\epsilon_0} \tag{4.30}$$

where Ω is the volume of the crystal, g is a reciprocal lattice vector. The reason for this manipulation is that by a good choice of the convergance parameter p the series can be made to converge very quickly. p is fixed such that the nearest neighbour terms summed for the reciprocal space series and for the real space series are of approximately the same magnitude.

When finding the Coulomb contribution to the matrix element we do have one useful simplification:

$$C^{xx}(kk0) - \sum_{k'} C^{xx}(kk'0) = 0 \tag{4.31}$$

by applying Laplace's equation

$$\nabla^2 \varphi_c = 0 \tag{4.32}$$

Then we find

$$C^{xx}(22_{\underline{q}}) = \frac{e^2}{4\pi\epsilon_0}\sum_{l'\neq l}\left[\frac{\operatorname{erfc}(\sqrt{p}r)}{r^3}\left\{\frac{3x^2}{r^2}-1\right\}+\frac{2e^{-pr^2}}{r^2}\sqrt{\frac{p}{\pi}}\left\{\frac{3x^2}{r^2}-1+2px^2\right\}e^{i\underline{q}\cdot\underline{r}}\right]_{\underline{r}=\underline{r}_{l2}-\underline{r}_{l'}}$$

$$+\frac{e^2}{4\pi\epsilon_0}\frac{16\pi}{a^3}\sum_{\underline{g}}\frac{(g_x+q_x)^2}{|\underline{g}+\underline{q}|^2}e^{-|\underline{g}+\underline{q}|^2/4p}-\frac{e^2}{4\pi\epsilon_0}\frac{4}{3}\frac{p^{3/2}}{\pi^{1/2}} \qquad (4.33)$$

The last term in (4.33) which is independent of $\underline{q}$ comes from the Coulomb contribution to the force constant at the origin which has to be explicitly subtracted off the reciprocal lattice series.

We also obtain

$$C^{xx}(23_{\underline{q}}) = \frac{e^2}{4\pi\epsilon_0}\sum_{l'\neq l}\left[\frac{\operatorname{erfc}(\sqrt{p}r)}{r^3}\left\{\frac{3x^2}{r^2}-1\right\}+\frac{2e^{-pr^2}}{r^2}\sqrt{\frac{p}{\pi}}\left\{\frac{3x^2}{r^2}-1+2px^2\right\}e^{i\underline{q}\cdot\underline{r}}\right]_{\underline{r}=\underline{r}_{l2}-\underline{r}_{l'3}}$$

$$+\frac{e^2}{4\pi\epsilon_0}\frac{16\pi}{a^3}\sum_{\underline{g}}\frac{(g_x+q_x)^2}{|\underline{g}+\underline{q}|^2}e^{-|\underline{g}+\underline{q}|^2/4p} \qquad (4.34)$$

By substituting equations (4.26), (4.27) and (4.33)and (4.34) into (4.23) we may find the Raman boundary eigenvalue from equation (4.20a) if $\underline{q}$ is set equal to $2\pi\hat{x}/a$.

Using this result, we have W^2_R in terms of the short range potential. Together with fitting ϵ_r and a, and choosing a suitable value for W^2_R, we have three parameters to fit to and the three 'free' parameters A_{+-}, ρ_{+-} and C_{--}. As before the short range cation-cation interaction was set to zero and A_{--}, ρ_{--} were taken from Catlow and Norgett (1973).

Initially we found a potential by fixing W_R at the experimentally measured frequency (Dickens and Hutchings 1978). However the large change in C_{--} required made the potential so soft that it was very unstable when tested using the HADES program. Therefore we fitted the Raman boundary frequency to a small positive value (0.2 THz) instead on the grounds

that this would be sufficient to annul the instability. Unfortunately the resulting potential was found to be unstable with respect to interstitial migration so we were forced to alter A_{--} and ρ_{--} to avoid this. However we did find that only slight adjustments to A_{--} and ρ_{--} were necessary to give a potential that is specified in section D.

4D. Potential Chosen

In table 1 we list the nine parameters of the short range potential that we found.

In table 2 we give the values of: the Frenkel energy E_o, the interstitial migration energy, ϵ_i, the vacancy migration energy, ϵ_v, the Raman zone boundary frequency, ω_R^2, the cohesive energy, ϵ_c and the elastic constants C_{11}, C_{12}, C_{44}. Experimental measurements of these parameters are also shown. It is clear from table 2 that we have satisfactory agreement for all the parameters we have calculated although the agreement for the interstitial and vacancy migration energies is poor. However overall the agreement was good enough for us to try the potential in the molecular dynamics simulation programmes with the results outlined in Chapter 5.

Table 1

Short Range Parameters for Lead Fluoride Potential

A^{--} (eV)	10225
ρ^{--} (Å)	0.225
C^{--} (eVÅ^6)	107.324
A^{+-} (eV)	122.66
ρ^{+-} (Å)	0.516
C^{+-} (eVÅ^6)	0
A^{++} (eV)	0
ρ^{++} (Å)	0
C^{++} (eVÅ^6)	0

Table 2

Comparison of Parameters from PbF_2 Potential with Experiment

	From PbF_2 Potential	From Experiment
E_o (eV)	1.116	1.0 [a]
E_i (eV)	.081	0.62 [b]
E_v (eV)	.082	0.18 [c]
W_R^2 (THz)	.164	39.0 [d]
E_c (eV)	22.5	25.3 [e]
C_{11}(dynes cm^{-2})	$5.56 \cdot 10^{11}$	9.30 [f] $\cdot 10^{11}$
C_{12}(dynes cm^{-2})	$1.44 \cdot 10^{11}$	4.40 [f] $\cdot 10^{11}$
C_{44}(dynes cm^{-2})	$1.26 \cdot 10^{11}$	2.06 [f] $\cdot 10^{11}$

a March et al. (1980)

b Liang and Joshi (1975)

c Liang and Joshi (1975)

d Dickens and Hutchings (1978)

e Weast (1980) (Formation energy of PbF_2 = 159.4 K cal/g mole Hayes (1974))

f Catlow et al. (1978)

Table 3

Details of Simulation Runs

T_{run} (K)	a*(Å)	ΔR (time steps)	T†
412	5.963	1495	400
593	6.005	2595	600
792	6.056	3995	800
928	6.073	4695	900
991	6.089	3895	1000

† We assume in the script that the runs are at these nominal temperatures.

* Dickens et al. (1976)

CHAPTER 5

MOLECULAR DYNAMICS RESULTS

5A. Real Space Analysis

We described the technique of the molecular dynamics simulation in section 4A. Now we indicate how certain quantities relating to the disorder can be obtained from the simulation, discuss our results and compare them where possible with experiment. We give in table 3* details of temperatures at which we made runs, the lengths of each run, ΔR, and the lattice constant a at that temperature (giving the length scale). The simulations were all done for a box of ninety six particles at a pressure of about 0 atmospheres corresponding to very low ie. atmospheric pressure. The time step used was $\Delta t = 10^{-14}$ s.

(i) Time Dependent Behaviour

As we commented in section A, the simulation can either be used to look at the behaviour of the ions as a function of time, measured in discrete time steps Δt, or by averaging over the system behaviour at different time steps to obtain static equilibrium averages. Here we look at the time dependent behaviour since we can obtain from this analysis values of the diffusion coefficient D_d and the conductivity σ which may be compared with experiment. We also obtain an estimate of the defect concentration although we consider another way of finding this important parameter in section B. Additionally we have information about the directions for which the hops are taking place.

* on page 68

First of all it is necessary to find the position of the underlying regular lattice. We use the cation positions for this as we have been able to check that, in agreement with experiment (see the introduction), the cations do not diffuse. This check was done by calculating the time dependent mean square displacement

$$\langle r_\alpha^2(t)\rangle = \frac{1}{N_\tau}\sum_\tau \frac{1}{N_\alpha}\sum_i \left[\underline{r}_{i\alpha}(t+\tau) - \underline{r}_{i\alpha}(\tau)\right]^2 \qquad (5.1)$$

where $\underline{r}_{i\alpha}(t)$ is the position of the ith ion of species α at time t. The sums go over time origins τ and N_τ , N_α are the numbers of time origins and ions of species α respectively (see Dixon and Gillan 1980). At long times $|t|$ we have (Sangster and Dixon 1976)

$$\langle r_\alpha(t)^2\rangle \longrightarrow B_\alpha + 6D_\alpha|t| \qquad (5.2)$$

where D_α is the self diffusion constant of species α and B_α is a constant. Thus if D_+ is zero, the cations are not diffusing and this is what we found at all temperatures. The cations are however vibrating about their regular sites and furthermore the cation sublattice as a whole is moving. (The sublattice recoils each time an anion hops by conservation of momentum). Therefore it was necessary to calculate the mean vector position for each simulation run and to average these positions to construct the position of the lattice.

Once the regular lattice sites have been established, it is possible to obtain a hopping catalogue for the anions. This catalogue records when an anion leaves a sphere of radius $d = a/6$ (a is the lattice constant) whose centre is at the anion regular site. The catalogue also indicates when that

anion enters a sphere of the same radius surrounding another regular site. The two events constitute a hop. It is clear that such a method of analysis assumes that there are no other sites to which the hops are made as the hops only occur between regular sites. The method is vindicated by the fact that and (1980) found using precisely this form of analysis on an $SrCl_2$ simulation, that when the radius of the sphere was decreased by a factor of two, the number of hops recorded only changed by 25%. Since the volume of the sphere would have been decreased eightfold when d was reduced by two, this suggests that most of the hops are taking place between sites within $a/_{12}$ of the regular site. Furthermore none of the hops recorded by the catalogue last more than a few vibration periods indicating that none of the ions are lingering on sites between the regular sites.

The hopping catalogue can first of all be used to find the directions of the hops. Three kinds of hop were found: between nearest sites along a cube edge (direction (1 0 0)) (91.5%), along a cube face diagonal ((1 1 0)) (8%) and along a cube body diagonal (.5%). The percentages shown are percentages of hops in each direction noted from a simulation run at 1000K; the figures indicate very clearly that by far the greatest number of hops is along the (1 0 0) direction. This is in complete agreement with and (1980).

These percentages may also be used to evaluate the mean square value of the hopping distance, $\overline{\sigma_i^2}$ Thus

$$\overline{\sigma_0^2} = \sum p r^2 = \left.\frac{1.09\, a^2}{4}\right|_{T = 1000K} \qquad (5.3)$$

Here the sum is taken over the three different values of r for each of the three directions specified above, r is the nearest neighbour distance in each direction and p is the percentage of hops in that direction. The figure of 1.09 is obtained from the percentages quoted above. From the total number of hops per unit time we obtain the mean rate ν at which each anion executes hops. If we assume that the directions of hops are statistically independent, then we can obtain the anion diffusion constant

$$D_- = \frac{1}{6} \overline{\delta_0^2} \nu \qquad (5.4)$$

(Corish and Jacobs 1973).

We used this analysis to obtain D_- at 400K, 600K, 800K, 900K and 1000K; our results are shown in table 4. It is inter ing to see that we obtain quite reasonable agreement with experimental values for D_- that are also shown in table 4. This we feel is a good indication that our simulation is producing a good representation of lead fluoride, bearing in mind the slightly arbitrary nature of the methods chosen to find the potential to be used in the simulation.

We may also evaluate the dc conductivity from the simulation using the Nernst Einstein relation

$$D_- = \frac{f_H k_B \sigma T}{\rho_- e^2} \qquad (5.5)$$

Corish and Jacobs (1973).

Here f_H is the Haven ratio, k_B is Boltzmann's constant, e the electronic charge and ρ_- the density of mobile ions given by

Table 4

Diffusion Constants and Conductivities

T(K)	$D_d/10^{-5}cm^2\ s^{-1}$	$D^a_{expt}/10^{-5}cm^2\ s^{-1}$	$\sigma(\Omega^{-1}m^{-1})$	$\sigma^b_{expt}(\Omega^{-1}m^{-1})$
600	.03	---	3.4	---
800	.94	1.7	79	270
900	2.2	3.0	150	410
1000	4.1	4.0	270	520

a Gordon and Strange (1978)

b Carr et al. (1978)

$$\rho_- = 8/a^3 \qquad (5.6)$$

where a is the lattice constant. (f_H is defined by (5.5)).

We have shown our results for σ in table 4 which we calculated using (5.5) and the values of D given in table The Haven ratio was set equal to unity as it is not clear precisely which value to take and it is known that it should not differ from unity by more than a factor of 30%. (Corish and Jacobs 1973).

We see from table 4 that we also obtain approximate agreement with experiment though this is not such a reliable comparison because of uncertainties over the Haven ratio. However table 4 does show that the simulated lead fluoride has the main characteristic of a fastionic, viz. a sharp increase in conductivity over a relatively narrow temperature range. This temperature range lies between 600K and 800K and may be compared with the fastionic transition temperature T_s found experimentally for lead fluoride of 705K (Derrington et al 1976). We have not examined more precisely the temperature range over which the transition occurs in our simulation as we are more interested in the qualitative nature of the disorder above the transition, and do not consider our simulation would give especially good results for the behaviour at the transition.

Finally we look at the defect concentration d_c A defect, as we have already indicated in the introduction, is a vacancy or an interstitial for the fluorites. The existence

of vacancies and interstitials may be found by looking at correlated sequences of hops. A correlated sequence is when a hop occurs from one site (1) to another (2), from site 2 to site 3 and so on.

We define the time at which a hop from site 1 to site 2 takes place as the mean of the times at which the anion leaves site 1 and arrives at site 2, and specify the hop from site 1 to site 2 by the ordered pair (1, 2). Then if the time t at which (1, 2) takes place is before the time t^1 at which (2, 3) takes place, we may consider this as indicating the presence of an interstitial on site 2 for time $t-t^1$. Similarly if $t-t^1$ is negative, this corresponds to a vacancy at site 2.

We can count the interstitials and vacancies from a pictorial representation in which the hopping events are represented as points on a line parallel to a time axis and the correlation arrows are drawn to connect the points. An arrow pointing parallel to the positive direction of the time axis indicates that an interstitial is present for the time represented by the length of the arrow. Likewise, an arrow pointing along the negative direction of the time axis indicates that a vacancy is present. The total number of vacancies plus interstitials is found at any instant by counting the number of correlation lines that cut the line perpendicular to the time axis, that intersects the time axis at that instant. We find the average defect concentration namely the number of vacancies (or interstitials) per site by averaging the number of vacancies (or interstitials) over the run. By charge neutrality, the numbers of vacancies and

and interstitials are equal at any instant.

In this way we found that the defect concentration was 2% at 1000K. This result is somewhat surprising in view of the defect concentrations measured by neutron scattering measurements (Shapiro and Reidinger 1979) and Dickens et al (1979) are about 40% at that temperature. In section B we go on to look at a way of explaining this discrepancy. The value of 2% is in line with the values of 3% found for $SrCl_2$ by the same method of analysis as that outlined above (Dixon and Gillan 1980). It indicates that lead fluoride does not appear to show qualitatively different behaviour from the other fluorites looked at with molecular dynamics simulations.

(ii) Radial Distribution Functions

The radial distribution function $g_{\alpha\beta}(r)$ for a particle of species α at the origin is related to $n_\beta(r)$, the average number of particles of species β at distances between r and $r + \Delta r$ by

$$g_{\alpha\beta}(r) = \frac{V}{N_\beta} \frac{n_\beta(r)}{4\pi r^2} \qquad (5.7)$$

(Sangster and Dixon 1976). Here V is the volume of the box containing the N_β particles of species β. With this normalisation, $g_{\alpha\beta}(r)$ tends to unity at large r.

We obtained $g_{\alpha\beta}(r)$ for temperatures 400K, 600K, 800K, 900K and 1000K. The results at 400K and 1000K are plotted in figures 4a and 4b. $g_{\alpha\beta}(r)$ is calculated as a histogram where the resolution is $1/100 \times a(T)$ ($a(T)$ is given in Table 3).

The general forms of the radial distribution functions are similar to those obtained by Rahman (1976) for CaF_2, by

de Leeuw (1976, 1978) for $SrCl_2$ and by Dixon and Gillan (1980) for $SrCl_2$. The cation-cation and cation-anion distribution functions are typical of those found in solids, having large and rather sharp peaks out to large distances and troughs which descend almost to zero. The anion-anion distribution functions by contrast are rather similar to those found in liquids, even at 400K where there is no diffusion. This indicates that by comparison with the cations, the correlations between the anions are relatively weak. It is worth noting that the distribution functions for the anions are even more liquid like than in $SrCl_2$ (Dixon and Gillan 1980). (Figures 4a, 4b)

We also obtained the radial distribution function between sites and particles in a way identical to that described above for the other radial distribution functions. This time one of the position vectors is that of a site, the empty cube centre site, and the other position vector that of the anions. Our results are shown in figures 5a, 5b for 400K and 1000K. We used this radial distribution function to calculate the mean square displacement $\langle \eta^2 \rangle_{rs}$ of the anions at the regular sites since by this means we have automatically excluded the hopping particles.*

$\langle \eta^2 \rangle_{rs}$ is obtained by approximating the density associated with an anion vibrating about its regular site as

$$\rho(r) = \gamma' \left(\frac{\alpha}{\pi}\right)^{3/2} e^{-\alpha r^2} \qquad (5.7a)$$

where γ' is some factor (less than unity) which allows for the fact that some anions are in other regions of the lattice. We ignore the distortion from sphericity caused by anharmonicity.

* $\langle \eta^2 \rangle^+_{rs}$ is found for the cations from the simulation by averaging η over all time steps

Fig. 4a

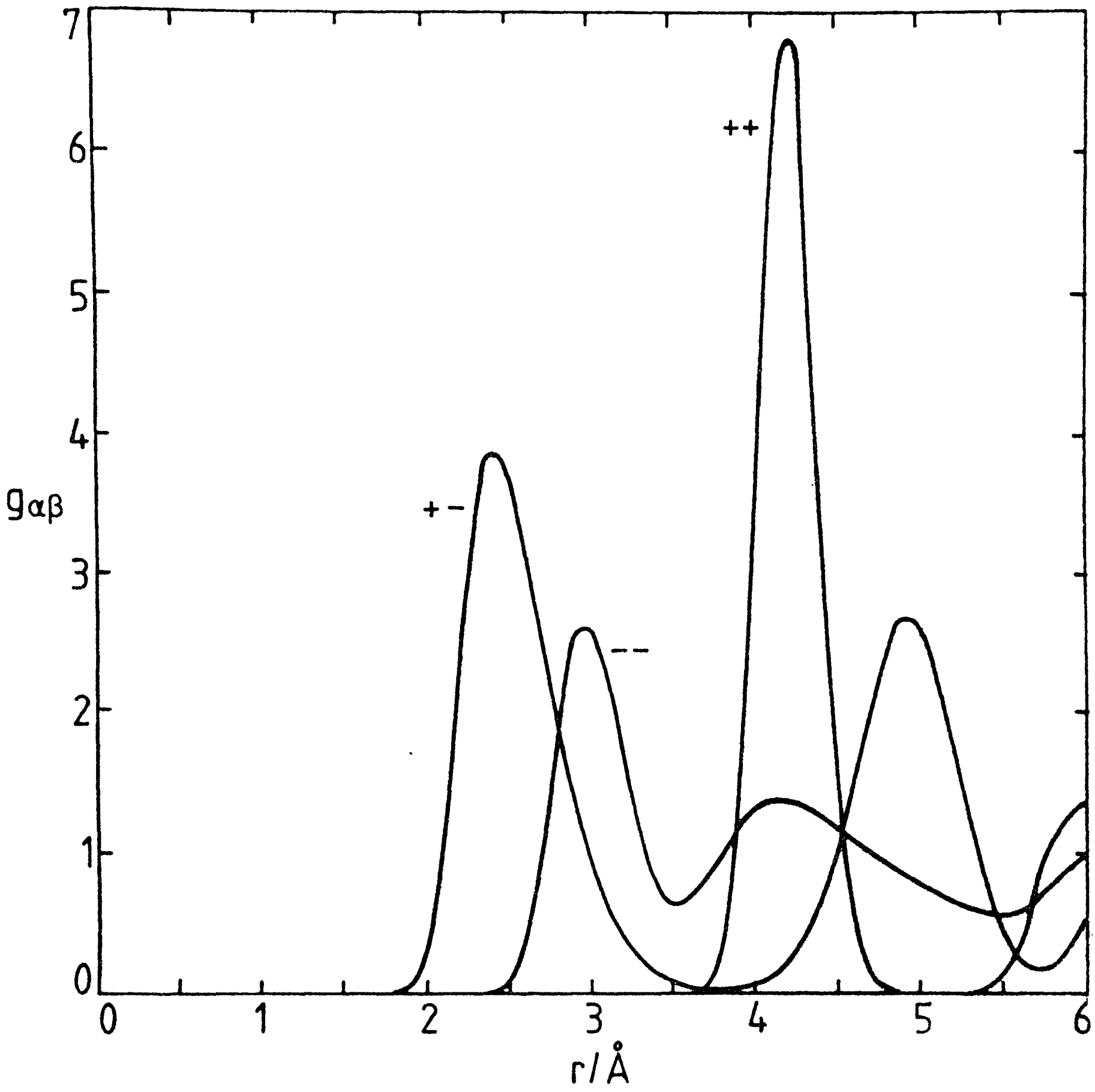

Radial distribution functions: T = 400 K

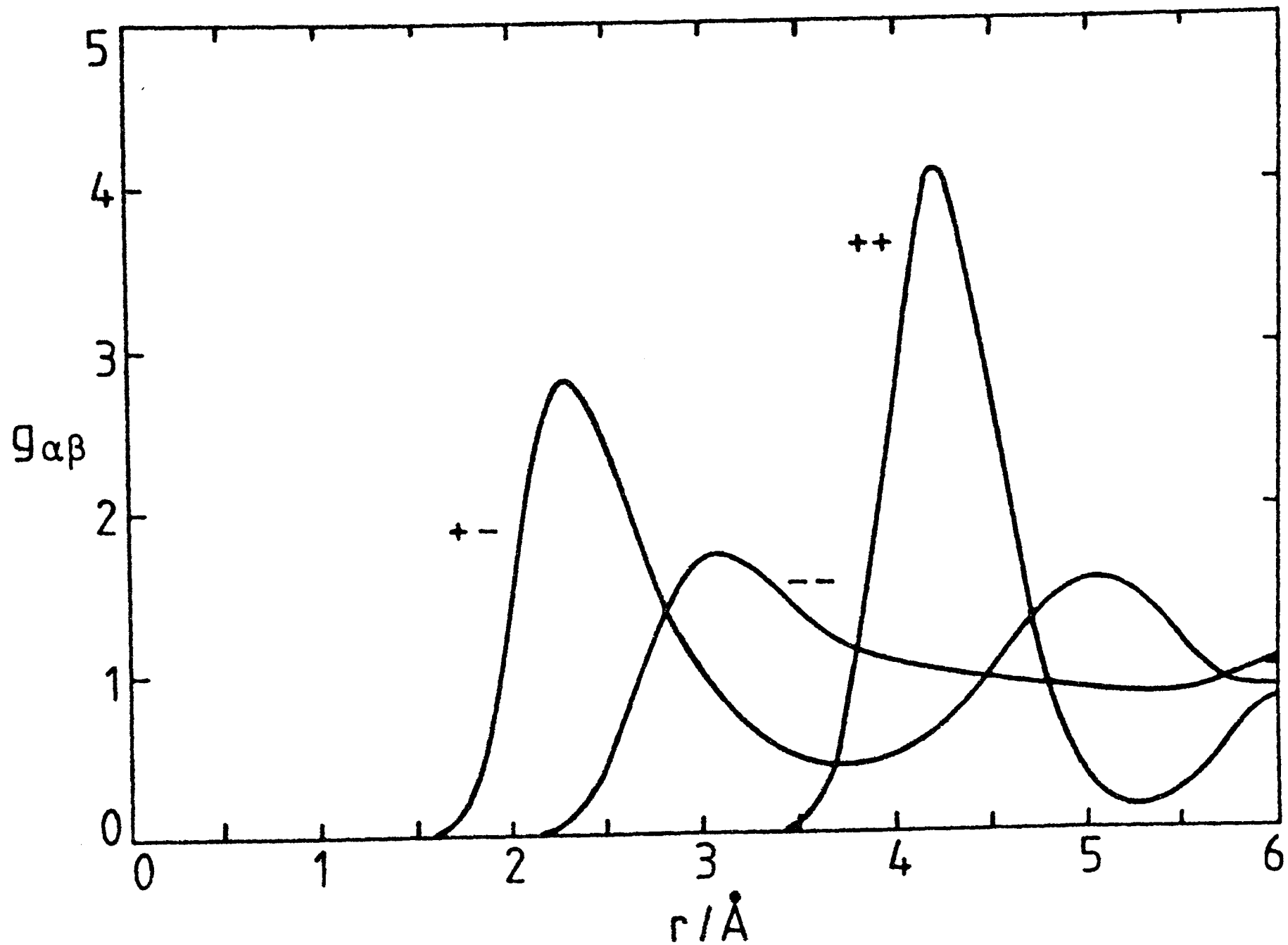

Radial distribution functions: T = 1000 K

Fig. 5a

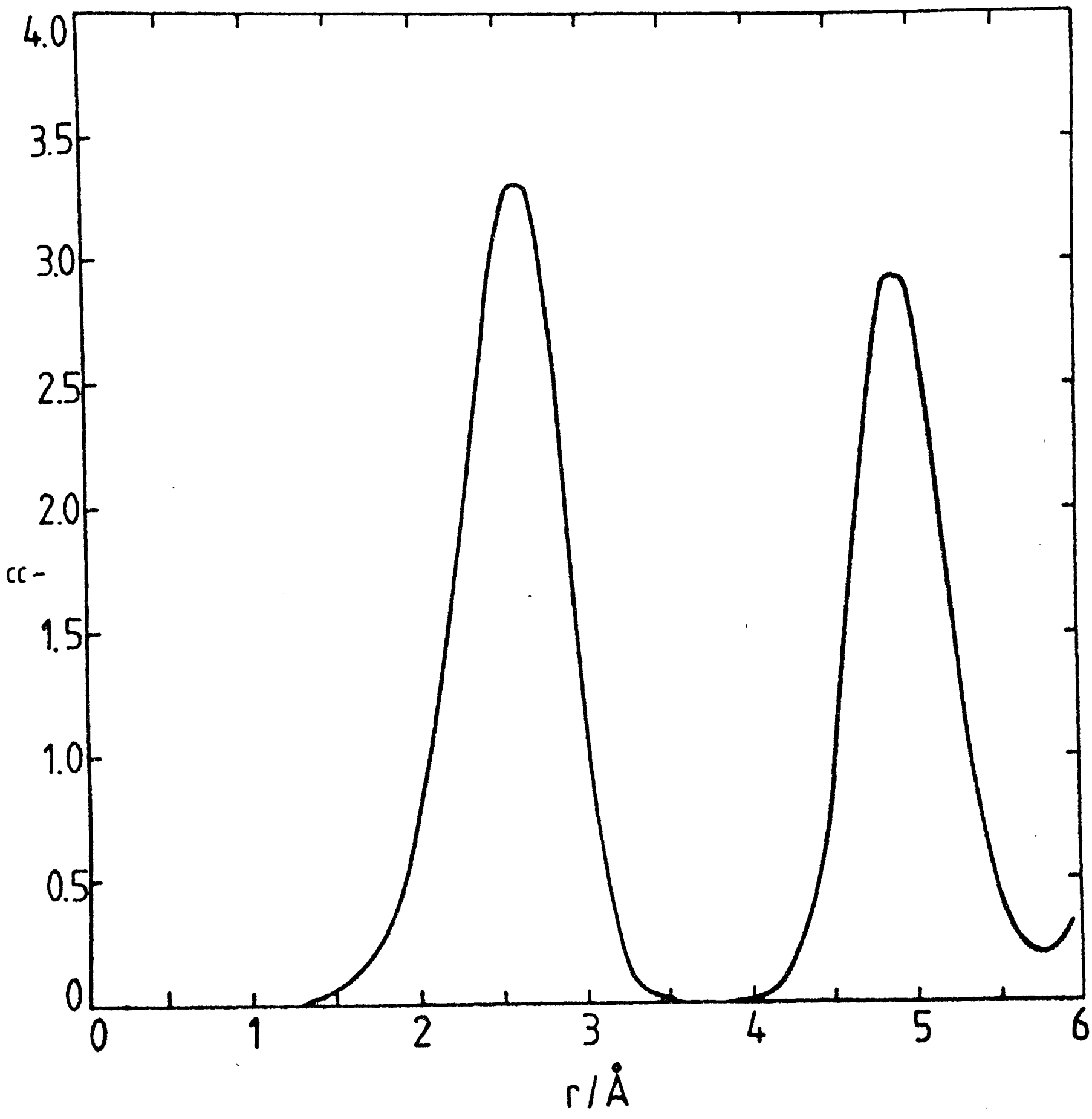

Distribution of anions w.r. to empty cube centre site:
T = 400 K

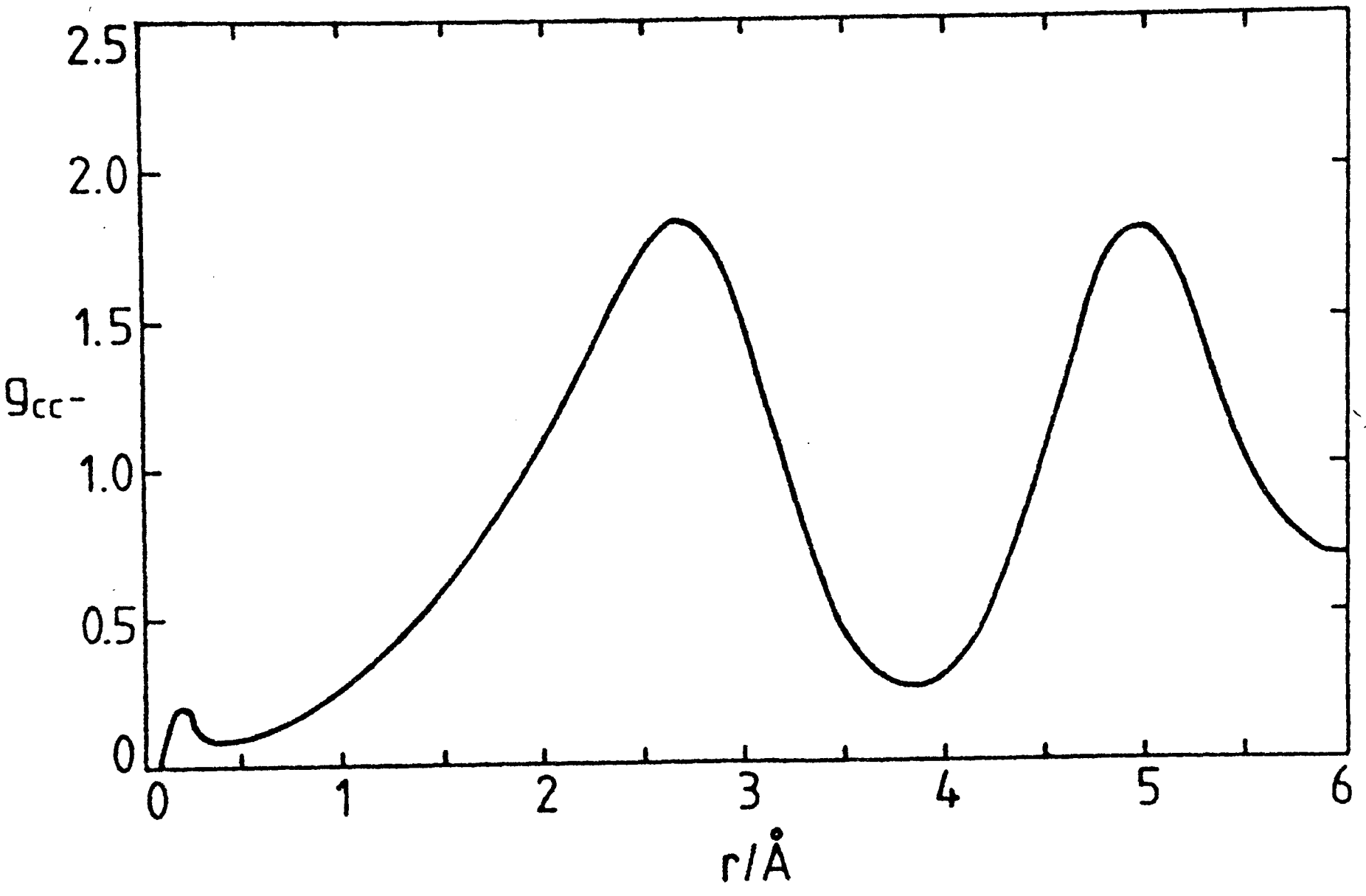

Distribution of anions w.r. to empty cube centre site:
T = 1000 K

Fig 5b

Now assuming the centre of the distribution be distributed with equal probability over a sphere of radius r_o (equals the distance from empty cube centre to the anion regular site = $\sqrt{3}a/4$ where a is the lattice constant). Also multiply by eight to count the eight anion neighbours of the cube centre site. Then the spherically averaged density due to anions on nearest neighbour sites is

$$\rho(r') = 8\gamma'\left(\frac{\alpha}{\pi}\right)^{3/2} \frac{1}{2}\int_0^{\pi} d\theta \sin\theta\, e^{-\alpha(r'^2 + r_c^2 - 2r' r_0 \cos\theta)} \qquad (5.8)$$

θ is the polar angle of the lattice position with respect to $\underline{r}'$ taken along the z axis. For large enough r' so that $2\alpha r_0 r'$ is much greater than unity we have

$$\rho(r') \simeq \frac{2\gamma'}{\alpha r_0}\left(\frac{\alpha}{\pi}\right)^{3/2} e^{-\alpha(r'-r_0)^2} \qquad (5.9)$$

Thus the value of $\langle r^2 \rangle$ is simply the second moment of the gaussian distribution where

$$r' = r - r_0$$

Then $$\alpha = \frac{\ln 2}{(r_{HWHM})^2} = \frac{3}{2\langle r^2\rangle} = \frac{3}{2\langle \eta^2\rangle_{rs}} \qquad (5.10)$$

where r_{HWHM} is the half width at half height for the gaussian $\rho(r')$ Equation (5.7) shows that $\rho(r')$ is proportional to the radial distribution function $g_{cc}(r)$ for the anions with respect to the cube centre site. Thus r_{HWHM} is the half width at half neighbour of the gaussian cube centred on $r = \sqrt{3}a/4$ for $g_{cc}(r)$.

We used equation (5.10) to obtain $\langle \eta^2 \rangle_{rs}$ for 400K, 600K, 800K, 900K and 1000K. Our results are given in table 5 where they are compared with the neutron scattering results of Dickens et al (1980) $\langle \eta^2 \rangle_e$. We see that we have reasonable agreement

Table 5

Mean Square Displacements of Anions

T(K)	$\langle\eta^2\rangle_{rs}$ (Å^2)	$\langle\eta^2\rangle_e^a$ (Å^2)
400	.30	0.10
600	.48	0.17
800	.67	0.30
900	.91	0.33
1000	1.12	0.35

[a] Dickens et al. (1980)

with these results.

(iii) Densities

The mean ion density $\rho_\alpha(\underline{r})$ gives the probability density of finding ions of species α at position $\underline{r}$ in the unit cell. It is defined by

$$\rho_\alpha(\underline{r}) = A < \sum_{i=1}^{N_\alpha} \delta(\underline{r} - \underline{r}_{i\alpha}) > \qquad (5.11)$$

where the sum goes over ions of species α, N_α being the total number of these species in the system and the brackets denote the equilibrium thermal average. Here the equilibrium average is found by averaging over all steps in a run. A is simply the reciprocal of the ion density in the regular lattice:

$$A = 8/a^3 \qquad \text{for anions} \qquad (5.12)$$

$$= 4/a^3 \qquad \text{for cations} \qquad (5.12a)$$

Thus a uniform distribution of ions would give a density of unity. Because our system is crystalline at all temperatures, the mean ion densities $\rho_\alpha(\underline{r})$ are periodic functions of the vector positions $\underline{r}$ even in the presence of anion disorder.

In order to calculate the $\rho_\alpha(\underline{r})$ we need to calculate the position of the underlying regular lattice. The method of doing this has already been described for the time dependent behaviour. The $\rho_\alpha(\underline{r})$ are computed by superimposing a cubic grid on the unit cell where each element of the grid had dimension $a/48$. Then the number of ions in each element was counted and the mean found over the different time steps. In order to improve the statistical accuracy we average over

the occupancies of symmetry related elements.

The data is presented in figures 6a, 6b. We have taken planar cross sections in the unit cell and constructed equal density contours. We have assumed the structure shown in Figure 2 where the anions are at (0 0 0), ($\frac{1}{2}$ 0 0) etc. The cross sections are taken in the $[0\ 0\ \frac{1}{2}]$ plane and the $[1\ 1\ 0]$ plane at temperatures of 600K and 1000K. Cation contours are shown by dotted lines and anion contours by smooth lines. The figure marking the contour is always to the right of the contour. There is symmetry about a vertical line bisecting the plot for the plots in the $[1\ 1\ 0]$ plane and about a diagonal for the plots in the $[0\ 0\ \frac{1}{2}]$ plane so that not all the contours have been marked.

It may be seen that at the lower temperature, 600K, both cations and anions are strongly localised about their respective regular sites. This is consistent with the fact that in the hopping analysis very few hops are recorded at that temperature and indicates that the transition to fastionic behaviour has not yet taken place. The spherical symmetry of the cation distribution indicates that the cation vibrations are not appreciably anharmonic in contrast with the anion distribution which shows a strong tetrahedral distortion towards the cube centre sites.

The high temperature (1000K) results are quite similar to the low temperature results. Both cation and anion distributions are broader in the $[1\ 1\ 0]$ plane but their basic form remains the same. The most interesting point is that in

Fig. 6a

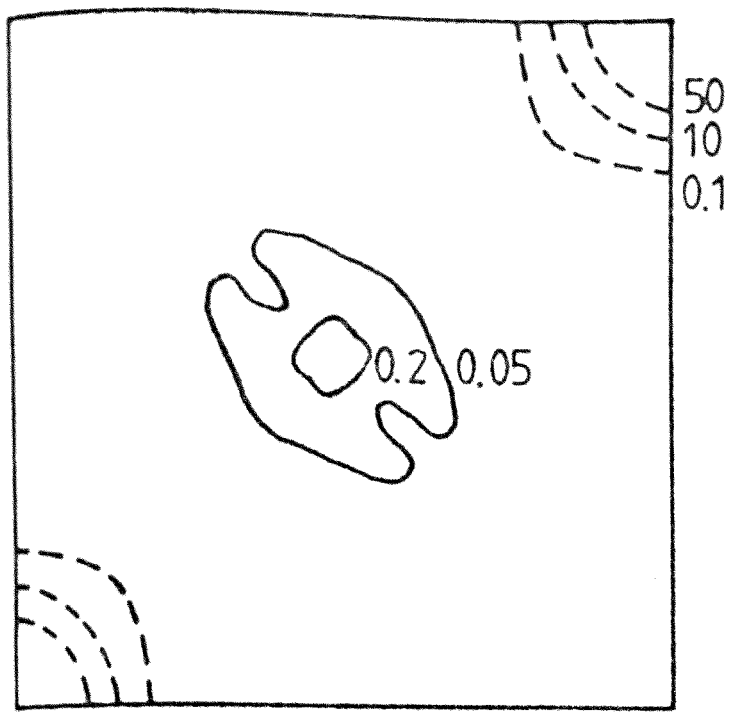

T = 600K
[00¼]plane

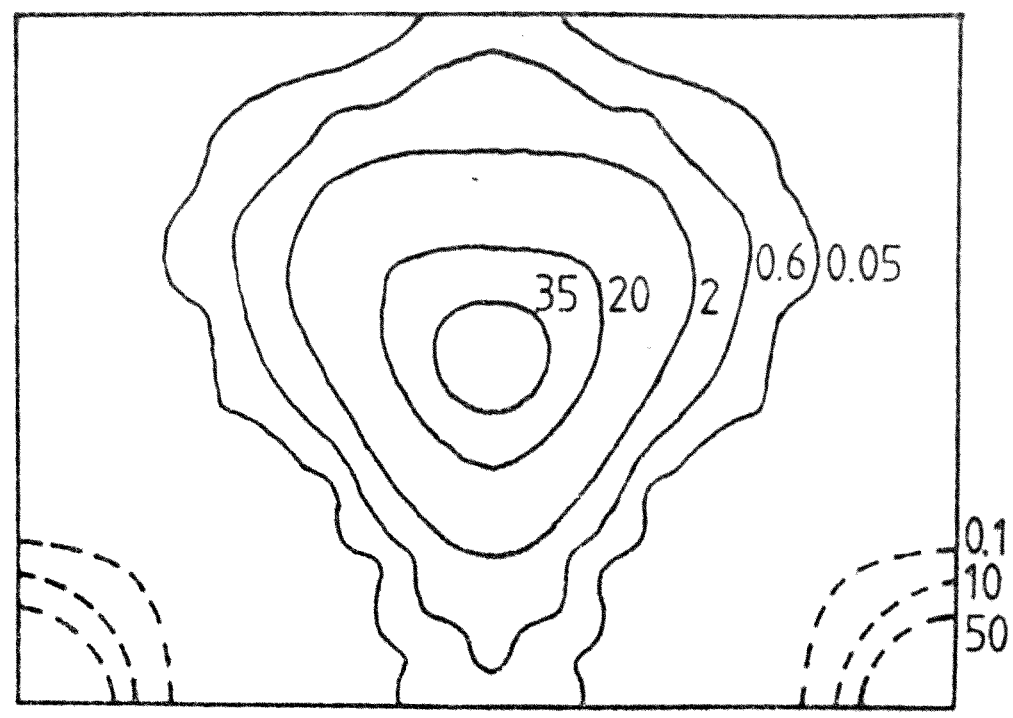

T=600K
[110]plane

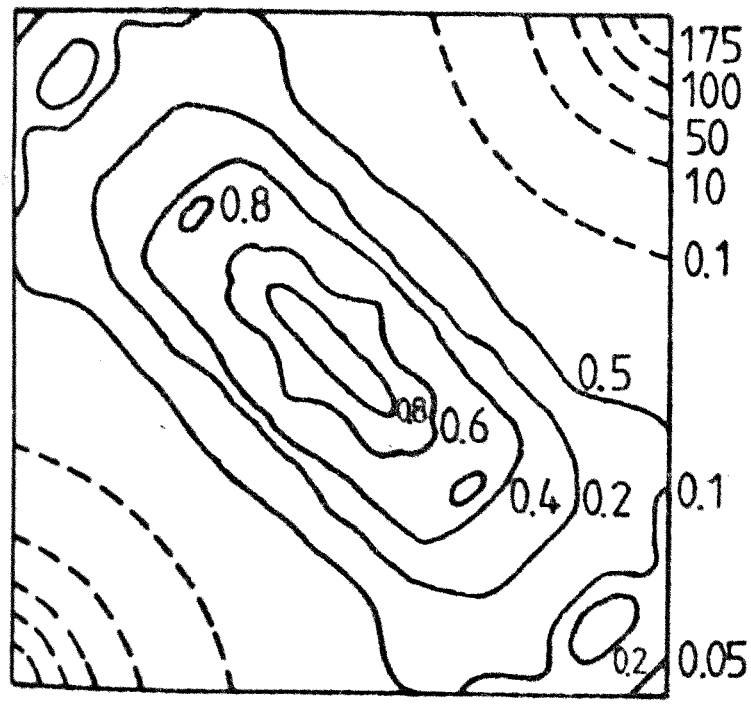

T = 1000K
[00¼] plane

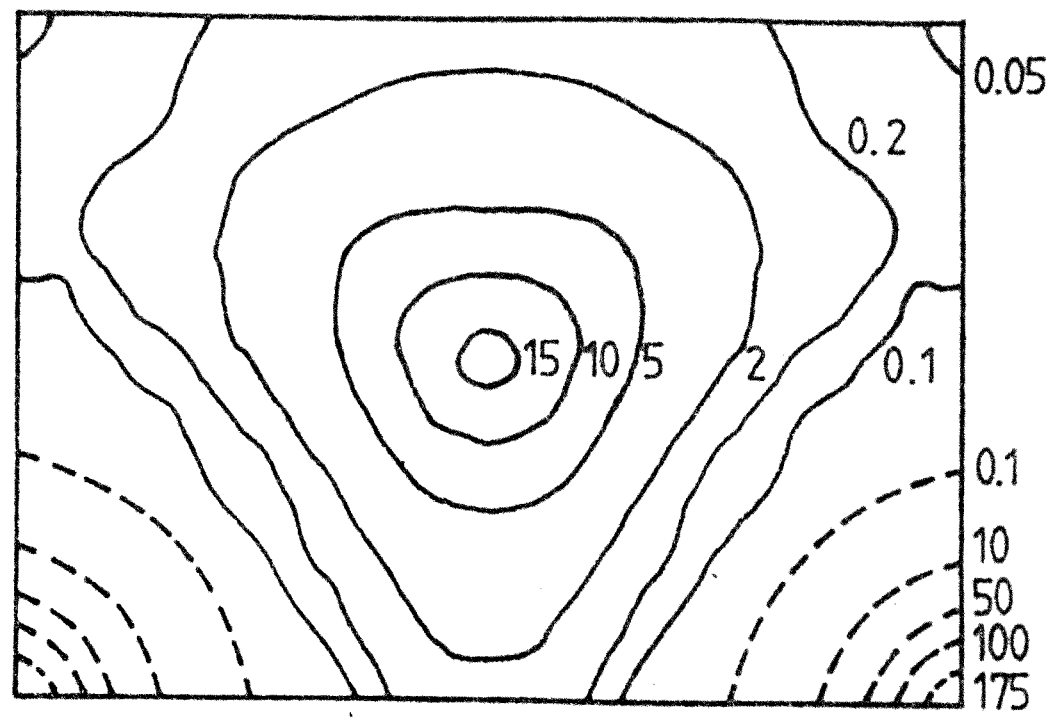

T=1000K
[110] plane

Fig. 6b

Density contours from lead fluoride simulation

Density contours from lead fluoride simulation

agreement with the results on $SrCl_2$ (Dixon and Gillan 1980) there is no peak in the anion density at the cube centre sites. Therefore the number of anion interstitials which reside on these sites for an appreciable time is negligible to within our statistical accuracy. The contours in the $(0\ 0\ \frac{1}{4})$ plane indicates density along and near the cube edges of the anion sublattice suggesting that the anions spend a significant fraction of their time hopping in these directions, and is consistent with the hopping analysis. Again this result is the same as for CaF_2 (Dixon and Gillan 1978) and $SrCl_2$ (Dixon and Gillan 1980).

We conclude then, that as with the hopping analysis, the results are very similar to the fluorites which have been looked at by simulation, CaF_2 and $SrCl_2$, so that the qualitative nature of the disorder in lead fluoride is like that in the other fluorites.

5B. k-Space Analysis

As we commented in section A, the defect concentrations we find from the hopping analysis differ by an order of magnitude from the defect concentrations quoted for PbF_2 from neutron scattering results. However, the methods of obtaining the defect concentration differ very greatly because the experimentalist has to work in momentum space. We describe in this section the method that is normally used to find the defect concentration experimentally (from neutron scattering), and show how we were able to apply the same method to our molecular dynamics simulation, treating the simulated lead fluoride as the 'crystal' from which we obtain data.

The defect concentration is, as we will show, an ill defined term and so it is more accurate to consider the neutron scattering measurements as finding the ion densities in momentum space. This is because the static disorder corresponding to the thermally averaged densities that we describe at the end of section A is obtained experimentally by looking at the intensities of Bragg peaks. These are obtained from the elastic scattering cross section. The intensities depend on the elastic structure factors

$$F_+(g) = \frac{1}{N_c} < \sum_{i=1}^{N_c} e^{igr_i} > \qquad (5.12)$$

where the sum is over all cations and N_c is the total number of cations, and

$$F_-(g) = \frac{1}{N_a} < \sum_{i=1}^{N_a} e^{igr_i} > \qquad (5.13)$$

summing over all anions, given that $N_a = 2N_c$ is the total number of anions.

Equations (5.12) and (5.13) are the Fourier transforms of the average densities of cations and anions respectively. Thus in principle it should be possible by Fourier transforming the set of elastic structure factors for sufficient reciprocal lattice vectors to obtain the ion average densities, albeit with finite resolution. We could then directly compare experimental results with the contours shown in figure 6. However the errors occurring due to overlap and extinction and the difficulty of obtaining the data at sufficient reciprocal space points to give a reasonable resolution, preclude this.

The experimentalists then commonly adopt the approach

of calculating the structure factor for various models of ion distributions with a number of free parameters eg. defect concentration and anharmonicity. These parameters are then found so as to minimise the difference between the model elastic structure factors and experimental structure factors. The model which gives the best fit is then considered to represent the ion distribution in the real crystal.

Given this approach, we have various ways in which we could compare our simulation results directly with experiment. The most straight forward is to evaluate the elastic structure factors from our simulation and compare them directly with the experimental structure factors. Unfortunately no experimental structure factors could be made available to us. We therefore achieved our comparison by treating the simulation structure factors as 'experimental' data and comparing these structure factors with a model that resembled those used by Dickens et al (1980) in the analysis of their measurements.

The model we chose is in fact a generalisation of models I to V of Dickens et al (1980) although here we use different notation. Our model is as follows: All the cations are on regular sites and have harmonic vibrations only with a mean square displacement $\langle \eta^2 \rangle_{cat}$. There are (1-D) anions on each regular site which have vibrations specified by a mean square displacement $\langle \eta^2 \rangle_{an}$. They also have anharmonic vibrations which we parametise through the anharmonicity γ. Here α, γ are defined from the potential seen by the (modelled) anions,

$$V = \alpha \eta^2 + \xi \gamma \eta_x \eta_y \eta_z \qquad (5.14)$$

where

$$\zeta = +1 \qquad \text{for anions at } (\tfrac{1}{4}\ \tfrac{1}{4}\ \tfrac{1}{4})\ a \tag{5.14a}$$

$$\zeta = -1 \qquad \text{for anions at } (-\tfrac{1}{4}\ \tfrac{1}{4}\ \tfrac{1}{4})\ a \tag{5.14b}$$

Here, as throughout this section, position vectors are relative to the cation in the unit cell. This form of the potential is obtained directly from symmetry considerations as the anions are at sites of tetrahedral symmetry. In addition there are μD anions on the 'diagonal' sites which we define as

$$\begin{aligned} a(\tfrac{1}{4}\ \tfrac{1}{4}\ \tfrac{1}{4}) + \quad & x\ a\ (1\ 1\ 1) \\ & x\ a\ (-1\ -1\ 1) \\ & x\ a\ (1\ -1\ -1) \\ & x\ a\ (-1\ 1\ -1) \end{aligned} \tag{5.15}$$

and

$$\begin{aligned} a(-\tfrac{1}{4}\ \tfrac{1}{4}\ \tfrac{1}{4}) + \quad & x\ a\ (-1\ -1\ -1) \\ & x\ a\ (-1\ 1\ 1) \\ & x\ a\ (1\ -1\ 1) \\ & x\ a\ (1\ 1\ -1) \end{aligned} \tag{5.16}$$

From figure 2 it may be seen that these defect positions lie on the lines joining anions to empty cube centre sites, the lines along which they vibrate anharmonically. x, the distance along these lines, is also a parameter in our model. We represent these anions as vibrating harmonically, with mean square displacement $\langle \eta^2 \rangle_{diag}$. The remaining $(1-\mu)D$ anions are placed halfway along the cube edges, namely the lines joining an anion to a nearest neighbour anion. In our model

they have a mean square displacement $\langle \eta^2 \rangle_{\substack{\text{cube} \\ \text{edge}}}$

We now derive the elastic structure factor for arbitrary reciprocal lattice vector which we can then compare with elastic structure factors from the simulation.

Equations (5.12) and (5.13) can be written as follows:

$$F_g^{\pm} = \mathcal{S}_g \langle e^{ig\cdot\eta_f} \rangle \qquad (5.17)$$

where the geometrical structure factor, $\mathcal{S}_g$ is

$$\mathcal{S}_g = \sum_s e^{ig\cdot\underline{r}_s} \qquad (5.18)$$

Here the sum is taken over ions on regular or defect sites within one unit cell at positions $\underline{r}_s$ with respect to the cation. η is the displacement of the ion from its regular or defect site at $\underline{r}_s$.

Next we average separately over regular sites, the diagonal sites and the cube edge sites:

$$F_g = \underset{\text{(regular sites)}}{\mathcal{S}_g \langle e^{ig\cdot\eta_f} \rangle} + \underset{\text{(diagonal sites)}}{\mathcal{S}_g' \langle e^{ig\cdot\eta_f} \rangle'} + \underset{\text{(cube edge sites)}}{\mathcal{S}_g'' \langle e^{ig\cdot\eta_f} \rangle''} \qquad (5.19)$$

and

$$F_{+g} = \mathcal{S}_g^{+} \langle e^{ig\cdot\eta_f} \rangle^{+} \qquad (5.20)$$

We look first at the regular cation sites using Bloch's identity (Marshall and Lovesey 1971) viz.

$$\langle e^{i\underline{g}\cdot\underline{\eta}_f} \rangle = e^{-1/2\langle(\underline{g}\cdot\underline{\eta}_f)^2\rangle} = e^{-W(\underline{g})} \tag{5.21}$$

where W(g) is the Debye-Waller factor that can be written as

$$W(\underline{g}) = g^2 \langle \eta^2 \rangle / 6 \tag{5.22}$$

Thus $$F_{+\underline{g}} = e^{-g^2\langle\eta^2\rangle^+/6} \tag{5.23}$$

At the regular anion sites, the anharmonic term has to be considered too. Using classical theory,

$$\langle e^{i\underline{g}\cdot\underline{\eta}_f} \rangle = \frac{1}{Z} \int e^{-\beta(\alpha\eta^2)} (1 + \xi\gamma\eta_x\eta_y\eta_z)\, e^{i\underline{g}\cdot\underline{\eta}_f}\, d\eta_f \tag{5.24}$$

where

$$Z = \int e^{-\beta(\alpha\eta^2)} (1 + \xi\gamma\eta_x\eta_y\eta_z)\, d\eta_f \tag{5.25}$$

and

$$\beta = 1/K_B T \quad , \quad K_B = \text{Boltzmann's Constant} \tag{5.26}$$

We find

$$\langle e^{i\underline{g}\cdot\underline{\eta}_f} \rangle = \langle e^{i\underline{g}\cdot\underline{\eta}_f} \rangle_{harm} \left[1 - i\gamma\beta\xi g_x g_y g_z \frac{(\langle\eta^2\rangle^3)}{27}\right] \tag{5.27}$$

where $\langle \quad \rangle_{harm}$ indicates that the average is to be calculated for a purely harmonic potential. This average is found in the same way as for cations: $\langle e^{i\underline{g}\cdot\underline{\eta}_f} \rangle_{harm} = g^2\langle\eta^2\rangle_{LAT}/6$ (5.28)

where $\langle\eta^2\rangle_{LAT}$ is the mean square displacement for anions at lattice sites

Next we calculate the geometrical structure factors for the anions. These are

$$S_{\underline{g}} = 2\cos\pi/2\,(h+k+l) \tag{5.29}$$

$$
\begin{aligned}
\mathcal{S}_g' &\equiv S_1(x) \\
&= 1/2\Big[\cos\pi/2\, a\left\{g_x(1+4_x)+g_y(1+4_x)+g_z(1+4_x)\right\} \\
&\quad +\cos\pi/2\, a\left\{g_x(1+4_x)+g_y(1-4_x)+g_z(1-4_x)\right\} \\
&\quad +\cos\pi/2\, a\left\{g_x(1-4_x)+g_y(1+4_x)+g_z(1-4_x)\right\} \\
&\quad +\cos\pi/2\, a\left\{g_x(1-4_x)+g_y(1-4_x)+g_z(1+4_x)\right\}\Big]
\end{aligned}
\tag{5.30}
$$

and

$$
\begin{aligned}
\mathcal{S}_g'' &\equiv S_2 \\
&= \cos\pi/2\, a\,(g_x+g_y+g_z)\times\frac{1}{3}\Big[2\cos\left(\frac{g_x\pi a}{2}\right)+ \\
&\quad 2\cos\left(\frac{\pi g_y a}{2}\right)+2\cos\left(\pi g_z a/2\right)\Big]
\end{aligned}
\tag{5.31}
$$

From equations (5.27), (5.28), (5.29), (5.30), and (5.31) (adapting (5.28) slightly for different defect sites) we obtain by substituting into (5.19)

$$
\begin{aligned}
F_g = {} & 2(1-D)e^{-g^2\langle m^2\rangle_{latt}/6}\Big[\cos\pi/2\, a(g_x+g_y+g_z) \\
& -\gamma\beta g_x g_y g_z\left(\frac{\langle m^2\rangle_{latt}}{27}\right)^3\sin\pi/2\, a\,(g_x+g_y+g_z) \\
& +\mu D\left(e^{-g^2\langle m^2\rangle_{diag}/6}\right)S_1(x) \\
& +(1-\mu)D\left(e^{-g^2\langle m^2\rangle_{\substack{cube\\edge}}/6}\right)S_2
\end{aligned}
\tag{5.32}
$$

We used equations (5.23) and (5.32) to find a set of elastic structure factors for the cations and anions respectively for the twenty-five smallest reciprocal lattice vectors of the fluorite lattice. This set was compared with elastic structure factors given in table 6 * for the same set of reciprocal lattice vectors calculated from a simulation run

* on page 96

at 1000K using equations (5.12) and (5.13) (for these I gratefully acknowledge Dr. Dixon).

The way in which we compared the two sets of structure factors was as follows. For each species of ions a programme was written to minimise the sum of the squares of the differences of the model structure factor and the simulation structure factor, summing over the reciprocal lattice vectors $\underline{g}$.

For anions the minimisation was achieved by allowing the parameters D, γ, $\langle \eta^2 \rangle_{tet}$, $\langle \eta^2 \rangle_{diag}$ and $\langle \eta^2 \rangle_{cube\ edge}$ to vary. The sum of squares, $\sum_{squares}$ was printed out once the difference between model and simulation structure factors had been minimised. As the model is not a perfect representation of the anion distribution, $\sum_{squares}$ will be non zero. We found it in all cases to be well above the lower limit that the minimisation programme set so that $\sum_{squares}$ is a measure of how successful the model is in fitting to the simulation structure factors. The whole procedure was repeated for different values of x, the distance of the 'diagonal' sites along the lines joining the anions to the empty cube centre sites. For each value of x, we allowed the fraction μ of the defects on the diagonal sites to take two values, $^2/3$ and 1, and did the minimisation for each value. We could have fitted μ and x along with the other parameters but then there would be so many parameters fitted that it would be difficult to establish how adequate the model was. By fixing μ and x, for each minimisation, we could compare the value of $\sum_{squares}$ for different minimisations. Clearly the values of μ and x that gave the least sum of squares would correspond to the distribution that gave the

best fit. μ was fixed at $^2/3$ and 1 because $\mu = ^2/3$ corresponds to model V of Dickens et al (1980) and $\mu = 1$ corresponds to their model V. Thus we had a direct comparison with their results.

Our values for x, μ, $\langle\eta^2\rangle_{salt}$, $\langle\eta^2\rangle_{cube\ edge}$, $\langle\eta^2\rangle_{diag}$, γ, D, $\sum_{squares}$ are shown in table 7 . Our results show up the very interesting fact that the defect concentration D varies between about 15% and 40% whilst the sum of squares changes very little for different values of x and μ . This indicates that there are no values of x and μ that are singled out as giving a much better fit to the simulation results. We would take this to imply that there are no well defined interstitial sites in agreement with our real space analysis.

In table 8 we compare our values of x, μ, $\langle\eta^2\rangle_{salt}$, $\langle\eta^2\rangle_{cube\ edge}$, $\langle\eta^2\rangle_{diag}$, γ and D for the smallest $\sum_{squares}$ we obtained with those of Dickens et al (1980) at 973K (our values are nominally at 1000K) It is worth noting that Dickens et al (1980) treated x as a parameter to be fitted and they did not try to compare D values for different x as we did.

Whilst agreement is not especially good, the fact that D especially varies so markedly for different values of x must be taken into account. It indicates that great caution must be used in interpreting the results from this type of model fitting.

The other conclusion we may make is that the value D is an order of magnitude greater than the value of the defect

Table 6

Structure Factors for PbF_2 from Simulation at 1000K.

$\underline{g} = (g_x, g_y, g_z)$	Cation Structure Factor	Anion Structure Factor
(1,1,1)	.907	-.113
(2,0,0)	.878	-1.083
(2,2,0)	.771	.644
(2,2,2)	.677	-.361
(3,1,1)	.700	.102
(3,3,1)	.540	-.100
(3,3,3)	.417	.115
(4,0,0)	.595	.266
(4,2,0)	.523	-.192
(4,2,2)	.459	.101
(4,4,0)	.355	.063
(4,4,2)	.312	-.033
(4,4,4)	.213	.024
(5,1,1)	.417	-.036
(5,3,1)	.322	.045
(5,3,3)	.250	-.047
(5,5,1)	.195	-.028
(5,5,3)	.151	.025
(6,0,0)	.311	-.062
(6,2,0)	.274	.040
(6,2,2)	.241	-.0328
(6,4,0)	.188	-.034
(6,4,2)	.166	.022
(7,1,1)	.192	.021
(7,3,1)	.150	-.023

Table 7

Lead Fluoride Structure Factor Fit to Molecular Dynamics Results (Anions)

X	μ	$\langle\eta^2\rangle_{latt}$	$\langle\eta^2\rangle_{cube\ edge}$	$\langle\eta^2\rangle_{diag}$	γ $eV\mathring{A}^{-3}$	D %	Σ squares
0.25	67	.65	.50	.46	.54	17.3	.009
	100	.57	.17	1.5	.79	38	.01
.05	67	.63	.63	1.8	.59	22.5	.008
	100	.54	.17	1.2	.81	42	.009
.075	67	.54	.69	.66	.62	36.8	.006
	100	.54	.17	.94	.68	38.8	.008
.1	67	.58	.44	.54	.44	26.7	.005
	100	.61	.17	.98	.48	23.2	.010
.125	67	.61	.32	.58	.47	19.5	.006
	100	.66	.17	2.3	.49	15.6	.012
.15	67	.62	.43	3.6	.56	19.7	.009
	100	.66	.17	2.7	.52	15.3	.013
.175	67	.64	.38	2.3	.49	16.2	.008
	100	.66	.17	3.9	.52	15.0	.013
.2	67	.66	.33	3.2	.46	15.0	.008
	100	.67	.17	5.2	.51	14.1	.012
.225	67	.66	.36	3.4	.47	14.7	.008
	100	.64	.17	6.0	.60	17.1	.013
.25	67	.66	.34	3.2	.44	14.6	.008
	100	.65	.17	4.7	.47	15.8	.013

(T = 1000K)

Table 8

Anion Distribution Parameters from k-Space Analysis

.	x	μ(%)	$\langle\eta^2\rangle_{latt}$	$\langle\eta^2\rangle_{cube\ edge}$	$\langle\eta^2\rangle_{diag}$	γ	D
(i)	.1	67	.58	.44	.54	.44	26.7
(ii)	.18	67	.35	1.14	1.71	.77	43.3

(i) Results from k space Analysis at 1000K.

(ii) Results of Model V of Dickens et al. (1980) at 973K.

Table 9

Cation Mean Square Displacements at 1000K

$\langle\eta^2\rangle_{cat}(\text{Å}^2)$	$\langle\eta^2\rangle^+_{rs}(\text{Å}^2)$	$\langle\eta^2\rangle^+_{expt}(\text{Å}^2)$ [a]
0.182	0.211	0.26

[a] Dickens et al. (1980)

concentration (2 %) obtained from the hopping analysis (section A). This appears to go a long way towards resolving the discrepancy between experimental results and our real space analysis.

We have also evaluated the mean square displacement $\langle \eta^2 \rangle_{cat}$ for the cations by fitting that in the manner described for the anions but using equation (5.23). We compare this value in table 9 with the value $\langle \eta^2 \rangle^+_{rs}$ obtained from our real space analysis (section A) and the value obtained by Dickens et al (1980), $\langle \eta^2 \rangle^+_{expt}$. It is apparent that agreement with our real space analysis is good, providing a useful check and that the agreement with Dickens et al (1980) is reasonable.

CHAPTER 6

CONCLUSIONS

We have used a lattice gas model to represent Frenkel defects in the fluorite fastionics. This model consists of mobile particles confined to sites on a cubic lattice which interact through the Coulomb interaction and which have a site exclusion property where no particles are allowed on the same site. The free energy of the particles in this model has been evaluated and from that the chemical potential. From these results we have shown that our system shows first order, second order and diffuse transitions indicating that the Coulomb interaction can cause co-operative behaviour on a lattice.

We have obtained the critical defect concentration for our model, this being

$$\nu_c = 8.92\,10^{-3} \tag{6.1}$$

We have also obtained the reduced critical temperature t_c and critical chemical potential less the reduced Frenkel energy, μ'_c. Here reduced units implies division by $k_B T_0$ where

$$T_0 = \frac{e^2}{k_B \epsilon \epsilon_0 a} \tag{6.2}$$

Our results for t_c and μ'_c are

$$t_c = 7.54.\omega^{-3} \tag{6.3}$$

$$\mu'_c = -0.13 \tag{6.4}$$

μ'_c is the negative of the Frenkel energy for the static lattice for a system which has critical behaviour so that we may compare

$$\xi_c = \frac{\mu'_c}{k_B T_c} = 17.4 \qquad (6.5)$$

with the value of $\epsilon_r / k_B T_c$ of March et al (1980) for the fluorites of about 20. Given that fastionics show diffuse transitions which may be close to second order phase transitions we conclude that our model shows that Coulomb interactions could be responsible for the co-operative behaviour in fluorites.

We have also estimated the critical temperature T_c and Frenkel energy E_c for CaF_2 and PbF_2 and we find that

$$T_c = 725\,K \quad \text{for } CaF_2 \qquad (6.6)$$

$$T_c = 166\,K \quad \text{for } PbF_2 \qquad (6.7)$$

and that

$$\epsilon_c = 1.09\,eV \text{ for } CaF_2 \qquad (6.8)$$

$$E_c = 0.25\,eV \text{ for } PbF_2 \qquad (6.9)$$

We have seen that these results do not give good agreement with experiment especially for lead fluoride but consider that this may be due to using the static dielectric constant ϵ_r to calculate T_o where a dielectric constant modified to allow for local field effects might be better. This does point up an inadequacy in our model. Another place in which our model might easily be improved is to introduce

a temperature dependence for the Frenkel energy, assumed constant for this work.

We consider that our model may be applicable to other fastionics, notably silver iodide at temperatures below the transition temperature where the structure changes and the defects cannot be considered as vacancy-interstitial pairs. The reason is that the model predicts how Coulomb interactions will lead to co-operative behaviour, not necessarily looking at a sharp transition. We also hope to extend the applications of our model to other instances, than fastionics, of Coulomb interactions in an ionic solid.

We have also focussed our attention on lead fluoride because its high static dielectric constant indicates that the Coulomb interactions between defects might be modified sufficiently to cause qualitatively different behaviour.

We have obtained an interionic potential assuming rigid ions for lead fluoride given by

$$\varphi_{\alpha\beta}(r) = \frac{Z_\alpha Z_\beta e^2}{4\pi\epsilon_0 r} + A_{\alpha\beta}\, e^{-r/\rho_{\alpha\beta}} - \frac{C_{\alpha\beta}}{r^6} \qquad (6.10)$$

where α, β are the species of the ions, ϵ_0 is the vacuum permittivity, Z_α the charge on an ion of species α. $A_{\alpha\beta}$, $\rho_{\alpha\beta}$, $C_{\alpha\beta}$ are the short range potential parameters. We have assumed

$$A_{++} = \rho_{++} = C_{++} = 0 \qquad (6.11)$$

and $$C_{+-} = 0\,, \qquad (6.12)$$

and obtained

$$A_{--} = 10225\ eV \quad , A_{+-} = 12266 eV \tag{6.13}$$

$$\rho_{--} = 0.225\ \text{Å} \quad , \rho_{+-} = 0.516\ \text{Å} \tag{6.14}$$

$$C_{--} = 107.324\ eV\text{Å}^6 \tag{6.15}$$

This potential gives a static Frenkel energy in good agreement with the experimental value of 1.0 eV (March et al 1980) and we can show that at low temperatures defects in a simulated system using the potential are stable at the cube centre site in agreement with experiment (Lidiard 1974). The potential also gives reasonable values for the cohesive energies and elastic constants.

We used the potential (6.10) in a molecular dynamics simulation of lead fluoride and have found that the nature of the disorder in lead fluoride is qualitatively similar to that in CaF_2 (Rahman (1978) and Dixon and Gillan (1978)) and $SrCl_2$ (Dixon and Gillan 1980). The disorder was examined by looking at the mean fraction of particles which are hopping between regular sites (2%) and by the diffusion constant and conductivity at several temperatures where we obtain reasonable agreement with experiment. We also looked at the radial distribution functions for cation-cation, cation-anion and anion-anion interactions. We showed that as for the other fluorites, eg. Dixon and Gillan (1980) the cations show a solid like radial distribution function when correlated with each other and with the anions, but the anions have more liquid like behaviour because of weaker correlations with each other. In addition we evaluated contours of the mean ion density in two planes of the structure and found that

here too the ion distributions show a close resemblance to those of CaF_2 (Dixon and Gillan (1978) and $SrCl_2$ (Dixon and Gillan 1980).

We also evaluated the elastic structure factors $F_{\pm}$ for our simulation where

$$F_{\pm}(g) = \frac{1}{N} < \sum_{i=1}^{N_+} e^{ig \cdot r_i} > \qquad (6.16)$$

where the sum is over all cations (+), or anions (-) and $N_{+(-)}$ is the total number of cations (anions) g is a reciprocal lattice vector. We then compared the value of F_- with that of a model in which the anion defects are partly on the diagonal lines joining their regular sites to the empty cube centre sites in the fluorite lattice and partly mid-way along the cube edges, the lines joining nearest neighbour anions. We obtained values for the defect concentration D, the mean square displacements of the anions at regular sites, $<\eta^2>_{latt}$ on the diagonal lines $<\eta^2>_{diag}$ and on the cube edges $<\eta^2>_{cube\ edge}$ and the anharmonicity in the potential γ. This was done by varying these parameters to minimise the sum of squares, the sums of squares of the differences between model structure factors and simulation structure factors (summing over different values of g). The position along the diagonal lines was fixed and so was the fraction of defects μ at the diagonal sites. The procedure was then repeated for different values of the distance x of defects along the diagonal lines from the regular sites and for μ = 67% and 100%. The model that gave the best fit to our results had

$$X = \cdot 1 \qquad (6.17)$$

$$\mu = 2/3 \tag{6.18}$$

$$D = 26.7\,\% \tag{6.19}$$

$$\gamma = .44\ eV\mathring{A}^{-3} \tag{6.20}$$

$$\langle m^2 \rangle_{latt} = .58\,\mathring{A}^2 \tag{6.21}$$

$$\langle m^2 \rangle_{diag} = .54\,\mathring{A}^2 \tag{6.22}$$

$$\langle m^2 \rangle_{cube\ edge} = .44\,\mathring{A}^2 \tag{6.23}$$

These values show approximate agreement with the results obtained by Dickens et al (1980) using the same method on their neutron scattering results.

However we did find that by slightly altering the value of x, D varied between 15% and 40%, without making a big difference to the sum of squares. We conclude that great caution must be taken when using these models to fit an assumed defect distribution to the elastic structure factor. The large variation in values of D is we consider due to the fact that there are no stable defect sites for the interstitials in the fluorites, as has been shown up by the analysis of the simulation in real space.

It is encouraging to note that by this method of analysis we have shown that we can obtain defect concentrations for lead fluoride of the same order of magnitude as those obtained experimentally even though a real space analysis indictes that the number of anions hopping between regular sites is about 2%.

We consider that a similar analysis might reveal the

same results for the other fluorite fastionics and it might be interesting to try this method on other molecular dynamics simulations.

Thus we would conclude that a molecular dynamics simulation is of value in helping to interpret experimental results.

PART I REFERENCES

Allnatt A R and Cohen M H J. Chem. Phys. 40 1860 (1964)

Andersen H C 1977 in 'Modern Theoretical Chemistry' 5 Ed. Berne B J (New York: Plenum Press)

Axe J D 1965 Phys. Rev. 139 A1215

Beeman D 1976 J. Computational Phys. 20 130

Boyce J B and Huberman B A 1979 Phys. Reports 51 190

Carr V M, Chadwick A V and Saghafian R J. Phys. C: Solid St. Phys. 11 L637

Catlow C R A, Comins J D, Germano F A, Harley R T and Hayes W 1978 J. Phys. C: Solid St. Phys. 11 3197

Catlow C R A and Norgett M 1973 J. Phys. C: Solid St. Phys. 6 1325

Cochran 1966 in 'Phonons in Perfect Lattices and in Lattices with Point Imperfections' pp 53-70 (London: Oliver and Boyd)

Cochran 1971 CRC Crit. Rev. Solid St. Sci. 2 1

Corish J and Jacobs P W M 1973 in 'Surface and Defect Properties of Solids' 2 Chap. 7 (London: Chemical Society)

de Leeuw S W 1976 'Thesis' University of Amsterdam

de Leeuw S W 1978 Molec. Phys. 36 765

Derrington C E, Navrotsky A and O'Keeffe M 1976 Solid St. Commun. 18 47

Dickens M H, Hayes W, Hutchings M T 1976 J. de Physique 37 Suppl. 12 Colloque 11 C353

Dickens M H, Hayes W, Hutchings M T and Smith C 1979 'Fast Ion Transport in Solids' Eds. Vashishta, Mundy, Shenov (New York: Elsevier North Holland)

Dickens M H and Hutchings M T 1978 J. Phys. C: Solid St. Phys. 11 461

Dickens M H, Hayes W, Hutchings M T and Smith C 1980 UKAEA Report - AERE M.PD/NBS/153

Diller K M 1975 UKAEA Report TP 642

Dixon M and Gillan M J 1978 J. Phys. C: Solid St. Phys. 11 L165

Dixon M and Gillan M J 1980 'Fast Ion Transport in Solids' Eds. Vashishta, Mundy, Shenov. (New York: Elsevier North Holland) pp 701-704 see also J Phys C: Solid St. Phys 13 1917

Dixon M and Gillan M J 1980a J de Phys Suppl 7 Coll 6-24

Dworkin A F and Bredig M 1968 J. Phys. Chem. 72 1227

Faux I and Lidiard A B 1971 Z. Naturf. A26 62

Gillan M J and Dixon M J Phys C: Solid St. Phys 13 1505

Gordon R E and Strange J H 1978 J. Phys. C: Solid St. Phys. 11 3213

Hansen J P and McDonald I R 'Theory of Simple Liquids' (New York: Academic Press)

Hardy J P and Flocken J W 1970 CRC Crit. Rev. Solid St. Sci. 1 605

Hayes W 1974 in 'Crystals with the Fluorite Structure' Ed. Hayes W (Oxford: Clarendon)

Hayes W 1978 Contemp. Phys. 19 469

Holzapfel G and Sickert H 1975 Festkorperprobleme XV, 317

Hooper A 1978 Contemp. Phys. 19 147

Jones D A 1955 Proc. Phys. Soc. B68 165

Kittel C 1971 'Introduction to Solid State Physics' (New York: John Wiley and Sons)

Kurosawa T 1957 J. Phys. Soc. Japan 12 338

Liang C C and Joshi A V 1975 J. Electrochem Soc. 122 466

Lidiard A B 1957 Handbuch Der Physik Ed Flügge S (Berlin: Springer) pp 246-348

Lidiard A B and Norgett M J 1972 in 'Computational Solid State Physics' Ed. Herman F, Dalton N W, Koehler T R (New York: Plenum) 385

Lidiard A B 1974 in 'Crystals with the Fluorite Structure' ed Hayes W (Oxford: Clarendon) pp 101-84

Marshall W and Lovesey S W 1971 'Theory of Thermal Neutron Scattering' (Oxford: Clarendon)

March N H, Richardson D D and Tosi M P 1980 Sol. St. Commun. 35 903

Mayer J E and Mayer M G 1940 'Statistical Mechanics' (New York: John Wiley)

Mayer J E 1950 J. Chem. Phys. 18 1426

Morita T and Hiroikek 1961 Prog. Theor. Phys. 25 337

Norgett M 1974 UKAEA Report AERE-R7650

Onsager L 1939 J. Phys. Chem. 43 189

Rahman 1976 J. Chem. Phys. 65 4845

Résibois P M V 1968 'Electrolyte Theory' (New York: Harper and Row)

Salamon M B 1979 in 'Physics of Superionic Conductors' (Berlin: Springer) pp 1-4

Samara G A 1979 J. Phys. Chem. Solids 40 509
Samara G A 1976 Phys. Rev B 13 4529

Sangster M J L and Dixon M 1976 Adv. in Phys. 25 247

Shapiro and Redinger 1978

Steele B 1978 New Scientist 87 705

Stell G 1964 in 'The Equilibrium Theory of Classical Fluids' Part II Eds. Frisch H L and Lebowitz J L (New York: Benjamin)

Stell G and Wu K C 1975 J. Chem. Phys. 63 491

Weast R C 1980 Ed. of CRC Handbook of Chemistry and Physics' (61st Edition).

PART II

A NUCLEAR QUADRUPOLE INTERACTION IN ORDERED MAGNETS

CHAPTER 1

INTRODUCTION

The nuclear quadrupole interaction that we study is the pseudoquadrupole effect which arises from the hyperfine interaction. Our theory applies to the size of the effect in ordered magnets especially ferromagnets where recently it has attracted interest.

The pseudoquadrupole interaction is a term of quadrupole symmetry in the nuclear Hamiltonian arising from the hyperfine interaction between a nucleus and a net electronic moment. Physically it arises as follows: through the hyperfine interaction, the magnetic field due to the nuclear spin polarises the electronic moment, setting up a back field which itself polarises the nucleus. It is called the pseudoquadrupole effect to distinguish it from other terms of quadrupole symmetry in the nuclear spin which are due to the electrostatic quadrupole moment of the nucleus coupling to a local electric field gradient. At low temperatures the pseudoquadrupole effect is simply obtained from the hyperfine interaction taken to second order in perturbation theory (Bleaney 1967).

The existence of the effect was first pointed out by Van Vleck (Kellogget al 1940). Baker and Bleaney (1958) looked at the effect for ions in a crystal field and showed that it could be large for certain low lying excited states, for instance in praseodymium ethyl sulphate where it was several times the size of the other quadrupole interactions.

Experimentally, the effect was isolated and measured by Clauser et al (1966) looking at $TmCl_3.6H_2O$. Segel and Stroud (1975) measure a quadrupole anomaly in gallium metal predicted by Pykkö (1971). A full summary of experimental and theoretical work is given by Pykkö (1971).

We are interested in the size of the effect in cubic magnets because it may obscure the quadrupole effects which arise from magnetic ordering especially the magnetically induced electric field gradient. Estimates have been made in this context for impurities in iron and nickel by Aiga and Itoh (1971), Gehring and Williams (1974), Gehring (1974) and Demangeat (1975, I and II).

Estimates of the effect in ferromagnets have been made by the following authors: Turov and Petrov (1969), Zevin and Kaplan (1975), Boasson and Kaplan (1978) and Looyestijn et al (1979). They used second order perturbation theory valid only at low temperatures. Stewart et al (1977) look at the pseudoquadrupole effect at dilute cobalt impurities in iron, though here they simply call it a 'back field' mechanism.

However a formalism valid at all temperatures may be obtained by looking at thermodynamic perturbation theory (Gehring and Walker (1981), to be published). We use this approach in Chapter 2 to show that the pseudoquadrupole effect can be simply related to the difference between transverse and longitudinal magnetic susceptibilities. This result is reasonable given that the effect arises from the response of the electronic moments to the field from the

nuclear spin.

We also show how the result can be used to predict the behaviour with temperature of the effect in both localised (Heisenberg) and itinerant magnets. Numerical estimates are given for pure iron and nickel and at impurities in these metals since here the quadrupole interactions have been measured and there is considerable interest due to the presence of magnetically induced gradients as described above.

The effect is also estimated by us for $GdAl_2$ where a large temperature dependent quadrupole interaction was measured by Degani and Kaplan (1973) and ascribed to the pseudoquadrupole interaction by Zevin and Kaplan (1975).

This account of the pseudoquadrupole effect in magnets is confined to those which are cubic and have zero or quenched orbital momentum because as shown in Chapter 2 there are terms in the hyperfine interaction which we do not take account of in our subsequent theory but which will contribute to the effect. These terms disappear for cubic symmetry and effectively zero orbital momentum. However, our formalism can be generalised to cubic antiferromagnets since the theory in Chapter 2 will apply to that case.

Finally, the material described above and given in Part II of this thesis is organised as follows: Chapter 2 contains a description of the origin of the effect and shows how it is related to the local transverse and longitudinal susceptibilities. The behaviour of the effect at different

temperatures including temperatures close to criticality is discussed in Chapter 3 and a formalism given for calculations in the localised and a simplified itinerant model. Numerical estimates at host and impurity nuclei in iron and nickel are given and comparisons made with experimental measurements. In Chapter 4 we look at the quadrupole interaction in $GdAl_2$ and consider explanations additional to the pseudoquadrupole interaction which we find is too small to account for the experimental data. Chapter 5 concludes Part II of this thesis.

CHAPTER 2

THE THEORY OF THE PSEUDOQUADRUPOLE EFFECT

2A. The Origin of the Effect

The Hamiltonian for the interaction of a nucleus spin $\underline{I}$ with an electron spin $\underline{S}$ and orbital momentum $\underline{L}$ may be written as:

$$H_{hf} = -g\mu_0 g_I \mu_N \left\{ \frac{8\pi}{3} \delta(\underline{r}) \underset{(i)}{\underline{I}} \cdot \underline{S} + \frac{1}{r^3} \underset{(ii)}{\underline{I}} \cdot \underline{L} + \frac{1}{r^3} \left[\frac{3}{r^2} \underset{(iii)}{(\underline{I}\,\underline{r})} (\underline{S}\,\underline{r}) - \underline{I}\,\underline{S} \right] \right\} \qquad (2.1)$$

where g, g_I are the electronic and nuclear g factors and μ_0, μ_N the Bohr and nuclear magnetons (Freeman and Watson 1961, I). This expression describes all the interactions which could lead to the pseudoquadrupole effect. The first term (i) is the Fermi contact term (Fermi 1930) and the second and third terms (ii) and (iii) respectively the orbital and dipolar contributions to the hyperfine interaction.

The interaction responsible for the pseudoquadrupole effect in cubic systems with quenched or zero orbital momentum is the Fermi contact term. Marshall (1958) has shown that the dipolar term will vanish at sites of cubic symmetry and it is clear that the orbital term will not contribute if the orbital moment can be neglected.

Because of the contact term, the nucleus couples to s state core electrons and to conduction electrons, whose wave functions overlap with the nucleus. These electrons in turn couple to magnetic d or f electrons via the exchange

interaction and covalent mixing (Freeman and Watson 1961, I). There is thus an effective coupling between the nucleus and the net magnetisation within the range of the coupling, that is the origin of the phenomena of the hyperfine fields and the Knight shift as well as of the pseudoquadrupole effect. Through this coupling the magnetic moments respond to the field of the nuclear spin so that a back field is set up that polarises the nucleus (again via the same mechanism) causing the pseudoquadrupole interaction (vide Chapter I).

We now set up our formalism for the pseudoquadrupole effect using thermodynamic perturbation theory.

The total Hamiltonian for our system will consist of electronic and nuclear contributions, H_{el} and H_{nuc} and $V = \sum_n V_n$ where V_n is the hyperfine interaction at the nth nucleus of spin $\underline{I}_n$. It comes from H_{hf} ((2.1)). We will show that V_n is given by $\underline{I}_n.\underline{B}_n$ where $\underline{B}_n$ depends on the magnetisation. Then, by expanding the free energy F in powers of V to order V^2 using the Brout (1960) identity we can obtain the terms of quadrupole symmetry in $\underline{I}$ which make up the quadrupole effect.

Defining

$$H(\lambda) = H_{nuc} + \lambda \sum_n V_n + H_{el} \qquad (2.2)$$

then

$$F = F(0) + \sum_n \int_0^1 d\lambda \langle V_n \rangle_\lambda \qquad (2.3)$$

where

$$\langle V_n \rangle_\lambda = \frac{Tr\ V_n e^{-\beta H(\lambda)}}{Tr\ e^{-\beta H(\lambda)}} \qquad (2.4)$$

(Brout (1960)).

Thus

$$\langle V_n \rangle_\lambda = \langle V_n \rangle_0 - \lambda \sum_m \int_0^\beta \left[\langle V_m(\eta) V_n \rangle_0 - \langle V_m \rangle_0 \langle V_n \rangle_0 \right] d\eta + O(V^3) \tag{2.5}$$

so that

$$F = F(0) + \Delta F_1 + \Delta F_2 + O(V^3) \tag{2.6}$$

where

$$\Delta F_1 = \sum_n \langle V_n \rangle_0 \tag{2.7}$$

$$\Delta F_2 = \int_0^1 d\lambda \; \lambda \sum_{n,m} \int_0^\beta d\eta \left[\langle V_m(\eta) V_n \rangle_0 - \langle V_m \rangle_0 \langle V_n \rangle_0 \right] \tag{2.8}$$

$$\beta = 1/k_B T \quad (k_B = \text{Boltzmanns Constant}) \tag{2.9}$$

and

$$V_n(\eta) = e^{\eta H(0)} V_n e^{-\eta H(0)} \tag{2.10}$$

ΔF_1 is the contribution to the free energy of the nuclear spins interacting with a magnetic field $\underline{B}_n$ arising from the electronic moments (ie. the normal hyperfine interaction):

$$\Delta F_1 = g_I \mu_N \sum_n \langle \underline{B}_n \rangle_0 \cdot \underline{I}_n \tag{2.11}$$

ΔF_2 contains the terms from only one nuclear spin which are responsible for the pseudoquadrupole effect, but also has contributions from cross terms $V_n \; V_m$ $n \neq m$ to which the Suhl Nakamura effect (Suhl (1960)), Nakamura (1958) is attributed.

We now describe our model for the hyperfine interaction V_n: We write V_n as:

$$V_n = \int A(\underline{r} - \underline{R}_n)\, \underline{M}(\underline{r})\, d\underline{r} \cdot \underline{I}_n \qquad (2.12)$$

where $A(\underline{r} - \underline{R}_n)$ represents the effective coupling between the nuclear spin $\underline{I}_n$ and the magnetisation $\underline{M}(\underline{r})$. For localised moments

$$\underline{M}(\underline{r}) = \underline{M}_m\, \delta(\underline{r} - \underline{R}_m) \qquad (2.13)$$

We do not attempt to calculate $A(\underline{r} - \underline{R}_n)$ from first principles but model it as follows:

Localised moments

$$A = A_0\, \delta_{m,n} \qquad (2.14)$$

if the nucleus is at a magnetic site,

$$= \frac{1}{z}\, A_1\, \delta_{m,n+\rho} \qquad (2.14a)$$

if the nucleus is at a non magnetic site and experiences a transferred hyperfine interaction with its z nearest neighbours at the sites $\{n+\rho\}$

Itinerant magnets:

$$A(\underline{k}) = \int A_i(\underline{r} - \underline{R}_n)\, e^{i\underline{k}\cdot(\underline{r}-\underline{R}_n)}\, d\underline{r} \qquad (2.15)$$

$$= A_i \quad |\underline{k}| \leq k_{max} \qquad (2.15a)$$

$$= 0 \quad |\underline{k}| > k_{max} \qquad (2.15b)$$

where $\frac{4}{3}\pi k_{max}^3$ = Brillouin Zone Volume (2.15c)

Our model assumes that it is reasonable to give A a finite range in <u>real</u> space in the localised case and a finite range in <u>momentum</u> space for itinerant moments. Whilst this is not exactly consistent, it will be appropriate as long

as $A(\underline{r} - \underline{R}_n)$ is approximately given by a Gaussian centred at $\underline{R}_n$.

2B. Localised Magnets

We write the hyperfine interaction term using equations (2.12), (2.13) and (2.14):

$$V_n = \sum_m A(\underline{R}_n - \underline{R}_m)\, \underline{M}_m \cdot \underline{I}_n \qquad (2.16)$$

$$\text{where } A(\underline{R}_n - \underline{R}_m) = A_o\, \delta_{m,n}, \quad n \text{ is a magnetic site} \qquad (2.17)$$

$$= \frac{1}{z} A_1\, \delta_{m,n+p}, \quad n \text{ is a non magnetic site} \qquad (2.17a)$$

We can also express equation (2.16) in terms of the Fourier transforms

$$\underline{M}_{\underline{k}} = \sum_m \underline{M}_m\, e^{i\underline{k}\cdot\underline{R}_m} \qquad (2.18)$$

$$A_{\underline{k}} = \sum_m e^{i\underline{k}\cdot(\underline{R}_n - \underline{R}_m)} A(\underline{R}_n - \underline{R}_m) \qquad (2.19)$$

as

$$V_n = \sum_{\underline{k}} e^{i\underline{k}\cdot\underline{R}_n} A_{\underline{k}}\, \underline{M}_{\underline{k}} \cdot \underline{I}_n \qquad (2.20)$$

Equations (2.11), (2.16) and (2.17) can be used to write A_o and A_1 in terms of the hyperfine field at saturation, $\underline{B}_o$:

$$g_I \mu_N \underline{B}_o = A_o \langle \underline{M}_n \rangle_o \qquad (2.21)$$

$$= A_o\, \underline{M}_o \quad n \text{ is magnetic} \qquad (2.21a)$$

$$= A_1 \langle \underline{M}_{n+\rho} \rangle_o \quad n \text{ is non magnetic} \qquad (2.21b)$$

$$= A_1\, \underline{M}_o \qquad (2.21c)$$

We can use equations (2.8), (2.16) and (2.21) to write the

pseudoquadrupole effect in terms of the magnetic susceptibilities and the saturation hyperfine field:

$$\Delta F_2^{nn} = -\frac{1}{2} \sum_n \sum_\nu \langle (I_n^\nu)^2 \rangle S_{nn}^{\nu\nu} \tag{2.22}$$

where $\nu = x, y, z$,

$$S_{nn}^{\nu\nu} = \frac{1}{\mu_0} \sum_m \sum_{m'} A(R_n - R_m) A(R_n - R_{m'}) \chi_{mm'}^{\nu\nu} \tag{2.23}$$

$$= \frac{1}{\mu_0} \sum_K |A(K)|^2 \chi_K^{\nu\nu} \tag{2.23a}$$

where

$$\chi_{mm'}^{\nu\nu} = \mu_0 \int_0^\beta d\eta \left[\langle M_m^\nu(\eta) M_{m'}^\nu \rangle - \langle M_m^\nu \rangle \langle M_{m'}^\nu \rangle \right] \left(\frac{V}{N}\right) \tag{2.24}$$

and

$$\chi_K^{\nu\nu} = \mu_0 \int_0^\beta d\eta \left[\langle M_K^\nu(\eta) M_K^\nu \rangle - \langle M_K^\nu \rangle^2 \right] \left(\frac{V}{N}\right) \tag{2.24a}$$

$\chi_{mm'}^{\nu\nu}$ and $\chi_K^{\nu\nu}$ are the space and wave vector dependent magnetic susceptibilities. Below T_c in a cubic magnet, $\chi^{xx} = \chi^{yy} \neq \chi^{zz}$

ΔF_2^{nn} may be separated into the terms of quadrupole symmetry which constitute the pseudoquadrupole effect and an isotropic term

$$\Delta F_2^{nn} = \sum_n \langle (I_n^z)^2 - \frac{1}{3} I(I+1) \rangle P_{pq} - \frac{I(I+1)}{6} \sum_n \sum_\nu S_{nn}^{\nu\nu} \tag{2.25}$$

where we define the pseudoquadrupole parameter

$$P_{pq} = \frac{1}{2} \left(S_{nn}^{xx} - S_{nn}^{zz} \right) \tag{2.26}$$

(analogously to the quadrupole parameter defined in Stone (1980)). We write P_{pq} in terms of the difference between the ~~local~~ longitudinal and transverse magnetic susceptibilities, $\tilde{\chi}$ (if the nuclei are at a magnetic site) and $\tilde{\tilde{\chi}}$ (if the nuclei

are at non magnetic sites) where

$$\tilde{\chi} = \sum_{\underline{K}} \left(\chi^{xx}_{\underline{K}} - \chi^{zz}_{\underline{K}} \right) \qquad (2.27)$$

and

$$\tilde{\tilde{\chi}} = \frac{1}{Z^2} \sum_{\rho\rho'} \left(\chi^{xx}_{n+\rho\, n+\rho'} - \chi^{zz}_{n+\rho\, n+\rho'} \right) \qquad (2.28)$$

$$= \frac{1}{N} \sum_{\underline{K}} |\gamma_{\underline{K}}|^2 \left(\chi^{xx}_{\underline{K}} - \chi^{zz}_{\underline{K}} \right) \qquad (2.28a)$$

where

$$\gamma_{\underline{K}} = \frac{1}{Z} \sum_{\rho} e^{i\underline{K}\cdot\underline{\rho}} \qquad (2.29)$$

The ρ's are defined in equation (2.14a)

Equations (2.27) and (2.28a) apply only for spins on a Bravais lattice; in Chapter 3 (section A) we show how (2.28a) can be generalised to spins on two sublattices.

Then from equations (2.21), (2.23a), (2.26), (2.27) and (2.28) we find that

$$\rho_{pq} = \frac{1}{2\mu_0} A_0^2 \tilde{\chi} \qquad \text{(n is a magnetic site)} \qquad (2.30)$$

$$= \frac{1}{2\mu_0} A_0^2 \tilde{\tilde{\chi}} \qquad \text{(n is a non magnetic site)} \qquad (2.30a)$$

where

$$A_0 = \frac{g_I \mu_N B_c}{m_e} \qquad (2.31)$$

Thus the temperature dependence of the pseudoquadrupole effect arises from the variation of the difference between the local transverse and longitudinal susceptibilities with temperature. We note that this effect goes as g_I^2 and as the square of the hyperfine field and is independent of the nuclear electrostatic quadrupole moment Q. Clearly it will

be zero above the transition temperature T_c where $\chi^{xx} = \chi^{zz}$ from cubic symmetry.

Next we look at itinerant magnets where the results have very much the same form.

2C. Itinerant Magnets

In this case the magnetisation $M(\underline{r})$ is a continuous function of $\underline{r}$ so that

$$V_n = \int d\underline{r}\; A_i(\underline{r} - \underline{R}_n)\, \underline{M}(\underline{r}) \cdot \underline{I}_n \qquad (2.32)$$

$$= \sum_{\underline{K}} e^{i\underline{K}\cdot\underline{R}_n} A_i(\underline{K})\, \underline{M}(\underline{K}) \cdot \underline{I}_n \qquad (2.32a)$$

where

$$\underline{M}(\underline{K}) = \frac{N}{V} \int d\underline{r}\; e^{i\underline{K}\cdot\underline{r}}\, \underline{M}(\underline{r}) \qquad (2.33)$$

and $A(\underline{k})$ is given by equation (2.15)

From equations (2.11) and (2.32a)

$$\Delta F_1 = \sum_n g_I \mu_N \underline{B}_0 \cdot \underline{I}_n \qquad (2.34)$$

$$= \sum_n \sum_K e^{i\underline{K}\cdot\underline{R}_n} A_i(\underline{K}) \langle \underline{M}(\underline{K}) \rangle \cdot \underline{I}_n \qquad (2.34a)$$

Thus

$$g_I \mu_N B_0 = \frac{V}{N^2} \sum_G A_i(G) \langle \underline{M}(G) \rangle \qquad (2.35)$$

$$\simeq \frac{V}{N^2} A_i(0) \langle \underline{M}(G = 0) \rangle \qquad (2.36)$$

$$= \frac{V}{N} A_i \underline{M}_0 \qquad (2.37)$$

(Here we assume that $A(\underline{k})$ is zero outside the Brillouin zone, as described in section A). We then use identical reasoning to that given in section B to obtain P_{pq}:

$$\Delta F_2^{nn} = -\frac{1}{2} \sum_n \sum_\nu \langle I_n^{\nu 2} \rangle_0 \, S_{inn}^{\nu\nu} \tag{2.38}$$

where

$$S_{inn}^{\nu\nu} = \frac{1}{\mu_0} \int dr \int dr' \, A_i(R_n - r) A_i(R_n - r') \chi_i^{\nu\nu}(r - r') \tag{2.39}$$

$$= \frac{1}{\mu_0} \sum_k |A_i(k)|^2 \chi_{ik}^{\nu\nu} \tag{2.39a}$$

$$\chi_i^{\nu\nu}(r - r') = \mu_0 \int_0^\beta d\eta \left[\langle M^\nu(r,\eta) M^\nu(r') \rangle - \langle M(r) \rangle \langle M(r') \rangle \right] \tag{2.40}$$

and

$$\chi_{ik}^{\nu\nu} = \mu_0 \int_0^\beta d\eta \left[\langle M_k^\nu(\eta) M_k^\nu \rangle - \langle M_k^\nu \rangle^2 \right] \tag{2.41}$$

From equation (2.25) we deduce

$$\rho_q = \frac{1}{2} \left(S_{inn}^{xx} - S_{inn}^{zz} \right) \tag{2.42}$$

$$= \frac{1}{2\mu_0} A_i^2 \, \tilde{\chi}_i \tag{2.42a}$$

where

$$\tilde{\chi}_i = \frac{1}{N} \sum_k \left(\chi_{ik}^{xx} - \chi_{ik}^{zz} \right) \tag{2.43}$$

and

$$A_i = \frac{N}{V} \frac{g_I \mu_N \beta_0}{M_0} \tag{2.44}$$

(from (2.37)).

Thus we have the same result as for the localised model, namely the pseudoquadrupole effect varies directly as the difference between the local transverse and longitudinal susceptibilities. The comments after equation (2.31) in section B will then apply here too.

We do not look at non magnetic sites in itinerant

magnets except at impurities in very dilute alloys which are discussed below.

2D. Impurities

As we discuss in the introduction and in section C of Chapter 3, there is interest in the origin of the interactions of quadrupole symmetry measured at dilute alloys to which the pseudoquadrupole effect might contribute. We therefore apply our theory to this case too.

(i) Localised Magnets

We have to consider separately the case for a magnetic impurity where there is a moment M_I and a 'non magnetic' impurity at which M_I is small compared to the host moment, or is zero.

By generalising equations (2.30) and (2.31) we obtain

$$P_{pq} = \frac{1}{2\mu_c} A^2_{I_{mag}} \left(\chi^{xx}_I - \chi^{zz}_I\right) \qquad (2.45)$$

for a nucleus at a magnetic site where

$$A_{Imag} \equiv g_I \mu_B B_I / M_I \qquad (2.46)$$

B_I is the hyperfine field at the impurity site

and χ^{xx}_I and χ^{zz}_I are the local susceptibilities at the impurity site. These susceptibilities may well be different from those of the pure host as we shall discuss in Chapter 3 section A.

At a non magnetic site,

$$P_{pq} = \frac{1}{2\mu_c} A^2_{I_{non}} \sum_{pp'} \left(\chi^{xx}_{n+p\,n+p'} - \chi^{zz}_{n+p\,n+p'}\right) \qquad (2.47)$$

where the impurity is at site n and ρ, ρ' specify its nearest neighbours. The hyperfine field at the impurity site is from a transferred hyperfine interaction with the nearest neighbour host moments so that for a moment M_H at host sites,

$$A_{I\,non} = \frac{g_I \mu_B B_I}{M_H} \qquad (2.48)$$

If we assume the dilution model applies, namely the impurity has zero moment and does not disturb the neighbouring host atoms, the susceptibilities will be those of the unperturbed host to a good approximation.

(ii) Itinerant Magnets

If we adapt equations (2.32), (2.39) and (2.42) we find

$$g_I \mu_N \underline{B}_I = \int d\underline{r}\; A_I(\underline{r} - \underline{R}_n)\, \underline{M}_n^I(\underline{r}) \qquad (2.49)$$

and

$$\rho_{\rho\eta}^I = \frac{1}{2\mu_0} \int d\underline{r} \int d\underline{r}'\; A_I(\underline{r} - \underline{R}_n) A_I(\underline{r}' - \underline{R}_n) \chi_I^{\nu\nu}(\underline{r} - \underline{r}') \qquad (2.50)$$

(where I refers to the impurity at site n).

For a magnetic impurity the main contribution to a hyperfine field will come from the magnetisation within the impurity cell (Freeman and Watson 1961, I). If we assume that other contributions can be ignored by comparison with that from the impurity cell then we find

$$g_I \mu_N B_I = A_I \int_{\text{impurity cell}} d\underline{r}\; M_I(\underline{r}) = A_I\, M_I \qquad (2.51)$$

For a non magnetic impurity the hyperfine field arises from interaction with the magnetisation in the neighbouring cells. We assume the dilution model is valid, a good assumption for impurities with low atomic number but not so

good otherwise (although neighbouring host moments differ from bulk moment by a few per cent at most). (Sayers 1976). Then we obtain the following approximation for P^I_{pq} analogous to the local moment case:

$$P^I_{pq} = \frac{1}{2\mu_0} A^2_{I\,non} \frac{1}{N} \sum_{\underline{k}} |\gamma_{\underline{k}}|^2 \left[\chi^{xx}_{\underline{k}} - \chi^{zz}_{\underline{k}} \right] \qquad (2.52)$$

where A_{Inon} is given in (2.48).

P^I_{pq} within the dilution model would differ from the pure case by the presence of $|\gamma_{\underline{k}}|^2$. We can assume that if we ignore $|\gamma_{\underline{k}}|^2$, P^I_{pq} would then provide an upper estimate of the pseudoquadrupole parameter.

Other Considerations

We have in the above theory ignored contributions from any unquenched orbital angular momentum at the impurity site. We know however that they will be present as there is an unquenched orbital moment (Demangeat 1975 I, II).

Nevertheless, we do not think that neglect of these contributions is a major source of error from the following reasoning.

It is possible to model the full hyperfine interaction (ie. including terms (ii) and (iii) in the Hamiltonian (2.1) using the approach outlined in sections A and C. The difference made by the presence of an orbital moment is that it will contribute to the magnetisation and so there will be a contribution to P_{pq} from the orbital susceptibility. The neglect of the latter at the impurities we look at in section C, Chapter 3 is unlikely to make a significant difference to

validity of our results in view of the other approximations made (which are discussed in that section).

However, it is interesting to note that if account were taken of the orbital contribution to the susceptibility, our theory would apply to examples where orbital momentum cannot be neglected.

CHAPTER 3

THE MAGNITUDE OF THE PSEUDOQUADRUPOLE EFFECT

We have shown in Chapter 2 that the pseudoquadrupole parameter P_{pq} is determined by the difference in the transverse and longitudinal susceptibilities $\tilde{\chi}$. In section A we evaluate the susceptibilities for the localised model within the molecular field and random phase approximations (RPA) and we look at the temperature dependence of the effect. Section B contains a discussion of the behaviour of $\tilde{\chi}$ near criticality. We describe a simplified itinerant model for $\tilde{\chi}$ in section C appropriate to iron and nickel, evaluate P_{pq} at host and impurity nuclei and compare the results with experiment.

3A. The Localised Model

Localised spin interactions are given by the Heisenberg Hamiltonian

$$H = -\tfrac{1}{2} \sum_{m,n} J(m-n)\, \underline{S}_n \cdot \underline{S}_m \qquad (3.1)$$

The molecular field approximation provides a means of determining the approximate way in which the susceptibilities behave at all temperatures. Here the Heisenberg Hamiltonian is replaced by a set of single ion Hamiltonians

$$H_{mf} = -\sum_n J(n)\, S^z_m \langle S^z_{m+n} \rangle \qquad (3.2)$$

Thus the spin-spin interactions are approximated by the effective field

$$\underline{h}_{mf} = \frac{1}{g\mu_B} \sum_m J(n-m) \langle S^z \rangle \, \hat{\underline{z}} \qquad (3.3)$$

$$= \frac{1}{g\mu_B} J(0) \langle S^z \rangle \hat{z} \qquad (3.3a)$$

($\hat{z}$ is the unit vector parallel to the z axis).

In the simplest version of molecular field theory, the transverse susceptibility is evaluated from an effective field

$$h_{eff} = h^x_m \hat{x} - \frac{1}{g\mu_B} J(0) \langle S^z \rangle \hat{z} \qquad (3.4)$$

where h^x_m is the external field (||x axis) at site m

giving

$$\chi^{xx} = \frac{\xi}{J(0)} \qquad (3.5)$$

where $$\xi = \mu_0 (g\mu_B)^2 \qquad (3.6)$$

χ^{zz}_0 is obtained from the fluctuation dissipation theorem and by using the derivative of the Brillouin function with respect to a small applied field $h^z \hat{z}$:

$$\chi^{zz}_0 = \frac{\partial \langle S^z \rangle}{\partial h^z} \Big|_{h^z=0} \mu_0 g\mu_B \qquad (3.7)$$

$$\langle S^z \rangle = S B \left(\beta S J(0) \langle S^z \rangle + \beta h^z g\mu_B S\right) \qquad (3.8)$$

$$\chi^{zz}_0 = \xi \left(\langle (S^z)^2 \rangle - \langle S^z \rangle^2\right) \beta \qquad (3.9)$$

Thus for $T < T_c$,

$$\tilde{\chi}_{mf} = \chi^{xx}_0 - \chi^{zz}_0 \qquad (3.10)$$

$$= \frac{\xi}{J(0)} - \xi\beta \left(\langle (S^z)^2 \rangle - \langle S^z \rangle^2\right) \qquad (3.11)$$

By expanding the Brillouin function

$$B_S(x) = \left(1 + \frac{1}{2S}\right) \coth\left(1 + \frac{1}{2S}\right) x - \frac{1}{2S} \coth \frac{1}{2S} x \qquad (3.12)$$

for small x we find that close to T_c where $\langle S^z \rangle$ is small

$$\tilde{\chi}_{mf} = \frac{2}{5} \xi \beta_c \langle S^z \rangle^2 \left[1 + \frac{1}{2S(S+1)}\right] + O\left[\langle S^z \rangle^4\right] \qquad (3.13)$$

At low temperature where $\langle S^z \rangle \simeq S$

$$\tilde{\chi}_{mf} \simeq \xi / J(0) - \xi \beta (S) \left[1 - \frac{\langle S^z \rangle}{S}\right] \tag{3.14}$$

By assuming an effective field that varies with $\underline{k}$

$$\underline{h}_{\underline{k}\,eff} = \left(h^x_m - \frac{1}{g\mu_B} J(\underline{k}) \langle S^x_{\underline{k}} \rangle\right) \hat{\underline{x}} - \frac{1}{g\mu_B} J(0) \langle S^z \rangle \hat{\underline{z}} \tag{3.15}$$

we obtain an interacting transverse susceptibility from molecular field theory:

$$\chi^{xx}_{\underline{k}} = \frac{\xi}{J(0) - J(\underline{k})} \tag{3.16}$$

The longitudinal susceptibility is found by expanding the Brillouin function about the change in $\langle S^z_{\underline{k}} \rangle$ due to an applied field h_k:

$$\chi^{zz}_{\underline{k}} = \frac{\xi S^2 \, d/dx \, B(x)}{k_B T - S^2 J(\underline{k}) \frac{d}{dx} B(x)} \Bigg|_{x = \beta S J(\underline{k}) \langle S^z \rangle} \tag{3.17}$$

This susceptibility decreases monotonically as the temperature drops, going to zero as absolute zero is reached.

A better approximation at low temperatures is the random phase approximation for which the transverse susceptibility is also given by equation (3.16) and the longitudinal susceptibility from

$$\chi^{zz}_{\underline{k}} = \frac{\xi}{NS} \sum_{\underline{k}'} \frac{n_{\underline{k}+\underline{k}'} - n_{\underline{k}'}}{J(\underline{k}+\underline{k}') - J(\underline{k}')} \tag{3.18}$$

$$\simeq \frac{\xi}{J(0) - J(\underline{k})} \frac{2}{NS} \sum_{\underline{k}'} n_{\underline{k}'} \tag{3.18a}$$

$$\simeq \frac{\xi}{J(0) - J(\underline{k})} \frac{2}{S} (S - \langle S^z \rangle) \tag{3.18b}$$

where

$$n_{\underline{k}} = \left[\exp\left[\left(J(0) - J(\underline{k})\right)\beta S\right] - 1\right]^{-1} \tag{3.19}$$

Low temperature approximations were made in deriving (3.18) and in further obtaining (3.18a) and (3.18b). Thus (3.18b) is only valid to leading order in $\frac{(S - \langle S^z \rangle)}{S}$. Therefore whilst it might appear that $\tilde{\chi}$ changes sign for $\frac{\langle S^z \rangle}{S} < \frac{1}{2}$, this is well outside the region where linear spin wave theory should hold. Physically, one would predict that $\tilde{\chi}$ is positive for a ferromagnet. For if there is a <u>net</u> alignment of spins in the z direction, the response to a field trying to align the spins (which are of fixed magnitude) further in the z direction must be less than to a field which would rotate them towards the x axis.

By assuming that the RPA is valid at low temperatures and the interacting molecular field theory is valid at all other temperatures we obtain the variation of $\chi_{\parallel}$, $\chi_{\perp}$ and $\tilde{\chi}$ shown in figure 1. We see that $\tilde{\chi}$ is positive at all temperatures in agreement with the argument above.

We are principally interested in $\tilde{\chi}$ at low temperatures where most experimental measurements of quadrupole interactions would be made and where $\tilde{\chi}$ is largest.

From equations (3.16) and (3.18), as $T \to 0$

$$\tilde{\chi} \to \tilde{\chi}_{SW} = \frac{1}{N} \sum_{\underline{k}} \frac{\xi}{J(0) - J(\underline{k})} - \frac{\xi}{NS} \sum_{\underline{k},\underline{k}'} \frac{n_{\underline{k}+\underline{k}'} - n_{\underline{k}'}}{J(\underline{k}+\underline{k}') - J(\underline{k})} \qquad (3.20)$$

$$\simeq \xi \left(\frac{2\langle S^z \rangle}{S} - 1 \right) \frac{1}{N} \sum_{\underline{k}} \frac{1}{J(0) - J(\underline{k})} \qquad (3.20a)$$

$$= \frac{\xi \eta_w}{J(0)} \left[\frac{2\langle S^z \rangle}{S} - 1 \right] \qquad (3.20b)$$

where

$$\eta_w = \frac{1}{N} \sum_{\underline{k}} \frac{1}{1 - \gamma_{\underline{k}}} \qquad (3.21)$$

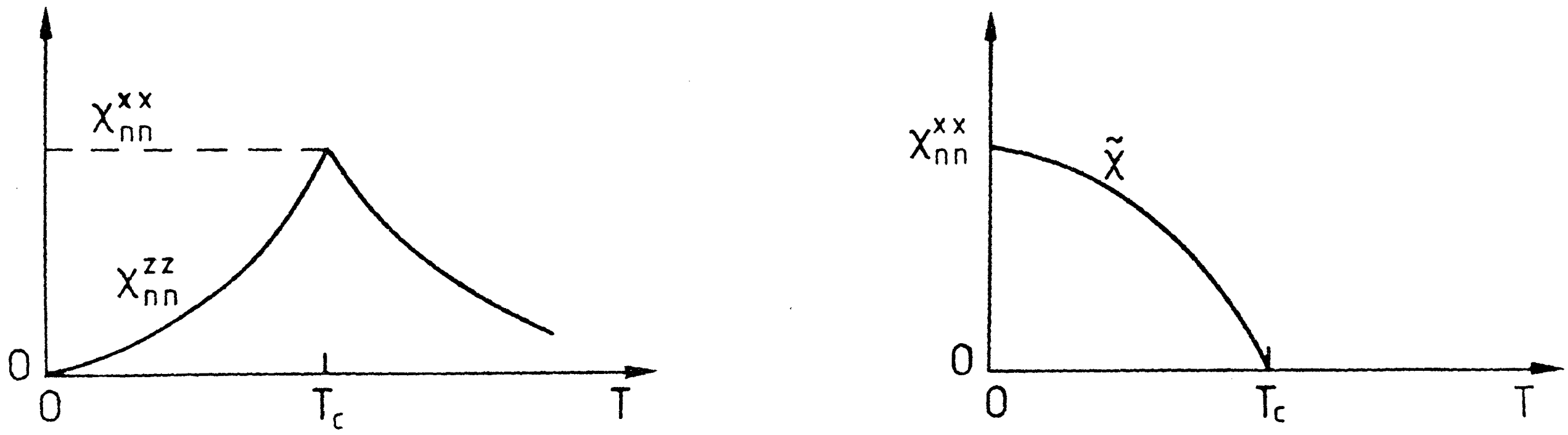

Localised model predictions for $\chi_{nn}^{xx}(T)$, $\chi_{nn}^{zz}(T)$ and $\tilde{\chi}(T)$

Fig. 1.

$$\gamma_{\underline{k}} = \frac{1}{z} \sum_{\underline{\rho}} e^{i\underline{k}\underline{\rho}} \qquad (3.22)$$

Equation (3.20b) applies for nearest neighbour exchange interactions only where the co-ordination number is z and the nearest neighbour displacements are given by $\{\underline{\rho}\}$. η_w has been evaluated for cubic lattices:

$$\eta_w = \begin{array}{lll} 1.5163 & \text{simple cubic} & (a)^* \\ 1.3918 & \text{body centred cubic} & (b)^* \\ 1.3441 & \text{face centred cubic} & (b)^* \end{array} \qquad (3.23)$$

Equation (3.21) shows that $\tilde{\chi}_{sw}$ and hence P_{pq} reaches its low temperature value as $\langle S^z \rangle$ (plus a constant term) in agreement with Zevin and Kaplan (1975). They looked at the rare earth intermetallic $GdAl_2$ for which the moments are at the gadolinium ions which lie on a diamond lattice (though they do not take account of this fact). We estimate the pseudoquadrupole effect for $GdAl_2$ in Chapter 4 so it is useful to have expressions for the longitudinal and transverse susceptibilities for the case of a diamond lattice. These are derived below using the RPA.

The diamond lattice consists of two face centred cubic lattices displaced by $\underline{\rho}_o = (\frac{1}{4}\ \frac{1}{4}\ \frac{1}{4})$ in units of the lattice constant of the conventional cubic unit cell. We label the spins on one sublattice 'S' and on the other sublattice 'T'. For $GdAl_2$, $|\underline{S}| = |\underline{T}| = S$. The susceptibilities $\chi^{vv}_{\underline{k}}(AB)$ are required, namely the response of spins on sublattice A to a spatially varying field acting on spins of sublattice B. They may be calculated from the Heisenberg Hamiltonian,

*(a) Mannari & Kageyama (1968) (b) Dvey Aharon (1978, Private Communication)

where the nearest neighbour spin displacements are $f_o + \underline{\mu}$.

$$H = J/2 \sum_{\underline{\mu},\underline{n}} \underline{S}_{\underline{n}} \cdot \underline{T}_{\underline{n}+\underline{f}_o+\underline{\mu}} - \gamma/2 \sum_{\underline{n}} h^x_{\underline{n}} \cdot S^x_{\underline{n}} \qquad (3.24)$$

This Hamiltonian is for nearest neighbour interactions only between spins on one sublattice and those on the other sublattice. Using linearised equations of motion for spins on each sublattice we find

$$\chi^{xx}_{\underline{k}}(SS) = \frac{1}{J(0)\left[1 - |\gamma^{\mu}_{\underline{k}}|^2\right]} \quad , \quad \gamma^{\mu}_{\underline{k}} = \sum_{\underline{\mu}} e^{i\underline{k}\cdot\underline{\mu}} \qquad (3.25)$$

$$\chi^{xx}_{\underline{k}}(TS) = \frac{\gamma^{\mu}_{\underline{k}}}{J(0)\left[1 - |\gamma^{\mu}_{\underline{k}}|^2\right]} \qquad (3.26)$$

For the diamond lattice, the other susceptibilities are given by

$$\chi^{xx}_{\underline{k}}(TS) = \left(\chi^{xx}_{\underline{k}}(TS)\right)^* \qquad (3.27)$$

$$\chi^{xx}_{\underline{k}}(TT) = \chi^{xx}_{\underline{k}}(SS) \qquad (3.28)$$

The longitudinal susceptibilities may be found from

$$\chi^{zz}_{\underline{k}}(AB) = \left.\frac{\partial \langle A^z_{\underline{k}} \rangle}{\partial h^z_{\underline{k}}}\right|_{h^z_{\underline{k}}\,(\text{at 'B' site}) = 0} \qquad (3.29)$$

$$\langle A^z_{\underline{k}} \rangle = NS\,\delta_{\underline{k},0} - \frac{1}{2SN} \sum_{\underline{k}} \langle A^-_{\underline{k}-\underline{k}'}, A^+_{\underline{k}'} \rangle \qquad (3.30)$$

Here $\underline{A}$ is a spin on a sublattice 'A'. (The linear spinwave approximation is used for equation (3.30)). We can find the correlation function $\langle A^-_{\underline{k}-\underline{k}'}, A^+_{\underline{k}'} \rangle$ from thermal Greens function theory (Zubarev (1960)):

$$\langle A^-_{\underline{k}-\underline{k}'}, A^+_{\underline{k}'} \rangle = i\,\frac{\left[G(\omega+i\epsilon) - G(\omega-i\epsilon)\right]}{e^{\beta\omega} - 1} \qquad (3.32)$$

where

$$G_{AA}(\omega) = \langle\langle A^-_{k-k'};\ A^+_{\underline{k}'} \rangle\rangle_{\omega} \qquad (3.33)$$

using the equation of motion

$$G_{AA}(t) = \delta(t)\langle[A^-_{\underline{k}-\underline{k}'}, A^+_{\underline{k}'}]\rangle + \langle\langle[A^-_{\underline{k}-\underline{k}'}, H]A^+_{\underline{k}'}\rangle\rangle \qquad (3.34)$$

and the Hamiltonian (3.24) we find $G_{AA}(\omega)$ in terms of $G_{BA}(\omega)$ and the Greens function $\langle\langle A^-_{-\underline{k}'}; A^+_{\underline{k}'}\rangle\rangle$ and $G_{BA}(\omega)$ in terms of $G_{AA}(\omega)$. After solving the simultaneous equations for G_{AA} and G_{AB} within the linear approximation to linear terms in $h_{\underline{k}}$ we find that

$$\chi^{zz}(ST) = 2\left(1 - \frac{M}{M_0}\right)\sum_{\underline{k}} \frac{1}{|\gamma_{\underline{k}}^{M}|^2 - 1} \qquad (3.35)$$

where M is the magnetisation and M_0 the saturation magnetisation. We also find

$$\chi^{zz}(ST) = 2\left(1 - \frac{M}{M_0}\right)\sum_{\underline{k}} \frac{1}{|\gamma_{\underline{k}}^{M}|^2 - 1}\ \gamma_{\underline{k}} \qquad (3.36)$$

and $$\chi^{zz}(TT) = \left(\chi^{zz}(ST)\right)^* \qquad (3.37)$$

$$\chi^{zz}(TT) = \chi^{zz}(SS) \qquad (3.38)$$

We conclude this section with a brief look at the theory of the pseudoquadrupole effect at magnetic impurities.

As discussed in section D, Chapter 2 the pseudoquadrupole effect depends on the difference between the <u>local</u> transverse and longitudinal susceptibilities at the impurity site.

The simple molecular field theory will give a rough estimate of the effect for a magnetic impurity. We generalise equation (3.5) to evaluate $\tilde{\chi}$, assume that χ^{zz} will be zero for very low temperatures and evaluate P_{pq} from the theory given in section D of Chapter 2.

Thus

$$\chi^{xx} \simeq \frac{\eta \xi}{2 J_I(o)} \tag{3.39}$$

where $J_I(o)$ is the exchange interaction between the impurity moment and nearest neighbour host moments.

Using equations (2.45) and (2.46) we find

$$\frac{P_{pq}^{max}}{} \simeq \frac{1}{2\mu_c}\left(\frac{g_I \mu_B B_I}{M_I}\right)^2 \chi_{nn}^{xx}(T=0) \tag{3.40}$$

$$\simeq \frac{1}{2J_I(o)}\left(\frac{g_I \mu_N B_{oI}}{S_I}\right)^2 \tag{3.41}$$

$$\simeq \frac{(S_I+1)}{S_I}\frac{(g_I \mu_N B_I)^2}{6 k_B T_c} \tag{3.42}$$

where S_I is the impurity spin.

χ^{xx} could also be evaluated for an impurity in a Heisenberg crystal using the theory given by Marshall and Lovesey (1971) to find the Green's function at the impurity site. We also require the relationship

$$\chi^{xx} = \left(\frac{g\mu_o}{4}\right)^2 \int_{-\infty}^{\infty} \frac{d\omega}{\omega}\left\{g_{\underline{k}}(\omega) - g_{-\underline{k}}(\omega)\right\} \tag{3.43}$$

where

$$g_{\underline{k}}(\omega) = i \mathcal{L}_{\epsilon \to o}\left[G_{\underline{k}}(\omega + i\epsilon) - G_{\underline{k}}(\omega - i\epsilon)\right] \tag{3.44}$$

and $G_{\underline{k}}(\omega)$ is the Greens function (Marshall and Murray 1969). We do not, however, pursue this line further as our experimental data is for itinerant magnets.

3B. Behaviour Near Criticality

As we have argued in section A, one would expect on physical grounds that $\tilde{\chi}$, the difference between transverse

and longitudinal susceptibilities, is positive. Unfortunately we have not been able to find a proof of this. In this section we give further arguments to suggest that close to the critical temperature T_c, $\tilde{\chi}$ may be positive.

The correct critical behaviour of $\tilde{\chi}$ is given by a classical approximation (unless T_c is close to zero):

$$\tilde{\chi} \sim \tilde{\chi}_{class} = \frac{1}{2k_B T}\left[\langle (S_n^x)^2 + (S_n^y)^2 \rangle - 2\langle (S_n^z)^2 \rangle + 2\langle S_n^z \rangle^2\right] \quad (3.45)$$

$$\simeq \frac{1}{2k_B T_c}\left[2\langle (S_n^z)\rangle^2 - \langle Q_n \rangle\right] \quad (3.46)$$

where

$$\langle Q_n \rangle = \langle 2(S_n^z)^2 - (S_n^x)^2 - (S_n^y)^2 \rangle \quad (3.47)$$

The quadrupole ordering has been obtained by Wegner (1972) in terms of the 'crossover' exponent φ. This exponent is discussed by Pfeuty et al (1974) and characterises the instability of the Heisenberg Hamiltonian to an Ising perturbation.* Therefore, given that from the definition of the exponent β

$$\langle S^z \rangle = B t^{\beta} + \text{higher terms} \quad (3.48)$$

where $t \equiv |T_c - T| / T_c$, B is a constant

and with the exponent inequality

$$2\beta = 2 - \alpha' - \gamma' \quad (3.49)$$

where α' is defined by $\lim_{\substack{T \to T_c \\ T < T_c}} C_H(T) = A_c \left| \frac{T_c - T}{T_c} \right|^{\alpha'}$, C_H is the magnetic specific heat at constant field H, A is a constant.

(Stanley 1971) we can write

$$\tilde{\chi} \simeq \frac{1}{2k_B T_c}\left[2B^2 t^{2-\alpha'-\gamma'} - A t^{2-\alpha'-\gamma}\right] \quad (3.50)$$

(i) (ii)

where A is a constant

If $\tilde{\chi}$ is positive, equation (3.50) implies that the

* A precise definition of this exponent is given in Fisher (1974)

second term (ii) must be less singular than (i) in the critical region so that

$$\rho \leq \gamma' \tag{3.51}$$

If the inequality holds, the behaviour of $\tilde{\chi}$ is given by the square of the magnetisation rather than $\langle Q_n \rangle$. There is some evidence that (3.51) does hold from renormalisation group calculations that have looked at both Q and γ'. Yamazaki (1974) has calculated ρ and γ' to order ϵ^3 for an n vector model in 4 - ϵ dimensions. His results show that, to that order in ϵ, $\rho \leq \gamma'$. Fisher and Pfeuty (1972) proposed that $\rho \leq \gamma'$ but we believe that our discussion (to be published as an appendix in Gehring and Walker (1981)) is the first attempt to find a physical reason for this inequality.

Further arguments in favour of $\tilde{\chi}$ being positive come from molecular field theory which is expected to be valid in four dimensions (where the fluctuations neglected become unimportant).

Looking at $\langle Q_n \rangle$ in the simple molecular field theory given at the beginning of section A,

$$\langle Q_n \rangle = 2\langle (S_n^z)^2 \rangle - \langle (S_n^x)^2 \rangle - \langle (S_n^y)^2 \rangle \tag{3.52}$$

$$= 3\langle (S_n^z)^2 \rangle - S(S+1) \tag{3.53}$$

$$= \frac{6}{5S(S+1)} \left[S(S+1) - \tfrac{3}{4} \right] \langle (S^z)^2 \rangle + O(\langle (S^z)^4 \rangle) \tag{3.54}$$

Equation (3.58) comes from the fixed length of the spins and (3.54) from expanding

$$\langle (S^z)^2 \rangle = \frac{\sum_{S^z=-S}^{S} (S^z)^2 \, e^{-\beta J(0) \langle S^z \rangle S^z}}{\sum_{S^z=-S}^{S} e^{-\beta J(0) \langle S^z \rangle S^z}} \qquad (3.55)$$

Equations (3.45) and (3.55) show that $\tilde{\chi}$ is positive and that it varies as $\langle (S^z)^2 \rangle$ and hence linearly with t.

If we use the interacting molecular field of section A we find that the dimensionality of our system comes in explicitly and we obtain different (and incorrect) results in three dimensions. The discrepancy can be explained by scaling theory as we discuss below.

We use equation (3.16) and

$$\chi_{\underline{k}}^{zz} = \frac{\xi}{k^2 + K_0^2} \qquad (3.56)$$

(eg. Marshall and Lovesey 1971) where K_0 is the inverse correlation length

In d dimensions we find for nearest neighbour exchange interactions

$$\tilde{\chi} = \frac{1}{N} \sum_{\underline{k}} \left(\chi_{\underline{k}}^{xx} - \chi_{\underline{k}}^{zz} \right) \qquad (3.57)$$

$$\simeq \frac{N \xi}{a^2 J_0} K_d \int_0^{K_0} dk \; k^{d-1} \left[\frac{1}{k^2} - \frac{1}{k^2 + K_0^2} \right] \qquad (3.58)$$

Here K_d is the appropriate angular factor (eg. $K_3 = 4\pi$), J_0 the exchange constant, a is the lattice parameter and the inverse correlation length is given by its molecular field approximation

$$K_0^2 = \frac{2t}{a^2} \propto t^{2\nu} \qquad (3.59)$$

The integral has been performed assuming that the dominant contribution is from the low k values.

In three dimensions,

$$\tilde{\chi} \propto K \tan^{-1} K_0/K \sim \xi^{\gamma} \sim \xi^{1/2} \qquad (3.60)$$

(We take the classical value for γ)

In just over four dimensions,

$$\tilde{\chi} \propto K_0^2 \sim \xi \qquad (3.61)$$

(at exactly four dimensions there will be logarithmic corrections (Ma 1976))

The result for four dimensions agrees with the real space simple molecular field calculation (after equation (3.55)) whereas the result for three dimensions does not.

This discrepancy is due to the fact that the scaling relation between ν and β (Stanley 1971), equation (3.62) below involves the dimensionality d and is only satisfied with classical exponents ($\nu = \beta = \frac{1}{2}, \eta = 0$) at d = 4:

$$2\beta = \nu (d - 2 + \eta) \qquad (3.62)$$

3C. The Itinerant Model

As discussed in the introduction, it is especially useful to have an estimate of the magnitude of the pseudoquadrupole effect in iron and nickel, at both host metal nuclei and at impurities in very dilute alloys. In this section we show how such an estimate can be obtained using a simple model to calculate the subsceptibilities based on Kim, Kubo and

Izuyama (1963).

The magnetism of iron and nickel is due to d electrons whose spins are aligned by exchange interactions. A large body of experimental evidence (reviewed by Herring (1966)) indicates that d electrons are itinerant. Thus any theory of magnetism in these metals must be founded on band theory.

Such a theory has been given by Kim, Kubo and Izuyama (1963), (KKI). Lowde and Windsor (1970) have shown that this theory provides a good description of the magnetism in nickel. Doniach (1968) has also argued that the RPA is a reasonable approximation to the ground state in nickel but he comments that in iron many body corrections are likely to be present. Recent theories have been shown to give an improved description of both the ground state and behaviour at finite temperatures, especially in iron (for reviews see Pettifor (1980) and Moriya (1979). We will however, use KKI's formulation as our results do not appear to justify a more accurate theory (see discussion at the end of this section).

KKI calculate the spin susceptibilities using a single band tight binding approximation. By ignoring the overlap between Wannier functions centred at different lattice sites compared with the overlap for the functions at the same site, they are able to write the susceptibilities in terms of 'reduced' susceptibilities $\chi'^{\mu\nu}$

$$\chi^{\mu\nu}_{\underline{k}} \simeq |F(\underline{k})|^2 \chi'^{\mu\nu}_{\underline{k}} \qquad (3.63)$$

$$= |F(\underline{k})|^2 \sum_{\underline{k}',\underline{k}''} \langle\langle a^{\dagger}_{\underline{k}+\underline{k}'} \underline{\underline{\sigma}}^{\mu} a_{\underline{k}} ; a^{\dagger}_{\underline{k}+\underline{k}''} \underline{\underline{\sigma}}^{\nu} a_{\underline{k}} \rangle\rangle_{\omega} \qquad (3.64)$$

where

$$\underline{a}_{\underline{k}} = \begin{pmatrix} a_{\uparrow \underline{k}} \\ a_{\downarrow \underline{k}} \end{pmatrix} \quad , \quad a^{+}_{\underline{k}} = \begin{pmatrix} a^{+}_{\uparrow \underline{k}} & a^{+}_{\downarrow \underline{k}} \end{pmatrix} \tag{3.65}$$

are the annihilation and creation operators for Block states, $\underline{\underline{\sigma}}^{\mu}$ the Pauli spin matrix for direction $\hat{\underline{\mu}}$ and $F(\underline{k})$ the form factor for magnetic electrons. They find the susceptibilities by evaluating equations of motion for the Greens function in equation (3.64) using the Hubbard Hamiltonian

$$H = \sum_{\underline{k}\sigma} \epsilon(\underline{k})\, a^{+}_{\underline{k}\sigma}\, a_{\underline{k}\sigma} + \frac{1}{2} v \sum_{\underline{K}}{}' \sum_{\underline{k}\sigma} \sum_{\underline{l}\sigma'} a^{+}_{\underline{k}+\underline{K}\sigma}\, a^{+}_{\underline{l}\sigma'}\, a_{\underline{l}+\underline{K}\sigma'}\, a_{\underline{k}\sigma} \tag{3.66}$$

Here $\epsilon(\underline{k})$ is the energy of a Block state $\underline{k}$, and the sum over $\underline{K}$ excludes $\underline{K} = o$. (This Hamiltonian involves a major approximation concerning the matrix elements of electron interaction discussed by KKI and in Marshall and Lovesey (1971)). By treating the equations of motion within the RPA they obtain the following expressions for the susceptibilities:

$$\chi^{+-}_{\underline{K}} = |F(\underline{K})|^2 \, \frac{\Gamma^{+-}_{\underline{K}}}{1 - v\,\Gamma^{+-}_{\underline{K}}} \tag{3.67}$$

where

$$\Gamma^{+-}_{\underline{K}} = \sum_{\underline{k}'} \frac{(f_{\underline{k}+\underline{K}'\downarrow} - f_{\underline{k}\uparrow})}{\epsilon_{\underline{k}+\underline{K}'} - \epsilon_{\underline{k}} + \Delta - \hbar\omega} \tag{3.68}$$

and

$$\chi^{zz}_{\underline{K}} = \frac{|F(\underline{k})|^2 \left(\Gamma^{++}_{\underline{k}} + \Gamma^{--}_{\underline{k}} + 2v\,\Gamma^{++}_{\underline{k}}\,\Gamma^{--}_{\underline{k}}\right)}{1 - v^2\,\Gamma^{++}_{\underline{k}}\,\Gamma^{--}_{\underline{k}}} \tag{3.69}$$

where

$$\Gamma^{++(--)} = \sum_{\underline{k}'} \frac{(f_{\underline{k}+\underline{k}'\uparrow(\downarrow)} - f_{\underline{k}\uparrow(\downarrow)})}{\epsilon_{\underline{k}+\underline{k}'} - \epsilon_{\underline{k}} - \hbar\omega} \tag{3.70}$$

Here $f_{\underline{k}\uparrow}$, $f_{\underline{k}\downarrow}$ are the fermi factors for the up and down spin bands respectively, $\epsilon_{\underline{k}}$ are the hole energies relative to the top of the band and Δ is the band splitting. $F(\underline{k})$ is defined

after (3.65).

ν is given by the conditions

$$\Delta = \frac{\nu \xi}{N} \sum_{\underline{k}} (f_{\underline{k}\uparrow} - f_{\underline{k}\uparrow}) \qquad (3.71)$$

and

$$\nu = 1/\Gamma^{+-}_{\underline{k}=0} \qquad (3.72)$$

(3.72) is the condition for a Goldstone mode to exist (for a discussion see Kubo and Izuyama (1969)).

At T = 0 the contributions to Γ^{+-} arise from terms when $f_{\underline{k}\downarrow} = 1$ and $f_{\underline{k}+\underline{k}'\uparrow} = 0$ and terms in which $f_{\underline{k}\downarrow} = 0$ and $f_{\underline{k}+\underline{k}'\uparrow} = 1$. These are shown in figure 2a. $\Gamma^{++}_{(--)}$ is due to transitions within an up (or down) spin band as shown in figure 2b.

For an order of magnitude estimate we use parabolic bands, an approximation which may be justified for nickel where there are few holes per atom and these lie at the top of the band where the density of states is a minimum. Clearly the approximation is much less justified for iron but as the use of RPA theory is also doubtful (as we have already mentioned) there seems no point in attempting a better calculation.

In this case the following expressions are obtained for the correlation functions.

$$\Gamma^{+-}_{\underline{k}}(\omega=0) = \frac{\xi_s m^* \nu}{N 4\pi^2 \hbar^2} \left\{ \left[\frac{k_{F\downarrow}^2}{2k} - \frac{(\Delta' + k^2)^2}{8k^3} \right] \log \left| \frac{2k k_{F\downarrow} + \Delta' + k^2}{2k k_{F\downarrow} - \Delta' - k^2} \right| \right. \qquad (3.73)$$

$$- \left[\frac{k_{F\uparrow}^2}{2k} - \frac{(\Delta' - k^2)^2}{8k^3} \right] \log \left[\frac{2k k_{F\uparrow} + \Delta' - k^2}{2k k_{F\uparrow} - \Delta' + k^2} \right]$$

$$\left. + k_{F\downarrow} \frac{(\Delta' + k^2)}{2k^2} - k_{F\uparrow} \frac{(\Delta' - k^2)}{2k^2} \right\}$$

Contributions to χ_{nn}^{xx}

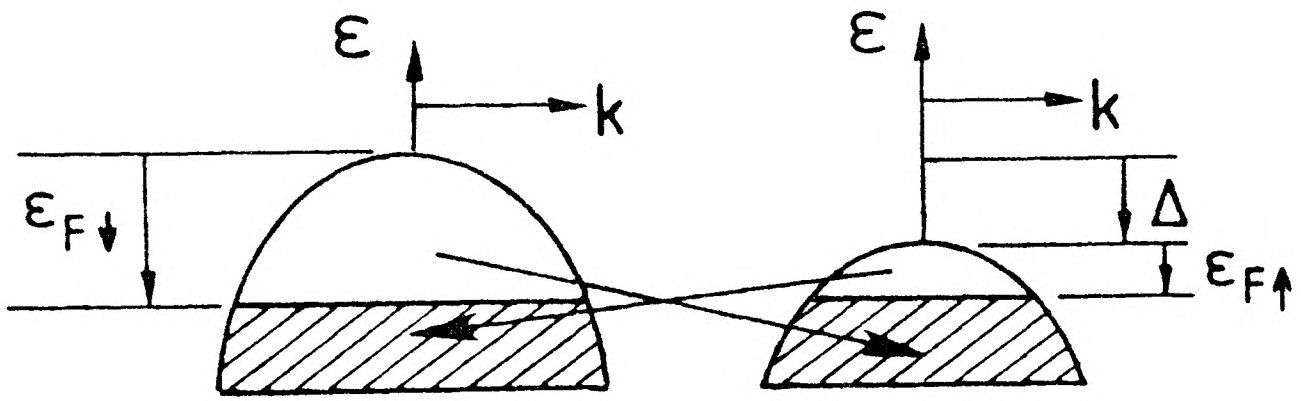

Fig. 2a.

Contributions to χ_{nn}^{zz}

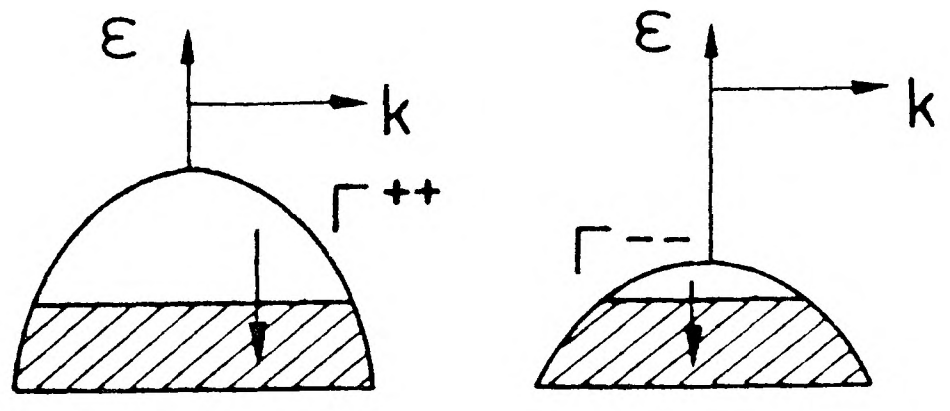

Fig. 2b.

and

$$\Gamma^{+-}(\omega=0) = \frac{\Sigma m^* V}{N 4\pi^2 \hbar^2}\left\{\left[\frac{k_{F\uparrow(\downarrow)}^2}{k} - \frac{k}{4}\right]\log\left|\frac{2k_{F\uparrow(\downarrow)}+k}{2k_{F\uparrow(\downarrow)}-k}\right| + k_{F\uparrow(\downarrow)}\right\} \qquad (3.74)$$

where $\Delta' = \Delta 2m^*/\hbar^2$, Ω is the volume of the crystal and $k_{f\uparrow(\downarrow)}$ are the Fermi wave vectors for the up (down) spin bands.

We can evaluate the spin wave stiffness coefficient Dc by expanding $\Gamma^{+-}_{\underline{k}}(\omega)$ for small ω and $|\underline{k}|$:

$$\lim_{k\to 0} \hbar\omega_{\underline{k}} = D_c k^2 \qquad (3.75)$$

$$D_c = \frac{\hbar^2}{2m^*}\left[\frac{4}{5}\frac{(k_{f\downarrow}^5 + k_{f\uparrow}^5)}{\Delta'} - (k_{f\downarrow}^3 + k_{f\uparrow}^3)\right]\frac{1}{(k_{f\downarrow}^3 - k_{f\uparrow}^3)} \qquad (3.76)$$

It is useful to have an estimate for $\chi^{xx}(T_c)$ $(= \chi^{zz}(T_c))$ to judge by how much χ^x and χ^z alter as the temperature decreases below T_c towards zero. Despite doubts about the validity of this theory near T_c (Edwards (1980) we make our estimate by calculating χ^{+-} using equations (3.67) and (3.68) but with $\Delta = 0$ since $\Delta \propto$ magnetisation (equation (3.71)). Since the Fermi temperature T_f is very much greater than T_c for both iron and nickel it should not be a bad approximation to assume that the Fermi factors can be calculated for the ground state. However we are forced to assume a temperature dependence for v, which is not consistent with the RPA theory, since equation (3.72) must be used for Goldstone modes to exist.

We give the values for $v(T=0)$ and $v(T=T_c)$ in table 2; their difference is a measure of the crudity of our model.

We also give a numerical estimate for D_c in table 4 as a further indication of where the model might be inappropriate.

Other authors (Wakoh et al (1971)) have found that D_c is much smaller than the experimental value D_e, as we do (using the parameters described below). This may be attributed to the use of the extreme tight binding approximation in which the electron-electron interaction is assumed site diagonal in a Wannier representation (Edwards (1980)). However, there is also considerable experimental uncertainty about D_e (Louwde (1979), private communication).

To make estimates of D_c, $v(T = 0)$ and $v(T = T_c)$ we used the following parameters which we obtained from experiment: the number of holes in the up and down spin bands (which for nickel is found from the electron g factor and the saturation magnetisation (Kittel 1971)) and Δ for nickel (for iron it is determined by the difference between the up and the down spin bands - see figure 2a). We evaluated m* from the experimental measurements of the electronic specific heat C_{el} which are quoted in Kittel (1971) using

$$C_{el} = \gamma T = \frac{1}{2}\pi^2 N k_B \frac{T}{T_F} \qquad (3.77)$$

where T_F is the Fermi temperature

It is necessary to assume that the d band holes would dominate C_{el} and additionally in iron that the contribution from spin down band holes can be neglected. The values we took for these parameters and references are given in table 1.

We find the itinerant susceptibilities from equations (3.67) and (3.69) and our expressions for the correlation functions for parabolic bands, equations (3.73) and (3.74). The itinerant susceptibilities, χ^{xx}_{nn} and χ^{zz}_{nn} are defined by

$$\chi^{xx}_{nn} = \sum_{|\underline{k}|<k_m} \chi^{xx}_{\underline{k}} \qquad (3.78)$$

Table 1

Parameters used in the Calculations

	$n\downarrow$	$n\uparrow$	g	m^* (in units of electron mass)	Δ(ev)	b′	c′	d′
N_i	0.54 a)	-	2.2 a)	28.5	0.34 b)	0	0.013	0.0037
F_e	2.6 c)	0.3 c)	2.1 d)	11.3	1.41	0.044	0	0.012

a) Kittel (1971)

b) Wohlfarth (1964)

c) Mott (1964)

d) Martin (1967)

Table 2

Calculated Parameters for Nickel and Iron

	D_c MeV $\mathring{A}^2$	D_e MeV $\mathring{A}^2$	$V_{T=0}$ 10^{+32} m^3	$V_{T=T_c}$ 10^{+32} m^3
N_i	48	550 a)	1.93	1.29
F_e	36	314 b)	2.07	1.94

a) Lynn (1974)

b) Stringfellow (1968)

$$\chi^{zz}_{nn} = \sum_{|\underline{K}|<K_m}{}' \chi^{zz}_{\underline{K}} \qquad (3.79)$$

where K_m is defined in equations (2.15). It is the radius of a spherical Brillouin zone whose volume is that of the Brillouin zone for an fcc (face centred cubic) lattice (nickel) and a bcc (body centred cubic) lattice (iron). This is so that using equation (2.42) we may find the pseudo-quadrupole parameter from

$$\rho_{pq} = \frac{1}{2\mu_o} A_i^2 \tilde{\chi}_i \qquad (3.79a)$$

and A_i is given by equation (2.44), χ^{xx}_{nn} and χ^{zz}_{nn} are thus approximations to the local susceptibilities in that we do not integrate over the full Brillouin zone to be consistent with our model for $A(\underline{k})$ (equation (2.15)). We parametrise the magnetic form factors which are required in equations (3.67) and (3.69) by

$$F(k) \simeq \exp\left[-b'k - c'k^2 - d'k^3\right] \qquad (3.80)$$

where b', c', d' are given in table 1 *This parametrisation of* $F(k)$ gave good agreement with the calculated values of Mook (1966) for nickel and Freeman and Watson (1961), II in iron especially at low k where $\chi^{xx}_{\underline{K}}$ and $\chi^{zz}_{\underline{K}}$ are largest. Our values for $\chi^{xx}_{nn}(T=0)\,(=\chi^{xx}_{nn})$, $\chi^{zz}_{nn}(T=0)\;(=\chi^{zz}_{nn})$ and $\tilde{\chi}_i\,.\,(T=0)\,(=\chi^{xx}_{nn}-\chi^{zz}_{nn})$ are given in table 3. We include our value for $\chi_{nn}(T_c)$ for a rough comparison.

It is possible to approximate our value for $\tilde{\chi}_i(T=0)$ by assuming that $\chi^{zz}_{nn} \simeq 0\, \chi^{xx}_{nn}$ may be found by assuming that $K^2\chi^{xx}_{\underline{K}}$ in the integral over the spherical Brillouin zone is replaced by its value in the limit of $K \to 0$. As is apparent from figures 3a and 3b which plot $K^2\chi^{xx}_{\underline{K}}$ as a function of k, this is a good approximation. Physically it implies that $\chi^{xx}_{\underline{K}}$ is dominated by the spin wave pole,

Table 3

Calculated Itinerant Susceptibilities

	χ_{nn}^{xx} (T=0)	χ_{nn}^{zz} (T=0)	$\tilde{\chi}_i$(T=0)	$\chi_{nn}(T_c)$
N_i	2.9	0.84	2.1	10
F_e	17	1.1	16	21

(All values given in units of 10^{-32} m^3)

Table 4

Comparison of $\tilde{\chi}$ (T=0) Evaluated in Different Approximations

	Itinerant model $\tilde{\chi}_i$	From spin wave theory D_c χ_{Ai}	D_e χ_{Aii}	From molecular field theory χ_{mf}
N_i	2.1	3.6	0.31	2.0
F_e	16	20	2.2	3.1

(All values given in units of 10^{-32} m^3)

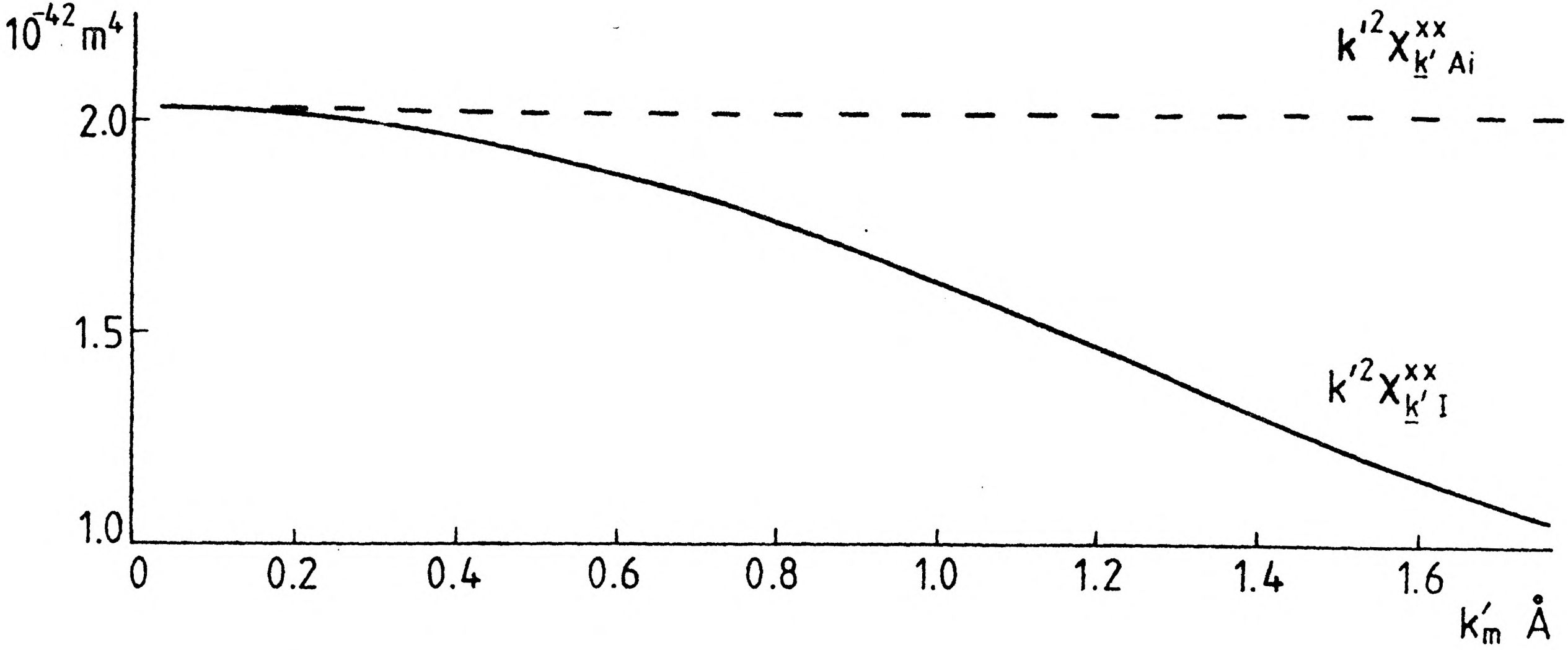

Itinerant model transverse susceptibility at T = 0 (Nickel)

Fig. 3a

251

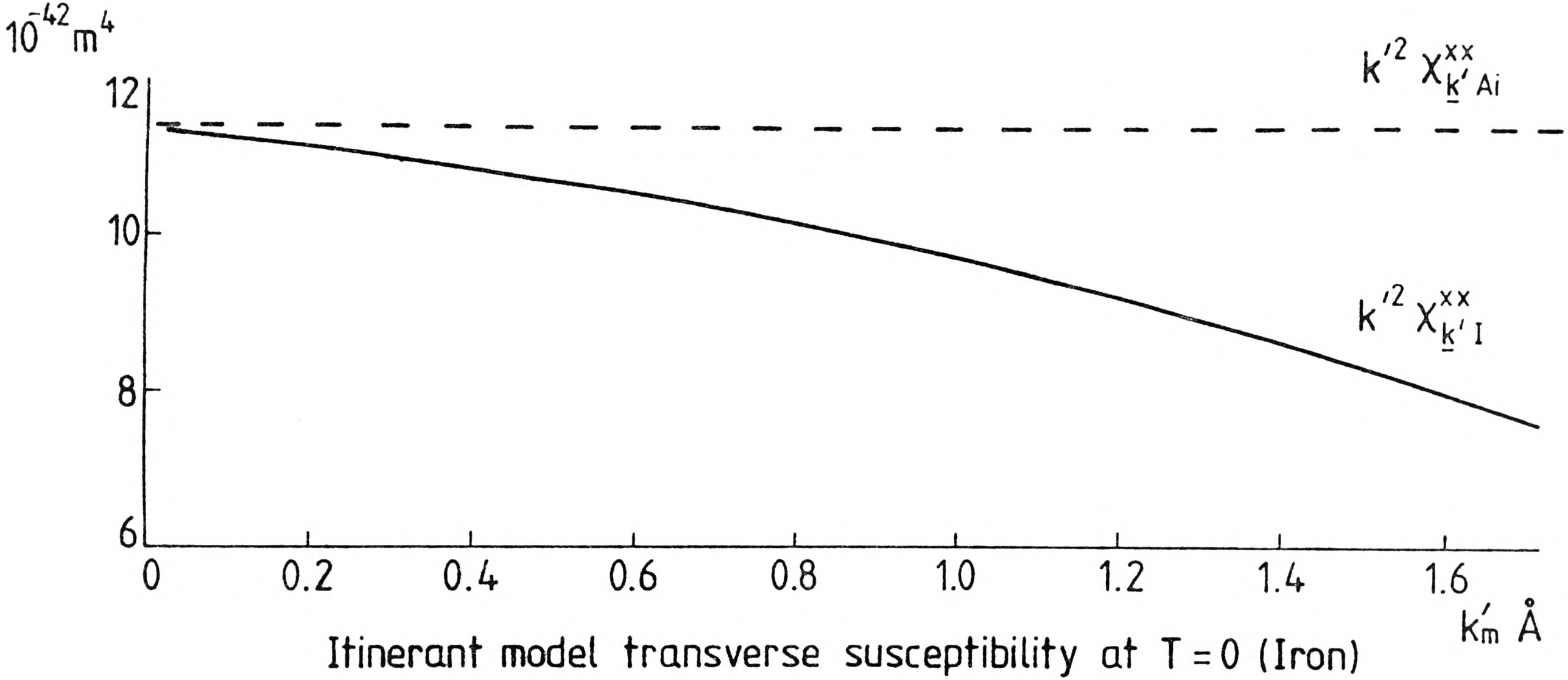

Itinerant model transverse susceptibility at T = 0 (Iron)

Fig. 3b

$$\chi^{xx}_{\underline{k}} \simeq \frac{(n_\downarrow - n_\uparrow)}{Dk^2} \qquad (3.81)$$

where D is the spin wave stiffness. We call this approximation to $\tilde{\chi}$, $\chi_{A(i)}$ where we use $D = D_c$ (equation 3.76)) and $\chi_{A(ii)}$ where $D = D_e$, the experimental spin wave stiffness.

$\chi_{A(i)}$ and $\chi_{A(ii)}$ are given in table 4 which includes estimates $\tilde{\chi}_{mf}$ obtained from molecular field theory using equations (3.16), (3.21), (3.22), (3.25) and

$$J(0) = \frac{S(S+1)}{3K_B T_c} \qquad (3.82)$$

This table shows that $\chi_{A(i)}$ is a good approximation to $\tilde{\chi}_{nn}(T=0)$, making a check on our results for the latter. However, $\chi_{A(i)}$ considerably underestimates $\tilde{\chi}_{nn}(T=0)$ owing to the large discrepancy between D_c and D_e. We see that the molecular field theory calculation gives good agreement for nickel but not for iron.

We then go on to estimate P_{pq} for the pure metal using equations (3.16) and (2.44). In (2.44) the saturation values of the magnetisation were substituted for M_o; these are 0.604 Bohr magnetons for nickel and 2.22 Bohr magnetons for iron (Martin(1967)). The other parameters we used to obtain A are given in table 5.

Our values are compared with experimental measurements of the quadrupole parameter P for iron in table 5. It is clear that our estimate for the pseudoquadrupole parameter P_{pq} is down by about two orders of magnitude compared with

Table 5

Host	Nucleus	I	g_I	B_c @ (Tesla)	A (MHz)	P_{pl} † (kHz)	P_e † (kHz)
Ni	^{61}Ni	3/2	.499 a)	7.6 b)	105	.19	-
Fe	^{57}Fe	3/2	.103 c)	34 c)	25.3	.067	14 d)
Ni	^{192}Ir	4	.47 e)	46.7 e)	607	6.3	300 f)
Ni	^{193}Ir	3/2	.108 g)	47 h)	140	0.34	700 i)
Fe	^{191}Ir	3/2	.097 g)	150 j)	10.5	1.20	1300 h)
Fe	^{193}Ir	3/2	.108 g)	150 j)	11.7	1.49	1700 h)
Fe	^{60}Co	5	.758 k)	29 l)	15.9	2.75	6.5 m)

a) Drain (1964)

b) Obenshain et al. (1971)

c) Violet and Pipkorn(1971)

d) Spijkerman et al. (1971)

e) Eska et al. (1971)

f) Fox and Stone (1969)

g) Davies and Owen (1969)

h) Wagner and Potzel(1971)

i) Aiga and Itho (1971)

j) Calvo et al. (1970)

k) Niesen and Huiskamp (1972)

l) Foster et al. (1977)

m) Callaghan et al. (1976)

* Experimentally measured quadrupole energies

† P_{pl}^I for impurity nuclei

@ B_I for impurity nuclei

the experimental parameter:

$$P_e = P_{pq} + P_q \qquad (3.83)$$

P_q is due to the electrostatic quadrupole moment of the nucleus and is given by,

$$P_q = \frac{3e^2 Q \; q}{4I\,(2I-1)} \qquad (3.84)$$

for a nucleus of quadrupole moment Q (e is the electronic charge) (Stone 1980) where q is the electric field gradient at the nucleus. Thus, even if our model were to significantly underestimate P_{pq} (we have no reason to believe that it would), it appears unlikely that the pseudoquadrupole effect would make a large contribution to P.

There is considerable interest in the quadrupole effect at impurities in iron and nickel as described in the introduction. For here there may be magnetically induced field gradients due to the rather subtle mechanisms of unquenched orbital momentum and magnetostriction (Gehring 1974). We therefore estimate the size of the splitting for impurities where experimental data is available. These are the effectively non magnetic impurity, iridium and the magnetic impurity, cobalt. The results are in table 5.

We treat iridium as a non magnetic impurity and use the theory of section D, Chapter 1 to find P_{pq} although here there is evidence for a small local moment and a virtual bound state in both Ni(Ir) (Demangeat (1975) I) and Fe(Ir) (Demangeat (1975) II). Thus the local susceptibility may be significantly affected making our assumption (in Chapter 1, section D), that P^I_{pq} given in the table provides an upper

estimate of the actual parameter, somewhat dubious.

However, we can see from the experimental measurements that, whereas g_I for ^{193}Ir is much larger than g_I for ^{192}Ir, P is less for ^{193}Ir than for ^{192}Ir. Therefore, the pseudo-quadrupole effect cannot have a significant effect on the measurements. Were the experimental values of P more accurate (Spijkerman et al (1971) for instance quote an error of 80% for their measurements in pure iron), we could even calculate P_{pq} from these two measurements. This is because the susceptibilities will be the same in the two cases so that the ratio r of the pseudoquadrupole parameters is given by the square of the ratio of the hyperfine constants. We also know the ratios of the 'real' quadrupole parameters P_q from equation (3.84) since q will be the same for both isotopes in the same host. Thus we can solve for P_{pq} and P_q from the equations:

$$P(^{193}Ir) = P_{pq}(^{193}Ir) + P_q(^{193}Ir) \qquad (3.85)$$

$$P(^{192}Ir) = r' P_{pq}(^{193}Ir) + s' P_q(^{193}Ir) \qquad (3.86)$$

Next we discuss Co(Fe). Cobalt has a moment in iron which is very close to that of its host. We therefore, assume that the local susceptibilities are close to that of the pure host to find P_{pq}. However it is likely that the cobalt impurity will locally modify the band structure, so that there could well be a different value for the susceptibilities. Since our estimate is so close to the experimental splitting (a factor of 3) we consider that a more accurate treatment might be advisable. Such a treatment would be

where $r' = \frac{A_{i\,192}}{A_{i\,193}}$, $s' = \frac{Q^{192}}{Q^{193}} \times \frac{I^{193}(2I^{193}-1)}{I^{192}(2I^{192}-1)}$; $A_{i\,192(3)} = A_i$ for $^{192(3)}Ir$

$I^{192(3)} = I$ for $^{192(3)}Ir$

$Q^{192(3)} = Q$ for $^{192(3)}Ir$

obtained using Wolfram's (1961) theory. He calculated the susceptibility using essentially an extended version of KKI. Also Campbell and Gomés (1967) find an expression for the local susceptibility in an appendix.

We can think of one example where the local transverse susceptibility and hence P_{pq} is likely to be large at an impurity. This is FeMn where measurements by Jaccarino et al (196 showed that the local hyperfine field had a very different temperature dependence from that of the host. This suggests that the local moment is only loosely coupled to the host moments. Jaccarino et al (1964) found that molecular field theory gave a surprisingly good fit to the magnetisations obtained from the experimental hyperfine field. It should therefore be possible to apply the molecular field estimate for P_{pq} (equation (3.42)) to this case. If the impurity moment-host moment coupling is weak, this suggests that $J_I(o)$ is small and hence P_{pq} will be large. A more accurate estimate might be obtained from the theory of Campbell and Gomés (1967) which has recently been shown to give very good results for the impurity moment (Kajzer and Parete 1980).

CHAPTER 4

QUADRUPOLE EFFECTS IN $GdAl_2$

4A. Experimental Results

Degani and Kaplan (1973) measured a sizeable temperature dependent quadrupole interaction at aluminium ions in the rare earth intermetallic $GdAl_2$. They showed that the interaction varied linearly with the magnetisation over a wide range of temperature, 4K to 112K, and commented that most origins of a magnetisation dependent electric field gradient would have a quadratic variation. In this chapter we look at various mechanisms that would be consistent with their observations, particularly the pseudoquadrupole effect proposed as an explanation by Zevin and Kaplan (1975).

$GdAl_2$ has the cubic Laves phase structure depicted in figure 4 (Wernick and Geller 1960). Gadolinium ions are arranged on a diamond lattice and the aluminium ions form tetrahedra of point symmetry $\bar{3}$ m whose axes of symmetry are parallel to the principal diagonals of the cubic unit cell. The cell contains eight gadolinium and sixteen aluminium ions and the length of one side is $a_o = 7.9\mathring{A}$.

Below $T_c = 176K$, the gadolinium ions order ferromagnetically along the $[1\ 1\ 1]$ direction, distinguishing aluminium ions at 'a' sites whose threefold symmetry axes coincide with the magnetisation vector from those at 'b' sites whose symmetry axes are parallel to $[\bar{1}\ 1\ 1]$, $[1\ \bar{1}\ 1]$ and $[1\ 1\ \bar{1}]$. Measurements of the echo decay modulation frequencies at the 'a' site shown in figure 4 were found to differ significantly

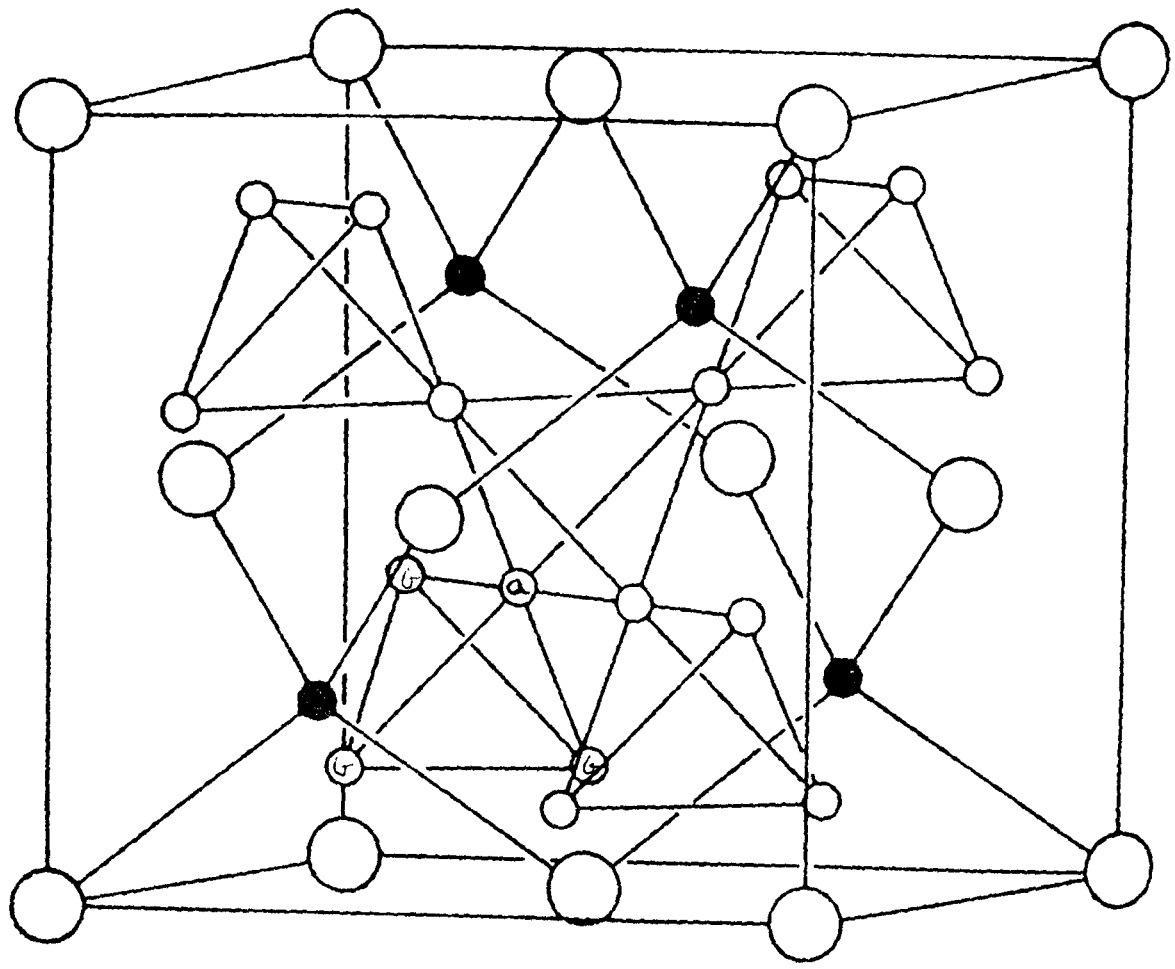

Fig. 4 Schematic representation of cubic laves phase structure of $GdAl_2$. The small open circles are the Al ions, the small full circles the Gd ions on one sublattice and the large open circles the Gd ions on the other sublattice. One 'a' site and 3 'b' sites are marked.

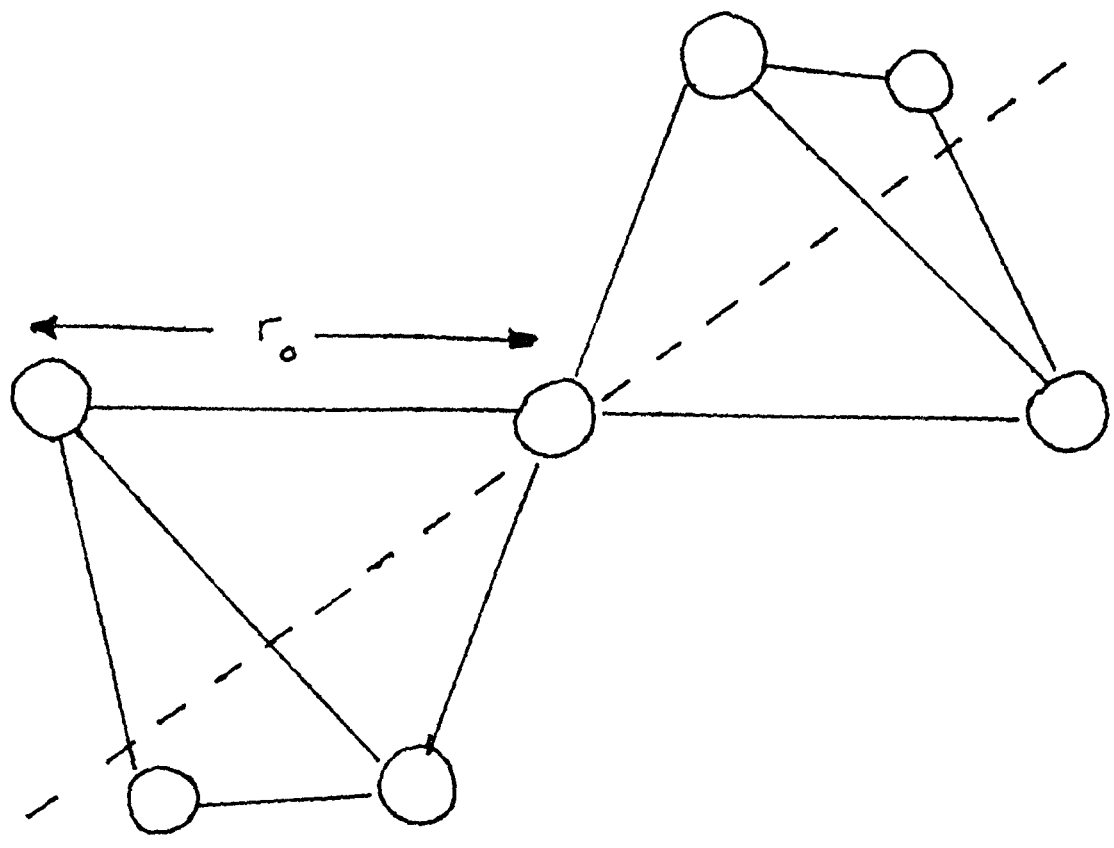

Fig. 5 The six nearest neighbour Al ions to a given Al ion. The dotted line marked the [1 1 1] axis of the cubic unit cell of $GdAl_2$

from those at the 'b' sites marked and to show a magnetisation dependence, an effect that may be explained by the assumption of a magnetically induced field gradient (efg). (Degani and Kaplan 1973). They find, from 'a' site measurements that the quadrupole parameter P is given by (defining P_c and P_m from this equation),

$$|P| = P_c - \frac{M}{M_o} P_m \qquad (4.1)$$

where

$$P_c = 0.314 \pm .004 \text{ MHz} \qquad (4.2)$$

$$P_m = 0.043 \pm .004 \text{ MHz} \qquad (4.3)$$

$$P = \frac{3e^2 Qq}{4I(2I-1)} \qquad (4.4)$$

Q is the nuclear electrostatic quadrupole moment, q the efg and M_o the saturation magnetisation.

The value of $|P|$ was measured in the para-magnetic phase by Jones and Budnick (1966) and was similar to P_c:

$$|P_{para}| = 0.320 \text{ MHz} \qquad (4.5)$$

No change of P_{para} with temperature was reported for their measurements which were taken between 350K and 575K. Jaccarino et al (1960) measured the quadrupole interaction at aluminium ions in the chemically similar but non-magnetic compound $LaAl_2$ but do not mention a temperature variation there either. It seems likely then that in $GdAl_2$ magnetic effects are responsible for the temperature dependence of the quadrupole parameter as Degani and Kaplan (1973) suggested.

4B. The Pseudoquadrupole Effect

The pseudoquadrupole effect is clearly a good candidate

for Degani and Kaplan's results (Zevin and Kaplan 1975) since it varies linearly with the magnetisation at low temperatures (equation (3.21)).

We use the theory in Chapter 3 section A to evaluate the susceptibilities for the local moments at the Gd atoms. However, we can not use it directly as the measurements have been made at the aluminium site so that equations (2.28), (2.30) and (2.31) must be employed. We may write $\tilde{\tilde{\chi}}$ (defined in (2.28)) in terms of $\chi^{\nu\nu}(SS)$, $\chi^{\nu\nu}(ST)$, $\chi^{\nu\nu}(TS)$ and $\chi^{\nu\nu}(TT)$ defined in Chapter 3 (just above equation (3.24)):

$$\tilde{\chi} = \frac{1}{z^2} \sum_{\underline{k}} \left\{ z_s^2 \, |\gamma_{\underline{k}}^s|^2 \left(\chi_{\underline{k}}^{xx}(SS) - \chi_{\underline{k}}^{zz}(SS) \right) \right.$$

$$+ 2 \mathrm{Re} \left[z_s z_t \, \gamma_{-\underline{k}}^s \, \gamma_{-\underline{k}}^t \, e^{i\underline{k}\cdot\underline{\rho}_0} \left(\chi_{\underline{k}}^{xx}(SS) - \chi_{\underline{k}}^{zz}(SS) \right] \right. \quad (4.6)$$

$$\left. + z_t^2 \, |\gamma_{\underline{k}}|^2 \left(\chi_{\underline{k}}^{xx}(TT) - \chi_{\underline{k}}^{zz}(TT) \right) \right\}$$

where $\gamma_{\underline{k}}^s = \frac{1}{z_s} \sum_{\underline{s}} e^{i\underline{k}\cdot\underline{s}}$, $z_s = \sum_{\underline{s}} 1$.

Here $\{\underline{s}\}$ and $\{\underline{t}\}$ denote displacements of ions on S and T sublattices respectively from a given aluminium ion for which they are nearest neighbours and $z = z^s + z^t$ (= 6).

Using equations (3.25) to (3.28) and (3.35) to (3.38) we find that

$$\tilde{\chi} = \frac{\tilde{m}}{J(0)} \quad (4.7)$$

where

$$\tilde{m} = \frac{z_s^2}{N z^2} \sum_{\underline{k}} \frac{\left(2|\gamma_{\underline{k}}^s|^2 + 2\mathrm{Re}\left[(\gamma_{\underline{k}}^s)^2 \gamma_{\underline{k}}^{\rho} \right] \right)}{1 - |\gamma_{\underline{k}}^{\rho}|^2} \quad (4.8)$$

$$= 0.73 \quad (4.9)$$

Here $\{\rho\}$ defines the displacement of nearest neighbour Gd ions to a given Gd ion (ie. the co-ordination vectors for the

diamond lattice). The result follows from the assumption of exchange interactions between nearest neighbour ions and the fact that $\{s\} = -\{t\}$ for the $GdAl_2$ structure.

We evaluate P_{pq} from equations (2.30), (2.31), (4.7) and (4.9) using the following figures: $g_I = 1.46$ (Kittel 1971), $B_o = 4.6T$ (Jones and Budnick (1966)) and we estimated J(o) from $T_c = 176K$ (Degani and Kaplan (1973)) using molecular field theory. This gives

$$P_m = .44\ kHz \tag{4.10}$$

by comparison with Degani and Kaplan's (1973) measurement of 43kHz (equation (4.4)). This P_m from our calculations is very much smaller than the value measured by Degani and Kaplan (1973). We conclude that the observed temperature dependent quadrupole interaction is not due to the pseudoquadrupole effect.

Our results may be compared with Zevin and Kaplan (1975) who estimate P_m as 22kHz. Their much larger estimate which we consider an overestimate comes from approximations in the spin wave sums when evaluating

$$P^{pseudo} = \frac{A_{11}^2}{N^2} \sum_{k \neq k'} \frac{n_k}{\epsilon_k - \epsilon_{k'}} \tag{4.11}$$

where A_{11} is the magnetic hyperfine constant in the z direction (equation (8) of their paper). (As is clear from equation (3.18) this is equivalent to

$$P_{PL} = \frac{A_o^2}{2\mu_o} \chi^{zz} \tag{4.12}$$

in our notation). We calculated a value of $\tilde{\eta}$ that would give their estimate for P^{pseudo} and showed that it was 6π (cf 0.73).

They also appear to overestimate the hyperfine constant A_o by a factor of 2.

4C. Other Mechanisms Consistent with Experiment

Single ion magnetostriction (as distinct from exchange magnetostriction - for a review see Kanamori (1963)) may provide an alternative mechanism. The distortion and hence the efg, q_m varies by symmetry arguments (Kanamori (1963)) as $\langle (S^z)^2 - \frac{1}{3} S(S+1) \rangle$ and vanishes above T_c in a cubic magnet, where q_m is the magnetostrictive contribution term to the total efg

We therefore assume that

$$q_m = q_m(T=0) \times \frac{\langle (S^z)^2 - 1/3\, S(S+1) \rangle_T}{\langle (S^z)^2 - 1/3\, S(S+1) \rangle_{T=0}} \qquad (4.13)$$

Using non interacting spin wave theory it is easily shown

$$\langle (S_i^z)^2 - \frac{S(S+1)}{3} \rangle = \frac{2}{3} S(S+1) - \langle S_i^- S_i^+ \rangle - \langle S_i^z \rangle \qquad (4.14)$$

$$= S(2S-1)\left[-\frac{2}{3} + \frac{\langle S^z \rangle}{S} \right] \qquad (4.14a)$$

since

$$\langle S_i^- S_i^+ \rangle = 2S \sum_k n_k \qquad (4.15)$$

$$= 2(S - \langle S^z \rangle) \qquad (4.15a)$$

Thus we obtain a linear variation of q with the magnetisation, in accordance with Degani and Kaplan's observations (using equation (4.4)). To calculate P_m, the rate at which P would change with $\langle S^z \rangle$ from this mechanism, we need to evaluate the efg at T = O so that we may find $q_m(T)$ and hence P from (4.4).

The magnitude of the efg at an 'a' site aluminium ion may

be estimated using the Thomas Fermi approximation for the potential of point charges screened by conduction electrons:

$$V(r) = \frac{e^{-k_o r}}{r} \qquad (4.16)$$

where

$$k_o^2 = \frac{e^2 m k_f}{\hbar^2 \pi^2 \epsilon_o} \qquad (4.17)$$

(Kittel 1971).

We investigate the reasonableness of this model by first looking at the efg in the paramagnetic phase, q_p. We consider nearest neighbour aluminium ions only as the screening length k_o^{-1} is small ($\sim 0{\cdot}2$ Å). These ions are at the corners of two tetrahedra (see figure 5)*. We find that our calculated value for q_p,

$$q_{p_{calc}} = 6(1-\gamma_\infty)\frac{e^{-k_o r_o}}{r_o^3}\left(\frac{2}{3}(k_o r_o)^2 + k_o r_o + 1\right) \qquad (4.18)$$

Here γ_∞ is the Sternheimer antishielding factor and r_o the nearest neighbour Al-Al distance. Taking $\gamma_\infty \sim 100$ (Cohen and Reif (1957), Q = 0.15 Barns (Sharma 1970), z = 3 and r = $\sqrt{2}/4\, a_o$ where a_o = 7.9 Å (Wernick and Geller 1960) we obtain

$$|P_{para}| = 3.4 \text{ MHz} \qquad (4.19)$$

Whilst this figure is too large by an order of magnitude of Jones and Budnick's (1966) measurement, the agreement is reasonable considering the approximations made and so we use this approach to calculate the efg in the ordered phase.from the magneto-striction, q_m

We assume that the efg from magnetostriction,

$$q_m = q_{pexpt} \times q_{mcalc}/q_{pcalc} \qquad (4.20)$$

where

$$\frac{q_{mcalc}}{q_{pcalc}} = \frac{[2(k_o r_o)^3 + (k_o r_o)^2 - 3(k_o r_o) - 3]\epsilon}{4(k_o r_o)^2 + 6(k_o r_o) + 6} \qquad (4.20a)$$

where q_{pexpt} is the experimental value of q_p.(4.20a) is obtained by assuming $q_{m\,calc}$ is given by the linear term in a Taylor expansion $q_m(\epsilon)$, where ϵ is the strain from magnetostriction

$$\rho^{ms}_{pq} = |P_{para}| \frac{q_{mcalc}{}^3}{q_{calc}} \qquad (4.21)$$

giving $\rho^{ms}_{pq} = 54.3$ Hz , using (4.13) and $\epsilon = 26.10^{-6}$ (Burd and Lee 1977) (4.22)

This calculation suggests that single ion magnetostriction is too small to account for the temperature dependent quadrupole interaction measured by Degani and Kaplan (1973).

Another possible explanation is that there is no magnetisation dependent quadrupole interaction and that the temperature dependence seen is due to lattice expansion. This is because both the magnetisation*and variation of q with T due to thermal expansion go as $T^{3/2}$ over a wide range of temperature, $.02T/_{T_c}$ to about $.6T/_{T_c}$ in both cases. Christiansen et al (1976) showed that the following relationship is valid in a very wide range of non cubic metals and intermetallics:

$$q(T) = q(0)\,(1 - BT^{3/2}) \qquad (4.23)$$

where

$$B \sim 10^{-5}\ K^{-3/2} \qquad (4.24)$$

B was generally positive, only one case (^{181}Ta in Be) being found where it was negative. In $GdAl_2$ the aluminium ions are at non cubic sites to that they do see a quadrupole moment due to the lattice. We used the data of Degani and Kaplan (1973)to find B on the basis that the temperature variation of the efg were entirely due to lattice expansion and discovered that B would be of the right order of magnitude.

*Nesbitt et al (1962)

We also showed using equations (4.4) and (4.23) that the quadrupole parameter P would increase from MHz at 350K to MHz at 575K whereas Jones and Budnick (1966) report P = 0.32 MHz for the range 350 to 575K. Furthermore this explanation does not account for the difference in observations at 'a' and 'b' sites discussed in section A, nor the lack of temperature dependence of the quadrupole splitting in $LaAl_2$, also discussed in section A. Thus this explanation, though it accounts neatly for the linearity of the efg with magnetisation over the large temperature range of 4K to 112K is unlikely to be valid.

We also considered volume striction. As the crystal expands, the efg at the aluminium sites responsible for the lattice contribution to the lattice coupling constant q will change. In this case the predicted temperature dependence would be that of the magnetic energy namely $T^{5/2}$ in simple spin wave theory. Thus the quadrupole splitting would have varied as $(M(T))^{5/2}$ where M(T) is the magnetisation rather than having the observed linearity. We have therefore not investigated this line further.

CHAPTER 5

CONCLUSIONS

We have shown that the pseudoquadrupole effect may be written in terms of the difference between the local transverse and longitudinal susceptibilities and the square of the hyperfine field. These susceptibilities can be calculated exactly at T = O for a localised (Heisenberg) spin model and estimated for the localised model at higher temperatures. They can also be calculated within the itinerant model for which we have given a simple theory.

We have used our itinerant theory to find estimates of the pseudoquadrupole parameter P_{pq} in pure iron and nickel and we have shown that P_{pq} is three orders of magnitude down from the experimentally measured quadrupole splitting P_e for iron. Our estimates for both iron and nickel suggest that in neither case is the effect likely to be experimentally observable, given an error of about 80% for P_e quoted in the measurements on iron.

We have extended our theory to look at dilute impurities in iron and nickel. For isotopes of iridium in iron and nickel we find that here too P_{pq} is several orders of magnitude less than values of P_e and we can show that for iridium in nickel, P_e is not significantly influenced by the pseudoquadrupole effect. However, our estimate of P_{pq} at cobalt impurities in iron is less than P_e by a factor of three only, so a more accurate theory is required to establish whether the pseudoquadrupole effect may be observable here. We also

consider that P_{pq} may be large at manganese in iron although we do not estimate its size.

In the rare earth intermetallic magnet with localised moments, $GdAl_2$, we have shown that the pseudoquadrupole effect is too small to account for the observed temperature dependent quadrupole splitting.

Our theory has been given for cubic ferromagnets but it may readily be extended to cubic antiferromagnets or any other colinear spin structure. We do not consider non cubic materials, as here the electric field gradients are large. Thus the pseudoquadrupole effect would generally be very much less than the 'real' quadrupole effects due to the electrostatic quadrupole moment of the nucleus.

Finally we note that the following conditions are favourable for an observation of the pseudoquadrupole effect in cubic magnets:

(i) A large value of the hyperfine constant

(ii) A small magnetically induced electric field gradient

(iii) A low value of the exchange constant J

(iv) Two isotopes (a) and (b) as dilute impurities in the same host such that the ratios of pseudoquadrupole to real quadrupole parameters

$$R = \frac{A_a^2 Q_b I_a (2I_a - 1)}{A_b^2 Q_a I_b (2I_b - 1)} \qquad (5.1)$$

is large. Here A is the hyperfine constant for the two different isotopes, Q the nuclear quadrupole moment and I the nuclear

spin.

Looyestijn et al (1979) have observed the pseudoquadrupole effect as a function of magnetic field for ^{17}O in $Rb_2CuCl_4.2H_2O$ in the paramagnetic phase. Here condition (iii) applies.

Part II REFERENCES

Aiga M and Itoh J 1971 J. Phys. Soc. Japan 31 1844

Baker J M and Bleaney B 1958 Proc. Royal Soc. A 245 156

Bleaney B 1967 in 'Hyperfine Interactions' Ed. Freeman A J and Frenkel R B (New York Academic Press) pp

Boasson H and Kaplan N 1978 S. State Commun. 27 983

Brout R 1960 Phys. Rev. 120 1519

Burd J and Lee E.W 1977 J. Phys. C: Solid St. Phys. 10 5481

Callaghan P T, Lattimer W M, Johnston P D and Stone N J 1976 Hyp. Int. 2 291

Calvo R, Passeggi C G, Isaacson R A 1970 Phys. Lett. 31A 407

Campbell I A and Gormés A A 1967 Proc. Phys. Soc. 91 319

Christiansen J, Heubes P, Keitel R, Klinger W, Loeffler, W, Sandner W and Witthuhn W 1976 Z Phys B 24 177

Cohen M H and Reif F 1957 Sol. St. Phys. 5 347

Clauser M J, Kankeleit E and Mössbauer R L 1966 Phys. Rev. Lett. 17 5

Davies J J and Owen J 1969 J. Phys. C: Solid St. Phys. 2 1405

Degani J and Kaplan N 1973 Phys. Rev. B 7 2132

Demangeat C 1975 I J Phys F: Metal Phys. 5 169

Demangeat C 1975 II J Phys F: Metal Phys. 5 1637

Doniach S 1968 J Appl. Phys. 39 751

Drain L E 1964 Phys. Lett. 11 114

Edwards D M 1980 J. Magn. and Magn. Mat. 15-18 Part I 262

Eska G, Hagen E, Butz T, Kiente P and Umlauf E 1971
Phys. Lett. B 36 328

Fermi E 1930 Z Phys. 60 320

Fisher M E and Pfeuty P 1972 Phys Rev B 6 1889
Fisher M E 1974 Rev. Mod Phys. 46 597

Foster H R, Chaplin D H, Lynam P, Swan D E and Wilson G V H
1977 Hyp. Int. 3 347

Fox R A and Stone N J 1969 Phys. Lett. 29A 341

Freeman A J and Watson R E 1961 I Phys. Rev. 123 2027

Freeman A J and Watson R E 1961 II Acta Crystallogr.
14 27

Gehring G A 1974 Physica Scripta 11 215

Gehring G A and Williams H C W L 1974 J. Phys. F:
Metal Phys. 4 291

Herring C 1966 in 'Magnetism IV' Eds. Rado G T and Suhl H
(New York: Academic Press)

Jaccarino V, Matthias B T, Peter M, Suhl H and Wernick J H
1960 Phys. Rev. Lett. 5 251

Jaccarino V, Walker L R and Wertheim G K Phys. Rev. Lett.
13 (1964) 752

Jones E D and Budnick J I 1966 J. Appl. Phys. 37 1250

Kajzer F and Parete G 1980 Phys. Rev. B 22 5471

Kanamori J 1963 in 'Magnetism I' Eds. Rado G T and Suhl H
(New York: Academic Press) pp

Kellogg, J M B, Rabi I I, Ramsey N F and Zacharias J R 1940
Phys. Rev. 57 677

Kim D J, Kubo R and Izuyama T 1963 J. Phys. Soc. Japan
18 1025

Kittel C 1971 'Introduction to Solid State Physics' (New
York: John Wiley and Sons)

Kubo R and Izuyama T 1969 Comments on Solid St. Phys 1 168

Looyestijn W L, Klaassen T O and Porulis N J 1979 Phys. Rev. B 19 4363

Lowde R D and Windsor C G 1970 Advances in Physics 19 813

Lynn J W 1974 'Ph.D.Thesis' Georgia Institute of Technology

Ma S-K 1976 'Modern Theory of Critical Phenomena' (London: Benjamin)

Mannari I and Kageyama H 1968 Prog. Theor. Phys. Suppl. 269

Marshall W 1958 Phys. Rev. 110 1280

Marshall W and Lovesey S W 1971 'Theory of Thermal Neutron Scattering' (Oxford: Oxford University Press)

Marshall W and Murray G 1969 J Phys. C: Solid St. Phys. 539

Martin D H 1967 'Magnetism in Solids' (London: Iliffe Books)

Mook H A 1966 Phys. Rev. 148 495

Moriya T 1979 J Magn. and Magn. Mat. 14 1

Mott N F 1964 Advan. Phys. 13 325

Nakamura T Prog. Theor. Phys. 20 547

Nesbitt E A, Sherwood R C, Wernick J H and Williams H T 1962 J. Phys. Soc. Japan 17 Suppl. B i 91

Niesen L and Huiskamp W J 1972 Physica 57 1

Obenshain F E, Glaser W, Czjzek G and Transit J E 1971 in 'Hyperfine Interactions in Excited Nuclei' Eds. Goldring G and Kalish R (New York: Gordon and Breach) pp 846-49

Pettifor D G 1980 J. Magn. and Magn. Mat. 15-18 847

Pfeuty P, Jasnow D and Fisher M E 1974 Phys. Rev. B 10 2088

Pykkö P 1971 J. Phys. F: Metal Phys. 1 102

Sayers 1976 J. Phys. F: Metal Phys. 1939

Segel S L and Stroud J D 1975 J. Phys. F: Metal Phys 5 1986

Sharma R R 1970 Phys. Rev. Lett 25 1622

Spijkerman J J, Travis J C, Pipkorn D N and Violet C E 1975 Phys. Rev. Lett 26 323

Stanley H E 1971 'Introduction to Phase Transitions and Critical Phenomena'(London: Oxford University Press)

Stewart G A, Barclay J A, Don C G, Lester L N, and Wilson G V H 1977 J. Phys. C: Solid St. Phys. 10 3651

Stone N J 1980 Hyp. Int. 8 83

Stringfellow M W 1968 J. Phys. C: Solid St. Phys. 1 950

Suhl H 1960 Phys. Rev. 109 606

Turov E A and Petrov M P 1969 'Yadern yi Magnitnyi Rezonans v Ferro-iAntiferromagnetikakh' (Moscow: Nauka) pp 88-157

Violet C E and Pipkorn D N 1971 J. Appl. Phys. 42 4339

Wagner F E and Potzel W 1971 'Hyperfine Interactions in Excited Nuclei' Eds. Goldring G and Kalish R (New York: Gordon and Breach) pp 681-91

Wakoh et al 1971

Wegner F J 1972 Phys. Rev. B 6 1891

Wernick J H and Geller S 1960 Trans. Metall. Soc. of AIME 218 866

Wohlfarth E P 1964 in 'Proceedings of the International Conference on Magnetism, Nottingham (London: Inst. of Physics) pp 51-54

Wolfram T 1961 Phys. Rev. 182 518

Yamazaki Y 1974 Phys. Lett. A 49 215

Zevin V and Kaplan N 1975 Phys. Rev. B 12 4604

Zubarev D N 1960 Usp. Fiz. Nauk. 71 71 (Sov. Phys. Usp. 3 320)